OPTIMIZATION OF ULTRASONIC WAVES IN AN ACRYLIC PIPE POWDER TRANSPORT SYSTEM

EVAN MURIMI WANJIRU

MASTER OF SCIENCE

(Mechatronic Engineering)

JOMO KENYATTA UNIVERSITY OF AGRICULTURE AND TECHNOLOGY

2012

Optimization of Ultrasonic Waves in an Acrylic Pipe Powder Transport System

Evan Murimi Wanjiru

A thesis submitted in partial fulfilment for the degree of Master of Science in Mechatronic Engineering in the Jomo Kenyatta University of Agriculture and Technology

2012

DECLARATION

This thesis is my original work and has not been presented for a degree in any other University.

Signature:..... Date.....

Evan Murimi Wanjiru

This thesis has been submitted for examination with our approval as the University Supervisors.

Signature:..... Date.....

Eng. Prof. John M. Kihiu

JKUAT, Kenya

Signature:..... Date.....

Prof. George N. Nyakoe

JKUAT, Kenya

Signature:..... Date.....

Prof. Stephen M. Mutuli

UON, Kenya

DEDICATION

This work is dedicated to my mum, Ms. E. W. Murimi.

ACKNOWLEDGEMENT

First, I would like to thank the Almighty God for giving me a chance to pursue and complete this course successfully. Secondly, I would like to acknowledge my supervisors, Eng. Prof. J. N. Kihiu, Dr. G. N. Nyakoe and Prof. S. Mutuli for their invaluable guidance and advice throughout my studies.

I am greatly indebted to Dr.-Ing. M. Neubauer, Dipl.-Ing. A. Renner and all staff of the Institute for Dynamics and Vibrations of the Gottfried Wilhelm Leibniz University Hannover, Germany for all the support they offered me.

I would like to thank Jomo Kenyatta University of Agriculture and Technology for granting me the scholarship throughout my studies. Special thanks goes to Mr. J. Kimotho for his selfless assistance, and the technologists in the Mechanical and Mechatronic Engineering Department Mr. D. Dzombo and Mr. M. Mumu for their assistance in the use of facilities in the department. I express my sincere thanks to all members of staff and all post graduate students in Mechanical and Mechatronic Engineering departments for their input to my work during post graduate seminars through their comments and suggestions.

Finally, I express my appreciation to my mother Ms. E. W. Murimi, and the entire family for their prayers, encouragement, guidance and love which kept me going.

TABLE OF CONTENTS

LIST OF TABLES

LIST OF FIGURES

LIST OF APPENDICES

LIST OF ABBREVIATIONS

AC	Alternating Current
DC	Direct Current
EMAT	Electromagnetic Acoustic Transducers
Nd:YAG	Neodymium: Yttrium Aluminium Garnet
PZT	Lead zirconate titanate
FDM	Finite Difference Methods
FEM	Finite Element Methods
TFMG	Thin film metallic glass
MEMS	Micro-electromechanical Systems
SH	Shear Horizontal

NOMENCLATURE

$\mathbf{c}$	Speed of sound $[m/s]$
$\mathbf{c_{ij}^D}$	Coefficients of the elastic constant tensor
$\boldsymbol{\gamma}$	Poisson's ratio
$\mathbf{d}$	Piezoelectric charge constant $[C/N]$
$\mathbf{[d]}$	Piezoelectric matrix relating strain/electric field
$\mathbf{\{D\}}$	Electric displacement vector
$\boldsymbol{\epsilon}$	Permittivity or relative dielectric constant $[Hz/F]$
$\mathbf{[e]}$	Piezoelectric matrix relating stress/electric field
$\mathbf{E}$	Young's Modulus $[N/m^2]$
$\mathbf{\{E\}}$	Electric field vector $[N/C]$
$\left[\boldsymbol{\varepsilon}^{\mathbf{T}}\right]$	Dielectric matrix evaluated at constant stress, i.e. mechanically free
$\left[\boldsymbol{\varepsilon}^{\mathbf{S}}\right]$	Dielectric matrix evaluated at constant strain, i.e. mechanically clamped
$\mathbf{f}$	Frequency [Hz]
$\mathbf{g}$	Piezoelectric voltage constant $[Vm/N]$
$\mathbf{h_{ij}}$	Elements of the piezoelectric constant tensor
$\boldsymbol{\phi}$	Scalar potential
$\mathbf{I}$	Moment of inertia of the cross section $[m^4]$
$\mathbf{J_1}$	First kind of Bessels functions of the first order
$\mathbf{k}$	Wave number
$\mathbf{L}$	Vector potential
$\boldsymbol{\lambda}$	Wavelength $[m]$
$\boldsymbol{\Lambda}$, $\boldsymbol{\mu}$	Lame's elastic constant
$\mathbf{r}$	Distance between an arbitrary point on the transducer and the observation point $[m]$

$\mathbf{R}$	Mean radius $[m]$
$\boldsymbol{\rho}$	Density of the material $[kg/m^2]$
$\mathbf{s}$	Compliance or the elastic constant of a material $[m^2/N]$
$\left[\mathbf{s^E}\right]$	Compliance matrix evaluated at constant electric field, i.e. short circuit
$\mathbf{S}$	Relative deformations tensor
$\mathbf{\{S\}}$	Strain vector
$\mathbf{\{T\}}$	Stress vector $[N/m^2$
$\mathbf{T_{ij}}$	Stress vector components $[N/m^2$
$\mathbf{u}$	Mechanical displacement vector $[m]$
$\mathbf{v}$	Velocity $[m/s]$
$\mathbf{V}$	Vibrating velocity at the sound source $[m/s]$
$\mathbf{w}$	Transverse displacement $[m]$
$\mathbf{Y_1}$	Second kind of Bessels functions of the first order
$\mathbf{Z_i}$	Impedance $[Pa.s/m^3]$
$\boldsymbol{\omega}$	Angular frequency $[rad/s]$

ABSTRACT

The transport of powder materials is an important aspect of process engineering. Various industries such as the food, chemical, pharmaceutical, coating, information and telecommunication industries have set a high demand on the performances of existing plants, which are mainly for bulk powder transfer. Modern systems demand powder transport systems which have a high quantitative accuracy. Therefore, the ultrasonic material transport process technology has in the last few years developed into an attractive alternative compared to the classical technologies. This technology involves transfer of powder through a pipe in which the ultrasonic waves are transmitted. However, this technology is not refined.

In this research, the traveling ultrasonic waves in an acrylic pipe were optimized by investigating the optimal placement of the transducer on the pipe, the optimal length and thickness of the pipe and the optimal frequency. The finite element analysis was used in modeling, due to its ability to analyze a material in small cells and then combine the results for the whole material. Thereafter, experiments were conducted in order to validate the model.

An optimal ultrasonic traveling wave was obtained at the resonant frequency of 48.4kHz at an optimal amplitude of 0.6mm can be used for powder transportation. The results showed that the optimal position of placing the transducer was 3mm from the edge of the acrylic pipe of optimal length of 500mm and internal and external diameter of 9mm and 14mm respectively. This optimization is important in developing new powder feeding mechanisms which have simple design, consume low power and exhibit high accuracy. Such a powder feeding device is useful where accurate control of powder in small quantities is required in industries such as pharmaceutical, manufacturing and chemical processing industries.

CHAPTER ONE

1.0 INTRODUCTION

1.1 Overview

A transport system is one of the essential equipment required in various fields of industry and it is important for higher productivity and production automation. There are several distinct methods for powder metering and dispensing: pneumatic methods [1], volumetric dosing, gravimetric dosing, screw and auger dispensers, electrostatic powder metering and control, magnetically mediated flow enhancement for controlled powder discharge of cohesive powders, acoustic or ultrasonic controlled powder dispensers and powder feeding devices based on the excitation of a traveling wave in a lossy ultrasonic transmission line [2]. Whilst it has been possible to handle small amounts of powder for some time using gravimetric or volumetric methods, these have not been able to deliver the required accuracy, speed or precision at the micro-dose level [3]. In the recent past, powder transportation using ultrasonic vibrations has generated a lot of interest. This has applications in several industrial fields requiring powder handling capability with very accurate mixing processes demanding for an exact control of powder feeding [4]. These industries include food, chemical, pharmaceutical, coating, information and telecommunication industries.

A non-contact manipulation technique that is capable of transporting small particles such as electronic components over long distances is highly attractive in the fields of manufacturing and biotechnology. Unlike air pressure methods, non-contact ultrasonic manipulation techniques do not require air compressors or tubes. In pharmaceutical biotechnology, a non-contact technique for transporting liquids is highly desirable be-

cause the conventional transportation technique that employs silicone tubes tends to contaminate the transported liquids (e.g., pure water and liquid drugs) through contact with the tubes. In these techniques, a particle that is much smaller than the wavelength of the acoustic standing wave is trapped at the nodal points [5]. The development of information and telecommunication industries has led to the development of semiconductor and optical industries. In the recent past, the demand of optical components has grown due to the demand of faster networks. On the other hand, conventional transport systems are not adequate for transporting precision optical components and semiconductors. Since the conveyor belt can damage precision optical components with contact force and a magnetic system would destroy the inner structure of semiconductor with magnetic field from the electromagnetic motors, a new system for transporting optical components and semiconductors is required [6].

An alternative to the existing systems is a transport system using ultrasonic wave excitation since it can transport granular components with improved accuracy and precision.

1.1.1 Ultrasonic waves

In general, the human ear is capable of receiving waves having a frequency lying between 15 and 15000 Hz. Below and above this range, mechanical vibrations fail to produce any sensation to the human ear. Though there is no standard limit, the vibrations lying above 15000 Hz are known as ultrasonics. If the velocity of sound waves in air is taken as 331 m/s, then the upper limit of wavelength of ultrasonic waves will be given by

$$\lambda = \frac{v}{f} \tag{1.1}$$

where λ is the wavelength, v is the velocity and f the frequency. Equation 1.1 gives a value of 2.2cm as the upper limit of the wavelength.

The most widely used methods for the generation of ultrasonic waves are the magnetostriction and piezoelectric methods. If a magnetic field is applied along the axis of a ferromagnetic material such as iron, cobalt and nickel in the form of a rectangular box, then a change in the length of the bar occurs. In a direct field, this change is small. If, however, the field oscillates, then the effect becomes much more pronounced because the internal elastic forces of the bar no longer oppose the change, and the only forces to be overcome are from the viscosity of the material. Further, if the oscillating field is resonant with the natural frequency of the bar, this effect becomes much more pronounced [7]. Electromagnetic transducers, also called electrodynamic transducers are also used as ultrasonic transducers. They are used at audio frequencies (kilohertz frequencies) as loudspeakers and microphones. Electromagnetic acoustic transducers (EMATs) are used in electromagnetic propagation and reception of ultrasound at megahertz frequencies. The main restriction for these transducers is the relatively high mass needed for the moving material and the consequent drop in sensitivity with frequency [8]. Laser pulses are also used to generate ultrasonic waves in metals. Common lasers used for ultrasound generation are solid state Q-Switched Nd:YAG and gas lasers (CO_2 or Excimers). The principles used are thermal expansion (also called thermoelastic regime) and ablation. In the thermoelastic regime the ultrasound is generated by the sudden thermal expansion due to the heating of a tiny surface of the material by the laser pulse. If the laser power is sufficient to heat the surface above the material boiling point, some material is evaporated and ultrasound is generated by the recoil effect of the expanding material evaporated. In the ablation regime, a plasma is often formed above the material surface and its expansion makes a substantial contribution to the ultrasonic

generation [9]. The advantage of using lasers in ultrasonic waves generation is the large frequency spectrum of the excited vibrations. However, the technique requires the complete knowledge of the structure of the laser-excited acoustic field in thin metal plates and the energy parameter of the laser radiation [10].

If DC voltages are externally applied to a piezoelectric, it responds with a mechanical deformation. Similarly, an AC field will cause the ceramic to alternate in size. In particular, the ceramic will have its own resonant frequencies at which it vibrates most easily, the values of which are determined by its composition, size and shape. If the ceramic is stimulated by an AC field at this frequency, it will oscillate with greater efficiency, converting electrical energy into mechanical (acoustical)energy [11]. At high frequencies of the AC field, the mechanical vibrations produced can be in the ultrasonic range.

1.1.2 Acrylic pipe

Structures and machines can have unwanted vibrations produced by the motions of engines, electric motors, or any mechanical device in operation. Such vibrations can be caused by imbalances in the rotating parts, uneven friction, the meshing of gear teeth, etc. and they can be damped by mechanisms which are essentially external to the system or the structure itself. The primary mechanisms of vibration damping important in mechanical systems are:

(i) **Internal damping -** It results from mechanical energy dissipation within the material due to various microscopic and macroscopic processes.

(ii) **Structural damping -** It results from mechanical energy dissipation caused by

friction due to the relative motion between components and by impacting or intermittent contact at the joints in a mechanical system or structure.

(iii) **Fluid damping -** arises from the mechanical energy dissipation resulting from drag forces and associated dynamic interactions when a mechanical system or its components move in a fluid.

There are two general types of internal damping: viscoelastic damping and hysteretic damping. Viscoelastic damping, strongly displayed in many polymeric, elastomeric and amorphous glassy materials, arises from the relaxation and recovery of the molecular chains after deformation. A strong dependence exists between frequency and temperature effects in polymer behavior because of the direct relationship between temperature and molecular vibrations [12]. In addition, experimental studies have showed that the damping and dynamic elastic properties of various solid materials increase with frequency over a finite bandwidth, and the increase is weak if the damping is low [13, 14].

Examples of these damping materials are; acrylic rubber, natural rubber, fluorocarbon, nylon, silicone, urethane and fluorosilicone [15].

Acrylic material has elastic properties similar to those of a metallic spring and has energy absorbing properties like those of a viscous liquid. These viscoelastic properties allow it to maintain a constant shape after deformation, while simultaneously absorbing mechanical energy. The viscosity follows Newton's law, increases with reduced temperature and increases with increased strain rate whereas the elasticity follows Hooke's law and increases with increased strain [12].

Kirekawa *et al.* [14] researched on the feasibility of acrylic material as a vibration energy absorbing device and found out that although the mechanical characteristics considerably varied with the ambient temperature and excitation frequency, the acrylic material

had great vibration energy absorbing capacity. An ultrasonic lossy transmission line can be used for generation of traveling ultrasonic waves. They cause the reflected wave to reduce in magnitude. Therefore, the wave transmitted from the driving transducer becomes dominant in the line. That is, the progressive wave is generated practically without attention to the acoustical matching at the receiving end [16]. The acrylic pipe has specific damping properties which allow the excitation of a progressive flexural radial wave in a pipe, using only a single piezoelectric actuator. Since the incident wave moves through a pipe, which consists of material with damping properties, it will be damped in its amplitude. During interference of incident and reflecting waves, the incident wave becomes dominant; therefore, a progressive wave is produced. By this, a wave front is sent along the pipe which causes compressions and dilatations at the inside of the pipe [17]. It is the ability of the pipe to produce the progressive waves that makes it superior to other materials like steel, which would need a mechanism to counter the reflected waves [16].

1.2 Problem statement

Most powder feeding devices are designed to feed large amounts of powder. However, present demands require the development of devices to feed small amount of powder with high quantitative accuracy and precision. Various feeding methods like vibrating conveyors, auger mechanisms and pneumatic systems which have a very low accuracy, can damage sensitive components, are noisy and have a high maintenance cost.

This has led to a need for an alternative method of transporting powder. A trial system for powder transportation where traveling ultrasonic waves are used to transport the powder in a hollow cylinder has been developed which transported the powder although

not under optimal conditions. This means that there was loss of energy and the full potential of the system was not attained. The strength of the traveling ultrasonic wave depends on the position and frequency of the vibrating transducer and the dimensions of the hollow acrylic pipe due to the interference of the incident and reflected wave and the ability of the acrylic pipe to damp out the wave [18].

Therefore, in this research, the transportation device was optimized in order to have an optimum traveling ultrasonic wave that can transport powder flowing through the acrylic pipe.

1.3 Objectives

The main objective was to optimize the traveling ultrasonic waves in a hollow acrylic pipe. To achieve this objective, the following specific objectives were accomplished;

1. To optimize the offset position of placing the transducer on the acrylic pipe.
2. To investigate the optimum length of the acrylic pipe.
3. To optimize the inner and outer diameters of the acrylic pipe.
4. To determine the resonant frequencies of the set-up through modeling and experiments.
5. To obtain the optimum frequency and amplitude of the traveling wave.

1.4 Significance of the study

Modern technology demands that a system for accurate and reliable powder transportation be in place, for instance, in modern copying machines [19]. In addition, a potential demand for a new method for conveying various powders and viscous liquids

has emerged in the food industry [20]. This thesis seeks to address the problem of small powder-feeding devices, e.g., copier feeding toner, which require a controlled powder feeding system which is highly accurate, reliable and quiet. The ability for the system to be miniaturized makes it a potential candidate in micro and nano-technologies [21,22]. Such a powder feeding device will lower the power consumption contributing to energy conservation. In addition, the improved accuracy and controllability will reduce in wastage of the powder during transportation.

CHAPTER TWO

2.0 LITERATURE REVIEW

This chapter discusses the research that has been done in powder transportation systems.

2.1 Classical powder transportation systems

The transport, metering and dosage of powder material are important in the process industry. The need to handle small quantities of powder to prepare mixtures, to achieve dosing as a function of position or to create images occurs in many industrial, technical and artistic activities. In the preparation of pharmaceutical products, small amounts of active chemicals are metered into a mixture of inert fillers, binders, flavourings and colours within critical dosing limits [23]. In the continuous preparation of paints, inks or glazes, powders that confer colour are metered into organic vehicles or glass frits [24]. In some cases, the requirement is to form a two-dimensional image or a succession of two-dimensional images, in powder [25]. Dosing in the polymer processing industry is critical in the extrusion of pipes or multiple coatings on wire by coaxial extrusion methods. The problem is to meter solid additives such as pigments, antioxidants, inert fillers, perhaps short staple fibres into the hopper along with pelletised or powdered polymer feedstock [26].

There are several mechanical methods used in powder conveying. These include: belt conveyors, screw conveyors, tables, bins, and elevators [27]. Vibratory conveyors consist of a trough which is vibrated sinusoidally by an electric motor with a fixed eccentric shaft(or rotating weight) or an electromagnet. The generated vibrations are then controlled to create a circular, elliptical, or linear movement of the granular material along

the conveyor surface. Linear vibrations are normally used for conveying and screening purposes whereas elliptical motion is used to drive screens, packers, shakeouts, or bin-dischargers. Circular drives are only used in annular conveyors [28]. The main advantages of vibratory conveyors are their simple construction, their suitability to handle hot and abrasive materials and their applicability as dosing equipment. Since the trough can be totally enclosed, they are also well suited to the transport of dusty materials. Their disadvantages are the noisy operation, the induced vibrations on their surroundings and their limited transport distance. Furthermore, the granular material may be damaged when it is subjected to large accelerations normal to the trough [29]. A screw conveyor, is another mechanical method of conveying powder. It consists of a driving unit in the form of a conveyor screw, obtained by welding a continuous flight to a tube, which rotates inside a duct. It is capable of handling materials in powder form by means of the rotating screw using the principle of Archimedean screw [30]. A rotating drum is also a mechanical method used in transportaion of powder. As the drum rotates, the powder heap rises with the rotation and it is taken to the receiver [31, 32]. Auger feed mechanisms have been employed to transfer freeze dried materials from a hopper to a mixing chamber. Such mechanisms do not dispense an accurate dose of material because the volume of material transferred in a given amount of time depends upon the speed of the auger motor and on the flow of material within the hopper. The motor speed fluctuates with the load on the auger such that the dose of material varies with hopper content [33].

A vibration feeder is a widely used device for transport of granular and particulate material in various manufacturing industries. Aleksandar *et al.* [34] considered the electromagnetic vibratory feeders to be compact, robust, reliable in operation, and easy for maintenance. However, their performance was highly sensitive to different kinds of

disturbances. For example, as the feeder vibrations occurred at its resonance frequency, vibration amplitude was highly dependent on a damping factor. On the other hand, the damping factor depended on the mass of the material on the feeder trough, the type of material, and the vibration amplitude. These disturbances could reduce drastically the vibration amplitude, thus reducing the performance of electromagnetic vibratory feeders.

Magnetic systems generate an undesirable magnetic field that can damage items such as electronic components; furthermore, the object is limited to being a magnetic material. In pharmaceutical biotechnology, a non-contact technique for transporting liquids is highly desirable because the conventional transportation technique that employs silicone tubes tends to contaminate the transported liquids (e.g., pure water and liquid drugs) through contact with the tubes [5].

Besides mechanical methods, air pressure, which requires air compressors or tubes has been used to transport powder. Anthony [1] described a pneumatic conveying system as a process by which bulk materials are transferred or injected using a gas flow as the conveying medium from one or more sources to one or more destinations. Air is the most commonly used gas, but may not be selected for use with reactive materials and/or where there is a threat of dust explosions. There are several methods of transporting materials using pneumatic conveying which generally fall into three main categories: dilute phase, dense phase, and air conveying. Dilute phase conveying is the most commonly used method of transporting materials. This process uses a relatively large amount of air to convey a relatively small amount of material and at lower pressures than dense phase systems. The material is transported at high velocities through the system while being suspended in air. To keep the material in suspension, it is necessary to maintain a minimum conveying air velocity. This system has the following limitations.

1. High power requirements.
2. The system is not suitable for abrasive particles or those susceptible to degradation as they are transported at high velocities causing wear in the pipe.
3. The product can be deformed or crushed.

Holdich *et al.* [35] classified a dilute system either as a positive pressure dilute phase or a negative pressure (vacuum) dilute phase. Positive pressure dilute phase systems operate above atmospheric pressure and are used to convey bulk materials from a single or multiple sources to one or multiple destinations, over medium distances and with greater capacity than possibly using vacuum systems. The system requires a blower to provide the motive force for the material. However, negative pressure conveying systems operate with air pressures below atmospheric pressure. In this case, particles are sucked through the system. All the above methods are usually useful in large powder feeding systems where accuracy of the amount of the powder fed is not an issue. However in modern technology, where more compact machines are being designed and miniaturization is also taking place, an alternative method of conveying the powder is needed.

There is a wide variety of methods using electrostatic control to meter powders and to create powder patterns on a surface [36]. Chen *et al.* [37] developed a simple electrostatic valve with external electrodes. This device had a horizontal electrostatic field created by the electrodes clamped to the side of a vertical pipe fed by a hopper as shown in Figure 2.1. At low applied voltages, the flow was independent of voltage V, but from experiments, when using a tube with inner diameter 7 mm, feeding metal powder, at voltage V greater that 2 KV, the flow rate was proportional to the voltage as shown in Equation 2.1.

$$Q \propto V^{-0.8} \tag{2.1}$$

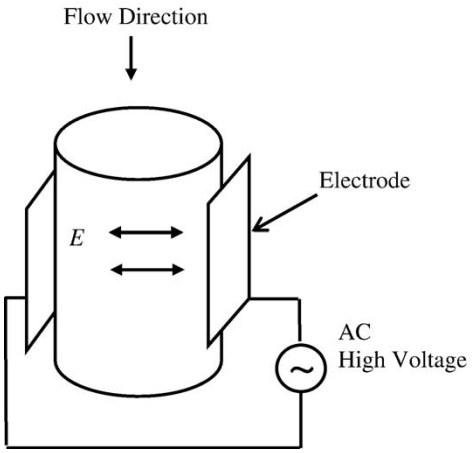

Figure 2.1: Electrostatic valve with external electrodes.

The valve worked because particles near the electrodes formed clusters and were pulled toward the sidewalls where particle friction was effectively increased. At higher voltages, a dense region developed just above the electrodes while the particle packing below became less efficient [37]. A comparable electrostatic valve, shown in Figure 2.2, had internal electrodes created using adjacent high voltage and ground electrodes consisting of cross-wires inside a vertical powder flow channel [38, 39].

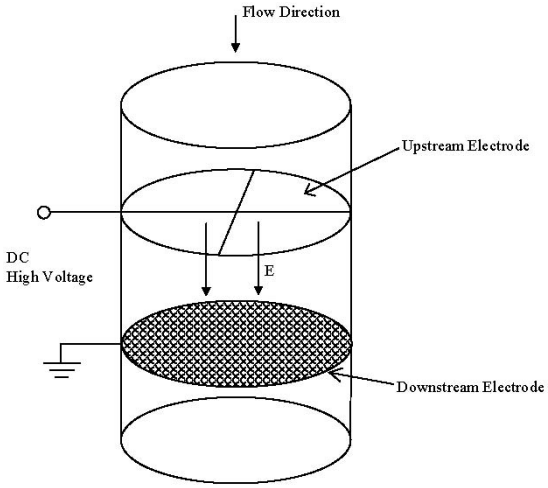

Figure 2.2: Electrostatic valve with internal electrodes.

A pulsed 10kV DC supply was used to achieve flow rate modification of $30-70\%$ of the free flow discharge rate using four particulate materials operated in a co-flow channel

with gas-assisted transport. A correction based on an effective increase in the gradient of interstitial gas pressure at the orifice predicted a reasonable fit to the mass flux-voltage curves for the electrostatic valve [40]. Olansen and Dunn [41] described the construction of a simple electrostatic powder dispenser without a gas flow based on electrostatic levitation and transport as shown in Figure 2.3. In this device, powder was supplied to a high voltage electrode situated between two grounded electrodes. Particles levitated from the source, approached the upper grounded electrode and returned. The upper electrode was shaped so that the particles were displaced radially, finally passing through a screen to an outlet. The dispenser worked in air or vacuum and was thus independent of a carrier gas. It's efficiency is related to the difference between the applied field and the minimum field for particle levitation.

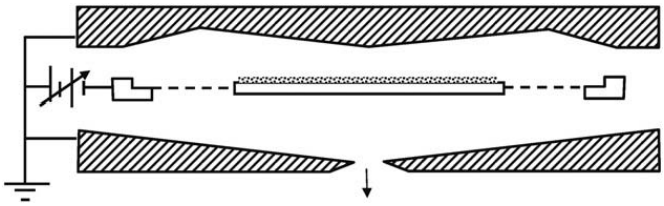

Figure 2.3: Electrostatic powder dispenser using levitation and lateral displacement.

2.2 Ultrasonic powder transport systems

There are three mechanisms for ultrasonic-based transportation: friction driving, wave-action and boundary layer interaction (acoustic streaming) [42].

Acoustic streaming is a steady circular airflow occurring in a high-intensity sound field. The factors that induce acoustic streaming are; spatial attenuation of a wave in free space and the friction between a medium and a vibrating object. When sound waves propagate, they are attenuated by absorption and scattering. This attenuation is, in general, insignificant in a short distance of propagation. However, the propagation of

a high intensity sound wave results in the attenuation of pressure significant enough to create steady bulk airflow. This type of streaming is usually associated with a medium of high viscosity. The other type of acoustic streaming is attributed to the friction between a vibrating medium in contact with a solid wall. As long as there is an oscillating tangential relative velocity, it is not important whether the source of a relative motion arises from either acoustic oscillations in the fluid or vibrations of the solid. Both cases lead to frictional dissipation within Stokes boundary layer. Unlike acoustic streaming resulting from spatial attenuation, this streaming has two components: inner and outer streaming. The inner streaming is created within the boundary layer due to the friction between the medium and the wall. Then, the inner streaming, in turn, induces relatively large-scale steady streaming outside the boundary layer. This process can be compared to the generation of electromagnetic field by a surface current on a conductor [43].

Friction driving is typically used in ultrasonic motors (USM) where the rotor is driven by friction forces between it and stator. The friction force is generated by the ultrasonic wave traveling or standing in the stator of USM [44].

The application of ultrasound to new functional devices such as actuators and motors has attracted much attention. Standing ultrasonic waves have been explored for powder transportation. A device developed by Kozuka *et al.* [45] used the standing ultrasonic waves, whereby a reflector was set in front of a transducer. The incident wave and the reflected wave generated a standing wave field as shown in Figure 2.4.

In this field, most of the solid particles received acoustic radiation pressure which pushed them toward nodes in the sound pressure distribution formed every half wavelength along the sound beam. Although it was possible to transport the particles by changing the driving frequency, the resonant frequency of this system kept changing with changing frequency. In addition, the moving direction and transportation distance varied

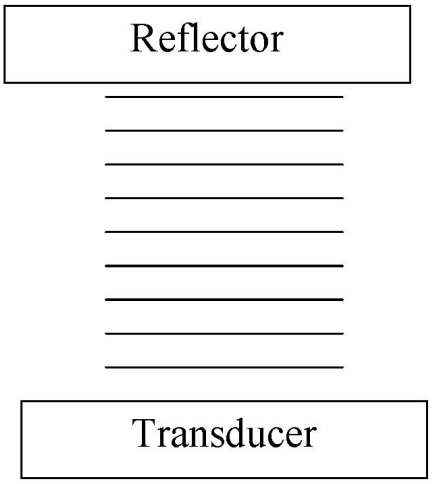

Figure 2.4: Generation of a standing wave field using a reflector.

depending on the distance from the reflector [46, 47].

Kozuka *et al.* [48] then improved on the previous device by developing another one which generated a standing wave field by two transducers whose sound beam axes crossed each other without using a reflector as shown in Figure 2.5. The sound field did not resonate

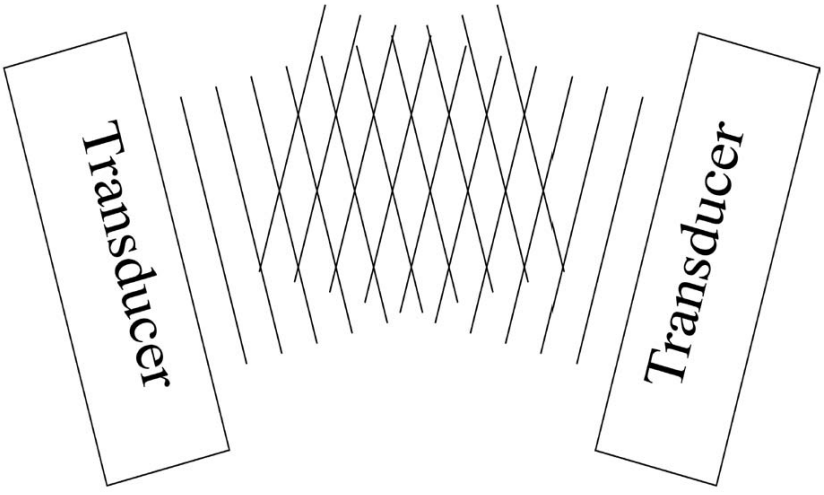

Figure 2.5: Generation of a standing wave field using two crossing sound beams.

since the sound beams were not reflected to each transducer making it stable for any frequency changes. By changing the phase difference between the transducers, the position

of the trapped particle shifted, and transportation occurred. In addition, by assigning slightly different frequency to each transducer, transportation at constant speed was realized. However, it was difficult to manipulate the particle at larger inclination angles of the sound beams. The sound pressure produced by a piston source in an infinite rigid wall can be expressed by the following Rayleigh's formula:

$$p = j\frac{\rho c \mathrm{V}_0}{\lambda}\exp(j\omega t)\int\int_F \frac{exp(-jkr)}{r}dF \tag{2.2}$$

Where, V_0, is the vibrating velocity at the sound source in m/s, ρ, is density of the medium in kg/m^3, c is sound speed in m/s, λ is wavelength in m, ω is angular frequency in rad/s, k is ω/c, and r is the distance between an arbitrary point on the transducer and the observation point in m.

An ultrasonic powder transportation device which consists of a pair of phase shifted bending vibrators facing each other across a gap as shown in Figure 2.6 was developed [49]. The upper vibrator was laterally shifted relative to the lower one by a quarter wavelength of the bending mode and the two vibrators were driven in temporal phases different from each other by 90 °. In such a condition, powder was transported in one direction through the gap. Yamane *et al.* [50] explained that a bending vibrator radiates directive ultrasound in four oblique directions. Since the bending vibration, that is, the lowest antisymmetry mode (A_0 mode) of Lamb waves has a low phase velocity, it can be phase matched to ultrasound in the air by adjusting the vibration frequency and the plate thickness. In such a condition, ultrasound is radiated in two opposite directions along the plates if they are facing each other side by side and excited in the same phase. However, if the plates are excited in phases different by 90° both in space and in time, ultrasound vibrated in the vibrators will add up in one direction

and cancel out in the other. In this case, unidirectional high intensity ultrasound would be generated along the plates and the sandwiched powder was transported in direction by the radiation pressure and accompanying acoustic streaming force. However, this system used multiple transducers making the design more complicated in operation and consume more power.

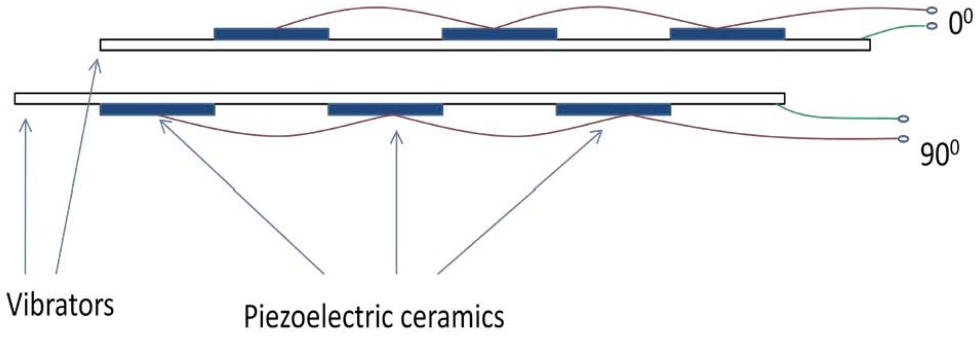

Figure 2.6: An ultrasonic powder transportation device consisting of a pair of phase shifted bending vibrators facing each other.

Ultrasonic linear motors using traveling ultrasonic waves have also been researched on in the recent past [42]. A particle at the surface of a transmission bar in which a flexural traveling wave was guided, moved elliptically. If a movable object was in contact with the bar, the object was forced to move through frictional force [51]. To generate the traveling wave, a pair of longitudinal vibrators were connected to the transmission bar where one of the vibrators excited a flexural wave in the bar and the other absorbed it. This required a mechanical impedance match between the transmitting and the receiving transducer [52]. However, the total efficiency of the trial motor was not high due to the losses in the vibration system [51].

Research has also been done on a device that used a rectangular stainless steel bar for an ultrasonic transmission line and two transducers for excitation and absorption of the wave as shown in Figure 2.7. In the device, a counter plan of acoustical matching was considered to suppress the reflected wave from the received end of the transmission

line because the transmission loss in the bar was very small [19]. This method had the disadvantage of using two transducers which consumed a significantly high amount of power.

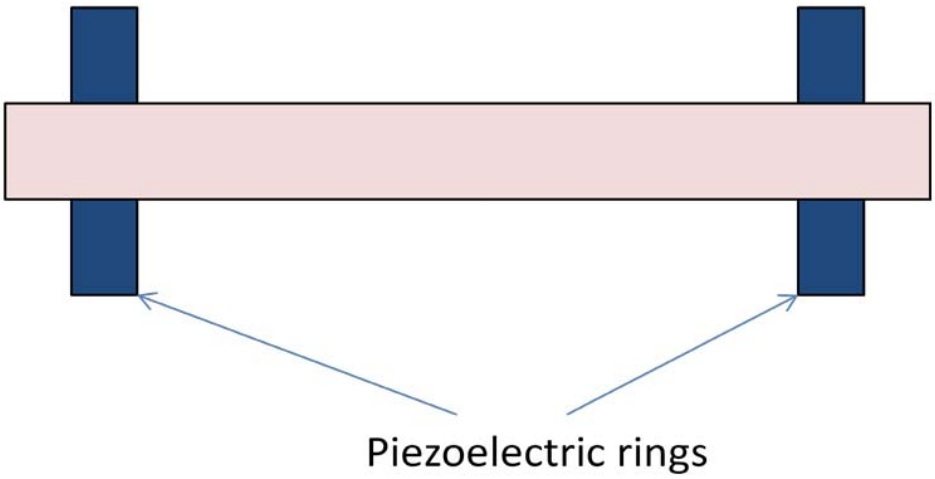

Figure 2.7: A traveling wave powder transportation device using two transducers.

Sun *et al.* [53] developed a microactuator composed of a stator and slider whose schematic drawing is shown in Figure 2.8. The stator consisted of two piezoelectric ceramic (PZT) tubes and one elastic pipe that were regarded as a bridge connecting the two PZT tubes. The elastic material was a thin film metallic glass (TFMG), which is an ideal material for micro-electromechanical systems (MEMS) and other micro elastic structures.

When high frequency harmonic voltages were applied, PZT tubes vibrated based on the converse piezoelectric effect. The TFMG pipe vibrated as a standing wave at its eigen-mode under the excitation of the PZT vibration. At some specific driving signals and under suitable boundary conditions, however, a traveling wave was generated on the TFMG pipe to drive the slider, which was a stainless pipe with high precision, to move in two directions.

Kanbe *et al.* [20] came up with a prototype powder transportation device, which had

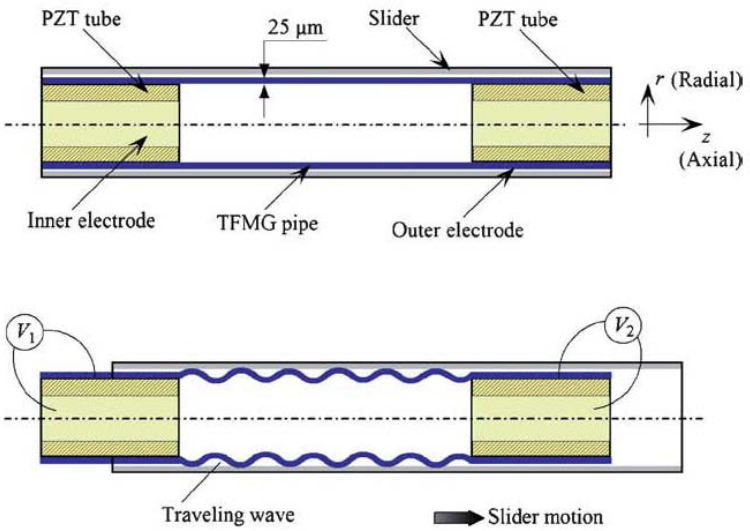

Figure 2.8: Generation of traveling Wave in Piezoelectric Ultrasonic Bidirectional Linear Microactuator.

a transmission line consisting of an acrylic pipe, with the set up similar to the one in Figure 2.7. In this case, the progressive wave was generated even without giving attention to acoustic matching at the receiving end. The use of a lossy transmission line caused the reflected wave to reduce in magnitude.

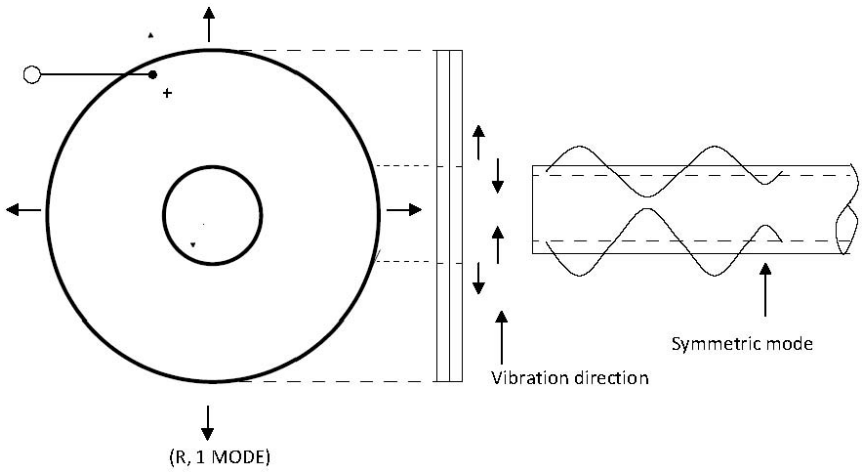

(a) Symmetric mode

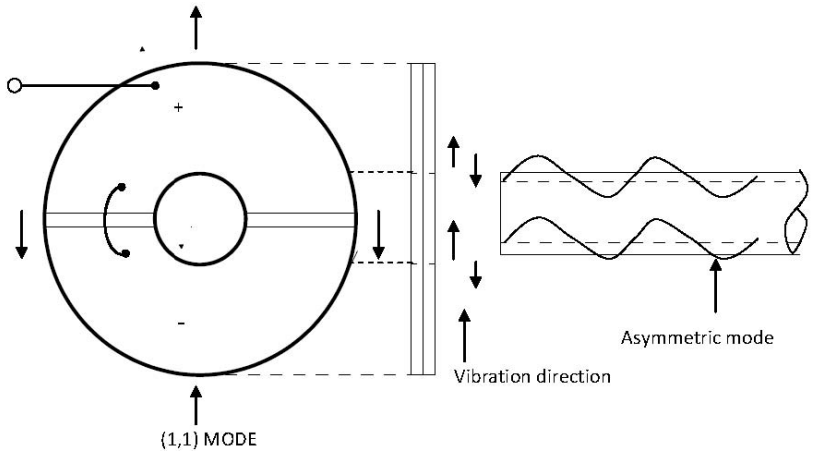

(b) Symmetric mode

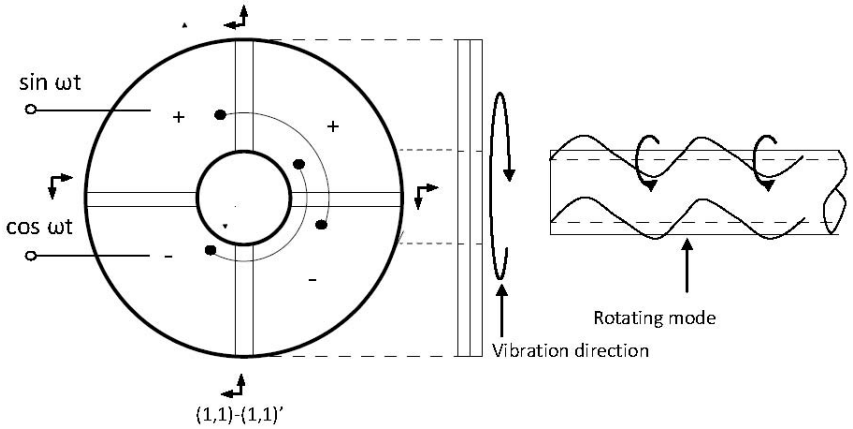

(c) Symmetric mode

In order to determine the best vibration mode of a piezoceramic ring to produce traveling ultrasonic waves to transport powder, Takano *et al.* [16] carried out a research by exciting flexural traveling waves in an acrylic pipe. Three kinds of flexural waves were excited corresponding to the vibration modes of the piezoceramic ring resulting to the waves shown in Figure 2.2. Figures **??**, **??**, and **??** show the symmetrical flexural mode excited by the (R,1) mode, the asymmetrical mode excited by (1,1) mode and the rotating flexural mode excited by degenerated (1,1)-(1,1)' mode respectively. The flexural progressive wave with rotation was excited into the pipe because two orthogonal flexural waves were driven by two electric signals with a phase difference of 90° [16]. From experiments on the vibration modes in acrylic pipes [19], the symmetric mode

transported more powder than the asymmetric mode, that is, the powder sending speed by the symmetric mode was about $15 - 20$ times faster than the asymmetric mode as shown in Figure 2.9.

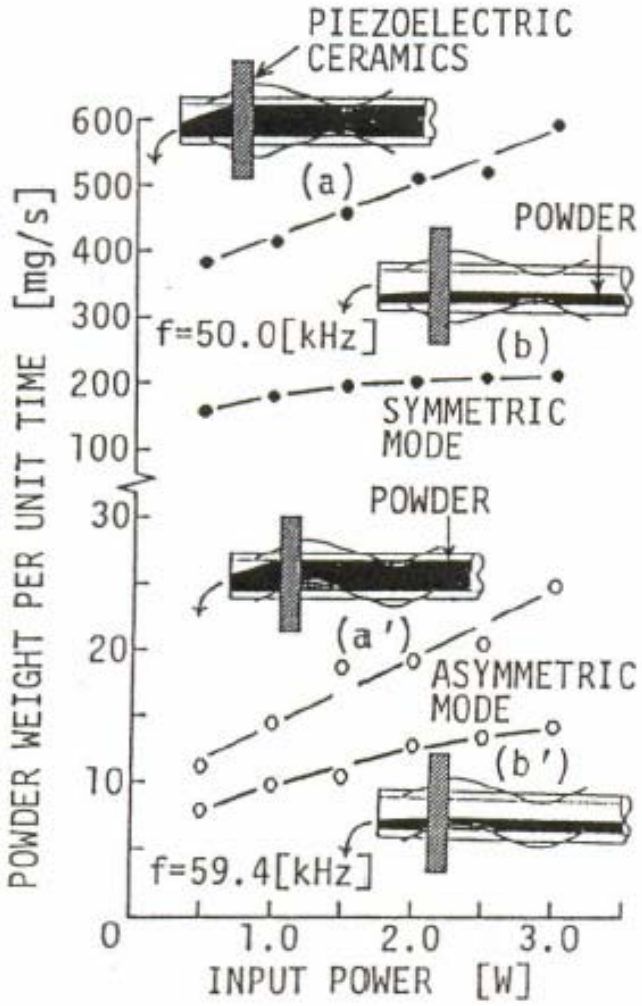

Figure 2.9: Powder sending characteristics of the device [19].

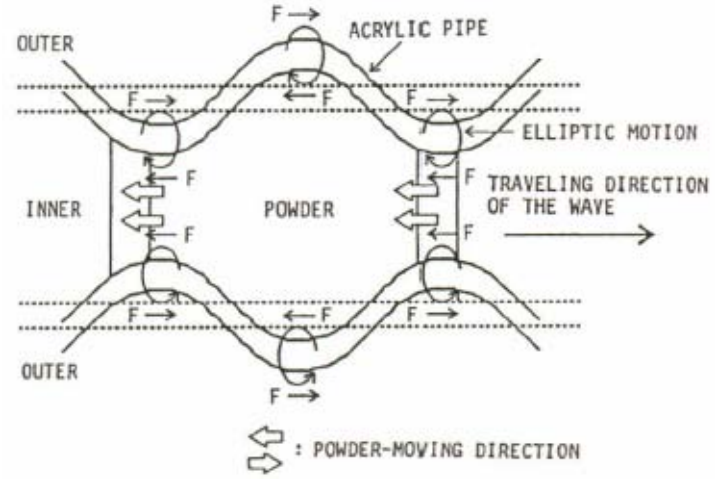

(a) Symmetric mode

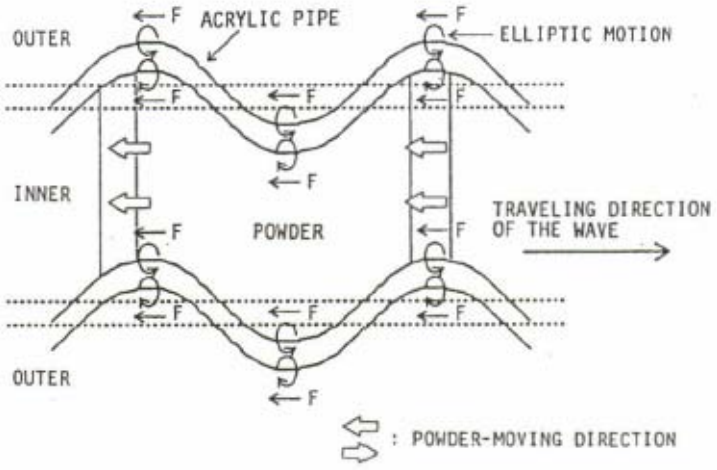

(b) Asymmetric mode

Figure 2.10: Elliptic motions of displacement and powder moving directions [19].

This is because the elliptic motion of the displacement of sending force, F, by the symmetric mode occurred in the same direction on the entire inner side of the pipe as shown in Figure 2.10a. Conversely, in the asymmetric mode, the elliptic motion of displacement is not uniform; that is, it was maximum at the top and bottom of the pipe, but non-existent in the middle area depicted in Figure 2.10b due to the absence of the elliptic force, F.

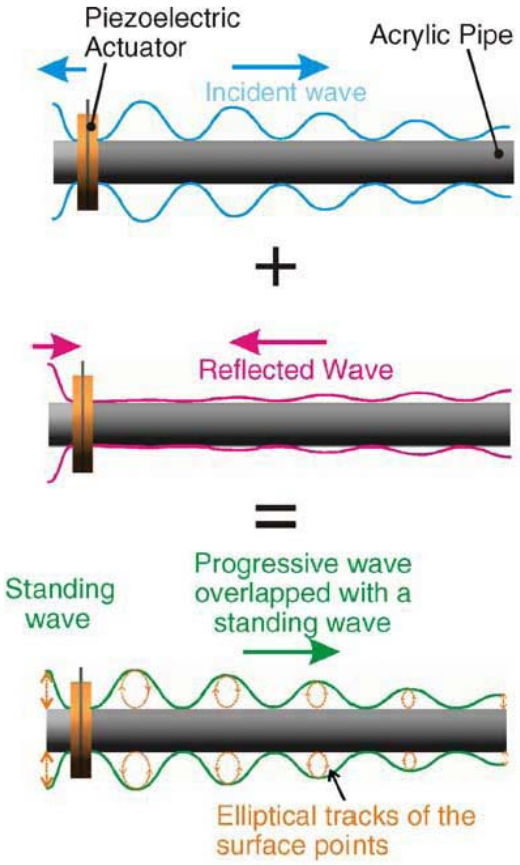

Figure 2.11: Traveling wave in an acrylic pipe [18].

Mracek *et al.* [18] developed a trial device for transporting small amounts of powder using a lossy transmission material (acrylic pipe) and only one transducer as shown in Figure 2.11. The device was used to move powder placed inside the pipe forward. During interference of the incident and the reflected waves, the incident waves became dominant producing a traveling wave. This resulted in the particles placed inside the pipe moved forward through the resulting elliptical movement of the surface area points.

2.3 Summary

From the foregoing literature review, it is evident that a lot of research in powder transportation has been undertaken. However, transportation, metering and dispensing

of small amounts of powder has been a challenge especially with the development of micro-electromechanical systems (MEMs). Accuracy, high power consumption and a possible alteration of the particle properties were the main drawbacks in traditional transportation methods that have led to the ultrasonic technology being sought as an alternative. This powder-feeding principle has the following advantages;

1. Simple mechanical structure
2. High accuracy
3. Low power consumption
4. No wear, simple maintenance
5. Vacuum and clean room compatibility
6. Operation at cryogenic temperatures is possible

Although research has been done on various devices that can transport small amounts of powder, the technology has not been refined, as only trial devices have been developed. The aim of this work was to refine this technology by optimizing the traveling ultrasonic waves in the powder transportation device. The parameters used to optimize were the offset position of placing the transducer and the length and diameter of the pipe. It was anticipated that this work would form a useful reference for further research in these powder transportation systems.

CHAPTER THREE

3.0 THEORETICAL BACKGROUND

In this chapter, the relevant theories on Finite element methods, (FEM), piezoelectricity, axisymmetric waves in a hollow pipe and manipulation of a particle by a traveling wave are discussed.

3.1 Finite Element Method

There are many engineering problems whose exact solutions cannot be obtained due to either the complex nature of governing differential equations or the difficulties arising from dealing with boundary conditions. In order to deal with such problems, numerical approximation problems have been developed. The two common classes of numerical approximation methods are finite difference methods (FDM) and finite element methods (FEM) [54]. The fundamental concept in the FEM numerical approximation methods is that any domain can be implemented as a collection of smaller subdomains (elements) of preferred shape. Corners of an element are called nodes at which the solutions to field variables are computed. There can be nodes in between corner points that are commonly called edge nodes [55].

In finite difference methods, the differential equation is written for each node, and the derivatives are replaced by difference equations resulting in a set of simultaneous linear equations. Although this method is easy to understand and employ in simple problems, it is difficult to apply in problems with complex geometries, complex boundary conditions or non-isotropic material properties. In contrast, the finite element method uses integral formulations, rather than differential equations to create a system of algebraic

equations. An approximate continuous function is then assumed to represent the solution for each element. The complete solution is finally generated by assembling the individual solutions, allowing for continuity at the inter-elemental boundaries [54].

3.1.1 Basic steps in Finite Element Method

The basic steps in finite element analysis are [56];

Preprocessing phase

(i) Creation and discretization of the solution domain into finite elements; that is subdividing the domain into elements and nodes.

(ii) Assumption of a shape function to represent physical behavior of an element.

(iii) Development of the element matrix for the subdomain (element).

(iv) Assembly of the element matrices for each element to obtain the global matrix for the entire domain.

(v) Application of boundary conditions, initial conditions and loading.

Processing phase

(vi) Solving the system of equations involving unknown quantities at the nodes (e.g., displacements) [57].

Postprocessing phase

(vii) Obtaining information of interest such as stress, strain and visualization of the response.

3.1.2 Element types

Elements used in finite element analysis are classified based on the shapes as:

(i) One dimensional elements - They are also called line elements and they are suitable for the analysis of one dimensional problem such as spring, truss and beam elements [58].

(ii) Two dimensional elements - suitable for solving two dimensional problems. Examples in stress analysis are plane stress, plane strain and plate problems [57].

(iii) Axi-symmetric elements - useful for the analysis of axi-symmetric problems such as analysis of cylindrical storage tanks, shafts, rocket nozzles [57].

(iv) Three dimensional elements - applied for three dimensional problems such as temperature, displacement, stress and flow velocity. Figure 3.1 shows the various element shapes in three dimensional elements. [57].

In this study, three dimensional elements will be applied since it relates to three dimensional problems. Displacement of the piezoceramic transducer producing the ultrasonic waves in the acrylic pipe will be analyzed.

3.1.3 Three dimensional elements

For three dimensional problems, a tetrahedron, which is the basic shape for an element has four nodes at the corners as shown in Figure 3.1a. Three dimensional elements with eight nodes are either in the form of a general hexahedron (Figure 3.1b)or a rectangular prism (also known as brick element, Figure 3.1c), which is a particular case of a

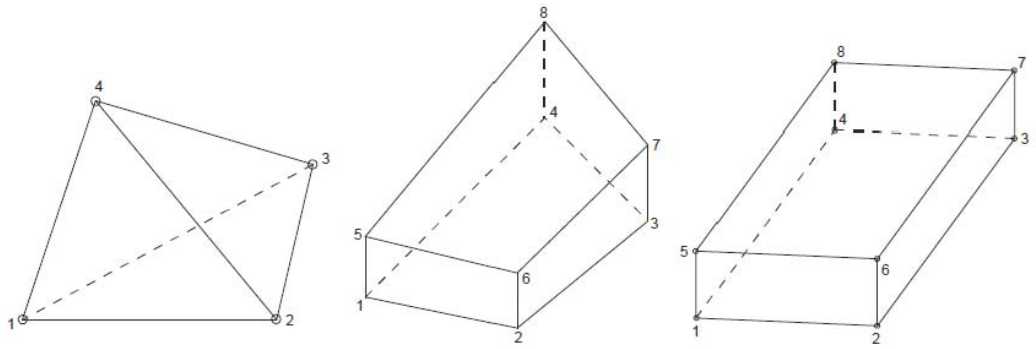

(a) tetrahedron element (b) hexahedron element (c) Rectangular prism

Figure 3.1: Examples of elements used in finite element analysis.

hexahedron [57]. Solid-type elements are constructed by modifying three-dimensional elements. The node points are situated in both the top and the bottom surfaces as shown in Figure 3.2 and have three degrees of freedom each, namely, the three components of displacement [59]. This is an eight-node solid element.

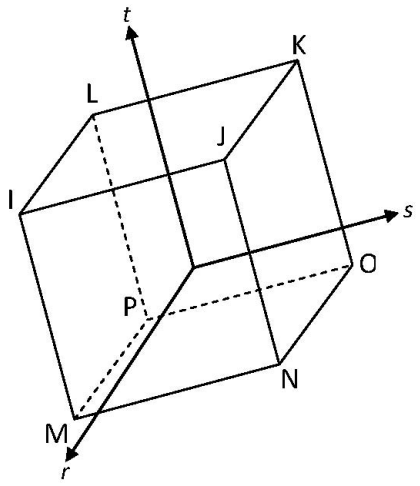

Figure 3.2: Nodes placed at each corner of the solid element.

A twenty-node solid element, shown in Figure 3.3 is a higher order version of the eight-node solid element. This element is more capable and more accurate for modeling problem with curved boundaries than eight-node solid element [54].

The deformation experienced by the element is explained in Appendix **A**.

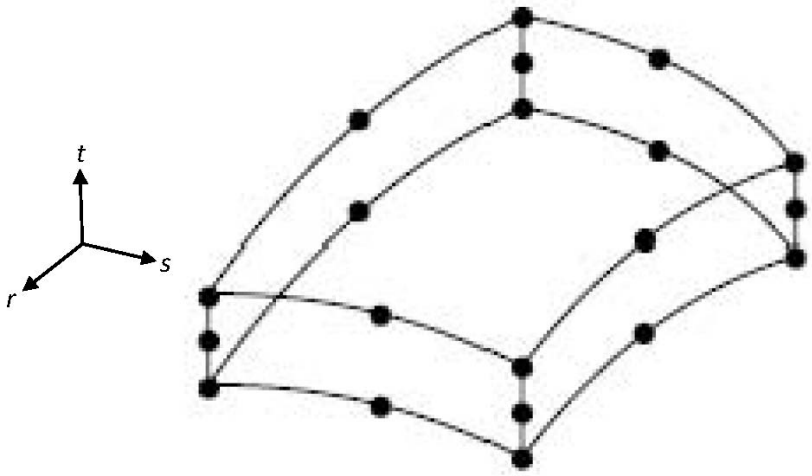

Figure 3.3: A twenty-node solid element.

3.2 Piezoelectricity

When mechanical stresses are applied to a piezoelectric solid, voltage is produced between its surfaces. This is the piezoelectric effect. Conversely, when a voltage is applied across certain surfaces of the solid, the solid undergoes a mechanical distortion. This is the inverse piezoelectric effect. The effect is exhibited by certain crystals whose charge symmetry is disturbed, and the charge asymmetry generates a voltage across the material. Examples include quartz, Rochelle Salt and many synthetic polycrystalline ceramics, such as bariumtitanate and lead zirconate titanates (PZT) [60]. Any polycrystalline ceramic is composed of randomly oriented crystals, and the bulk properties are similar to those of crystallites. In the case of a ferroelectric ceramic, most of the crystallites, or specifically the domains, can be aligned by applying a strong DC field to become a piezoelectric ceramic. The more of the domains that are aligned, the higher is the piezoelectric effect. In the manufacture of piezoceramics, a suitable ferroelectric material is first fabricated into the desired shape and electrodes are applied. The piezoceramic element is then heated to an elevated temperature while in the presence of a

strong DC field. This polarizes the ceramic (aligns the molecular dipoles of the ceramic in the direction of the applied field) and provides it with piezoelectric properties. If DC voltages are externally applied, the ceramic responds with a mechanical deformation. Similarly, an AC field will cause the ceramic to alternate in size. In particular, the ceramic will have its own resonant frequencies at which it vibrates most easily, the value of which are determined by its composition, size and shape. If the ceramic is stimulated by an AC field at this frequency, it will oscillate with greater efficiency, converting electrical energy into mechanical (acoustical) energy [11].

Most commercially available ceramics (such as barium titanate and PZT) are based on the perovskite structure shown in Figure 3.4. The perovskite structure (ABO_3) is the simplest arrangement where the corner-sharing oxygen octahedra are linked together in a regular cubic array with smaller cations (Ti, Zr, Sn, Nb etc.) occupying the central octahedral B-site, and larger cations (Pb, Ba, Sr, Ca, Na etc.) filling the interstices between octahedra in the larger A-site [61].

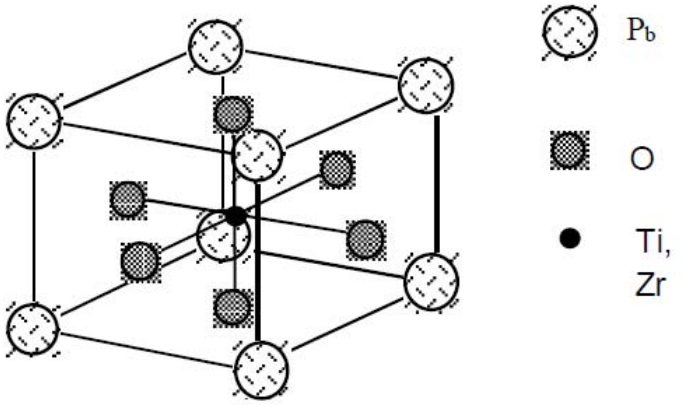

Figure 3.4: The Perovskite structure.

In materials such as PZT, each cell of the crystal lattice spontaneously polarizes along one of a series of allowed directions. This is due the positive and negative charge sites not coinciding, so the elementary cell has a built-in electric dipole, which maybe reversed or switched to certain allowed directions by the application of electric field. This

spontaneous polarisation disappears at a critical temperature (the Curie point). Above the Curie point, the structure is centrosymmetric, with positive and negative charge sites coinciding, so there are no dipoles present in the material (this is known as the paraelectric behavior). Such materials are termed as ferroelectric since this electrical behavior presents a physical analogy with magnetic behavior ferromagnetic materials [62]. The dipoles are not randomly oriented throughout the material. Neighbouring dipoles align with each other forming regions of local alignment known as Weiss domains. Within a Weiss domain, all the dipoles are aligned, giving a net dipole moment to the domain, and hence a net polarization (dipole moment per unit volume). The polarization direction between neighboring Weiss domain within a crystallite can differ by 90° or 180°, and owing to the random distribution of Weiss domains throughout the material, shown in Figure 3.5a, no overall polarization or piezoelectric effect is exhibited. The ceramic is made piezoelectric in any chosen direction by a poling treatment, which involves exposing it to a strong electric field (> 2000 V/mm) at a temperature slightly below the Curie point. In this field, the domains most nearly aligned with the field will grow at the expense of other domains, and the material will also lengthen in the direction of the field as shown in Figure 3.5b. When the field is removed, the dipoles remain locked in approximate alignment shown in Figure 3.5c, giving the ceramic material a remanent polarization and a permanent deformation making it anisotropic giving the material the piezoelectric properties. The poling treatment is usually the final treatment of PZT component manufacture [62].

3.2.1 Piezoelectric constants

Since piezoelectric ceramics are anisotropic, their physical constants are tensor quantities and relate to both the direction of the applied stress or electric field and to the directions

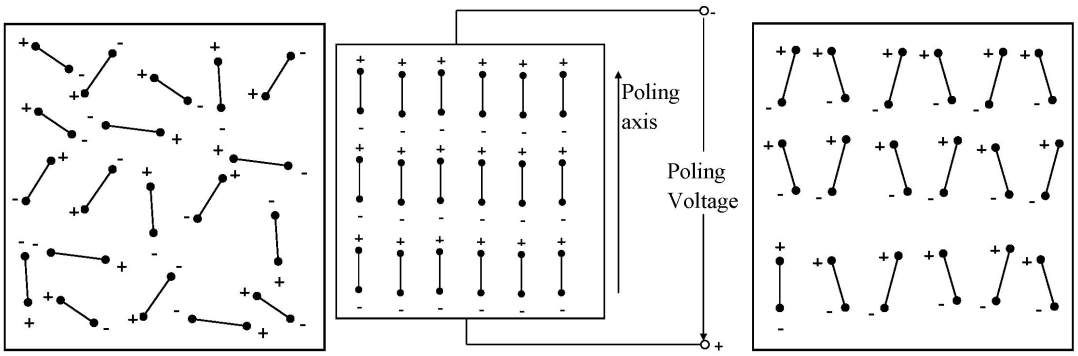

(a) before polarization (b) during polarization (c) after polarization

Figure 3.5: Electric dipole moments in Weiss domains.

perpendicular to these. For this reason, the constants are generally given two subscript indices which refer to the direction of the two related quantities. A superscript index is used to indicate the quantity that is kept constant.

The direction of positive polarization is usually chosen to coincide with the Z-axis of a rectangular system of crytalographic axes X, Y, Z. If the directions of X, Y, and Z are represented by 1, 2, and 3 respectively, the various constants maybe written with subscripts referring to these in Figure 3.6.

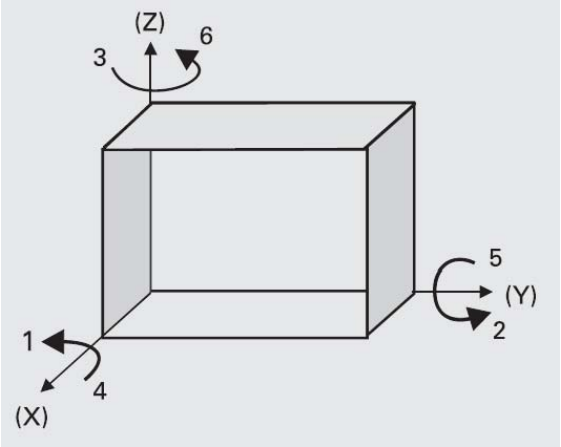

Figure 3.6: Designation of the axes for positive polarization of a piezoelectric material.

3.2.1.1 Permittivity

The permittivity (ε) or relative dielectric constant is a measure of polarizability of the material. The absolute permittivity (or dielectric constant) is defined as the electric displacement per unit electric field. The first subscript gives the direction of the dielectric displacement and the second gives the direction of the electric field. For example: ε_{11}^{T} is the permittivity for the dielectric displacement and electric field in the direction 1 under conditions of constant stress. ε_{33}^{S} is the permittivity for the dielectric displacement and electric field in direction 3 under conditions of constant strain [63].

3.2.1.2 Compliance

Compliance (s) or the elastic constant of a material is defined as the strain produced per unit stress. It is the reciprocal of the modulus of elasticity. The first subscript refers to the direction of the strain, and the second to the direction of the stress, for example: s_{11}^{E} is the compliance for a stress and accompanying strain in direction 1 under conditions of constant electric field. s_{36}^{D} is the compliance for a shear stress about axis 3 and accompanying strain in direction 3 under conditions of constant electric displacement [63].

3.2.1.3 Piezoelectric charge constant

Piezoelectric charge constant (d) is the electric polarization generated in a material per unit mechanical stress applied to it. Alternatively, it is the mechanical strain experienced by a material per unit electric field applied to it. The first subscript refers to the direction of polarization generated in the material (at $E = 0$) or to the applied field strength and the second refers respectively to the direction of the applied stress or to the direction

of induced strain. For example: d_{33} is the induced polarization per unit applied stress in direction 3. Alternatively, it is the induced strain per unit electric field in direction 3. d_{31} is the induced polarization in direction 3 per unit stress in applied direction 1. Alternatively, it is the mechanical strain induced in the material in direction 1 per unit electric field applied in direction 3 [63].

3.2.1.4 Piezoelectric voltage constant

Piezoelectric voltage constant (g) is defined as the electric field generated in a material per unit mechanical stress applied to it. Alternatively, it is the mechanical strain experienced by a material per unit electric displacement applied to it. The first subscript refers to the direction of electric field generated in the material or to the applied electric displacement and the second refers respectively to the direction of applied stress or to the direction of the induced strain. For example: g_{31} is the induced electric field in direction 3 per unit stress applied in direction 1. Alternatively, it is the mechanical strain induced in the material in direction 1 per unit electric displacement applied in direction 3. g_{15} is the induced electric field in direction 1 per unit shear stress applied about axis direction 2. Alternatively, it is the shear strain induced in the material about axis 2 per unit electric displacement applied in direction 1 [64].

3.2.2 Piezoelectric relations

The electrical behavior of an unstressed medium under the influence of an electric field is defined by the electric field strength, E and the dielectric displacement, D. Their

relationship is shown in Equation 3.1.

$$D = \varepsilon E \tag{3.1}$$

in which ε is the permittivity of the medium. The mechanical behavior of the same medium at zero electric field strength is defined by two mechanical quantities namely; the stress applied, T and the strain, S. The relationship is in Equation 3.2.

$$S = sT \tag{3.2}$$

Where, s denotes the elastic compliance of the medium [64].

Piezoelectricity involves the interaction between the electrical and the mechanical behavior of the medium. This interaction can be closely approximated by linear relations (Equation 3.3) between electrical and mechanical variables [11].

$$\left.\begin{aligned} S &= s^E T + dE \\ D &= dT + \varepsilon^T E \end{aligned}\right\} \tag{3.3}$$

3.2.3 Vibration modes of a piezoelectric ring

Considering the ring shown in Figure 3.7, there are three possible fundamental modes of vibrations in a piezoelectric ring when an electric field parallel to the poling direction is applied [65].

1. The thickness (axial) mode vibration occurs when the applied frequency is coincident with the thickness resonant frequency, f_{r-t} which induces a change in thickness, $\Delta\tau_r$ with τ_r being the thickness. $\tau_r \pm \Delta\tau_r$.

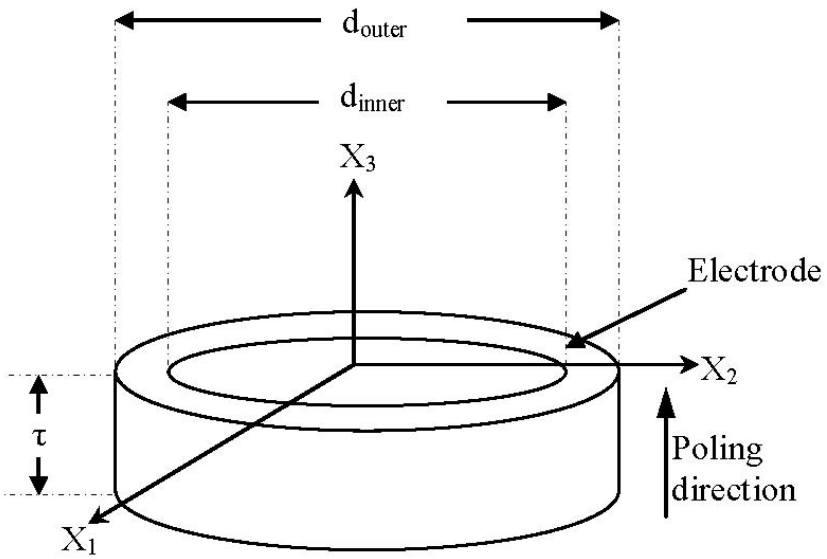

Figure 3.7: Schematic diagram of a piezoceramic ring.

2. The radial mode vibration occurs when the applied frequency is coincident with the radial resonant frequency, f_{r-r} which induces a change in the mean diameter, Δd_{mr} such that $d_{mr} \pm \Delta d_{mr}$. The radial mode always appears as the lowest frequency as the diameter is the largest dimension.

3. The wall thickness mode f_{r-w} occurs when the frequency is coincident with the resonant frequency along the wall thickness direction, causing a change in the wall thickness, Δw_r such that $w_r \pm \Delta w_r$ [66].

The thickness resonant frequency, f_{r-t}, radial resonant frequency, f_{r-r} and wall thickness resonant frequency, f_{r-w} are given in Equations 3.4, 3.5 and 3.6 respectively.

$$f_{r-t} = \frac{1}{2\tau_r \sqrt{\rho . s_{33}^D}} \tag{3.4}$$

$$f_{r-r} = \frac{1}{\pi d_{mr} \sqrt{\rho . s_{11}^E}} \tag{3.5}$$

$$f_{r-w} = \frac{1}{2w_r\sqrt{\rho.s_{11}^E}} \tag{3.6}$$

Where, $d_{mr} = (d_{outer} + d_{inner})/2$ is the mean diameter, $w_r = (d_{outer} - d_{inner})/2$ is the mean wall thickness, ρ is the density, τ_r is the thickness of the ring, s_{11}^E is the elastic compliance at constant electric field and s_{33}^D is the elastic compliance at constant charge density [67].

The radial mode vibration has three vibrations modes.

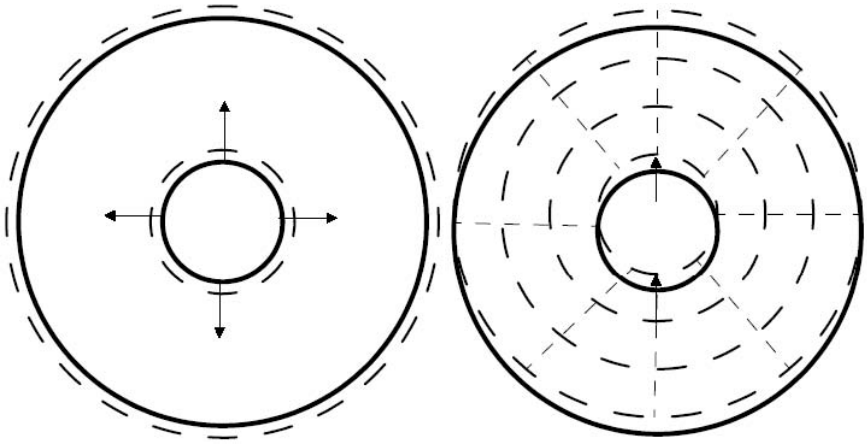

(a) (R,1) MODE (b) (1,1) MODE

Figure 3.8: Radial vibration modes of a piezoceramic ring.

Figure 3.8a is the first radial mode vibrating in its direction symmetrically, called the (R,1) mode and Figure 3.8b is one of the non-axisymmetric modes vibrating in its radial direction asymmetrically, called the (1,1) mode. A non-axisymmetric mode has an orthogonal mode with the same form as the degenerated mode as shown in Figures 3.9a and 3.9b.

When the degenerated modes are excited by two electric signals with a phase difference of 90° as shown in Figure 3.9c, a mode rotation occurs at the inner and outer circumference of the annular plate [16].

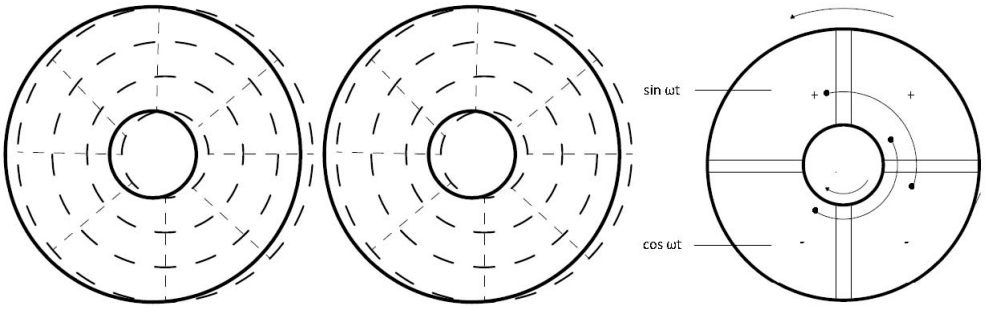

(a) (1,1) MODE (b) (1,1)' MODE (c) (1,1)-(1,1)' MODE

Figure 3.9: Degenerated modes of non-axisymmetric mode.

3.2.4 Analytical Modeling of a Piezoelectric Ring

Radmanovic et al [68] considered a piezoceramic ring polarized across the thickness (that is parallel to the z-axis), with an outer radius a, inner radius b, and thickness $2h$, and with completely metalized circularringed (plane) surfaces supplied with alternating excitation voltage. The set of constitutive piezoelectric equations used presents tensors of mechanical stresses (T) and an electric field (E) inside the material in function of the tensor of relative mechanical deformations (dilatations) (S) and dielectric displacement (D). In the case of the piezoceramic ring in Figure 3.10, components of the electric field E_r and E_θ are equal to zero on two plane surfaces, because they were metalized.

The following assumptions were made [69]:

1. Coordinate axes r and z are directions of pure (uncoupled) modes of wave propagation, with mechanical displacements in the radial and thickness direction $u_r = u_r(r,t)$ and $u_z = u_z(z,t)$.

2. Components of the electric field E_r and E_θ are negligible (equal to zero) everywhere inside the material.

3. Due to axial symmetry, only symmetric (radial and thickness) modes of oscillation

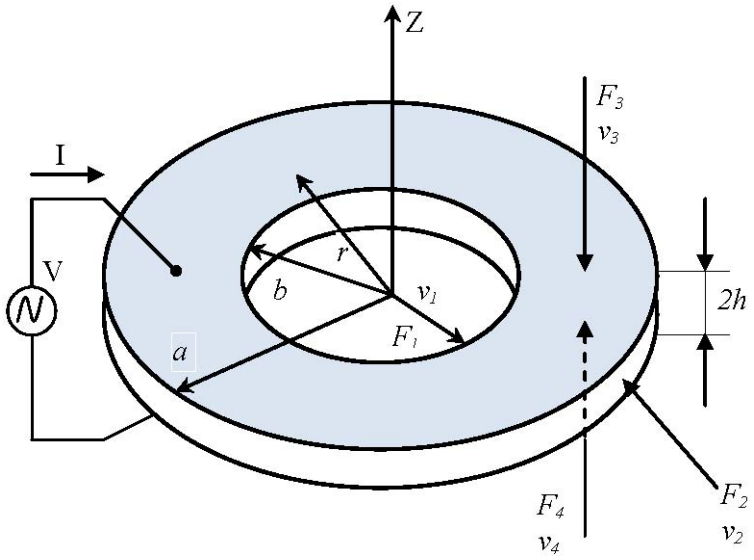

Figure 3.10: Loaded piezoceramic ring

are excited.

4. The waves are harmonic ($D_z = D_0 \mathbf{e}^{j\omega t}$)

Every ring surface was loaded with acoustic impedance Z_i, where v_i and F_i are velocities and forces on those contour surfaces $P_i (i = 1, 2, 3, 4)$. The set of constitutive equations which described the oscillation of a piezoceramic ring, in a polar-cylindrical coordinate system is [70]

$$\left.\begin{aligned} T_{rr} &= c_{11}^D S_{rr} + c_{12}^D S_{\theta\theta} + c_{13}^D S_{zz} - h_{31} D_z \\ T_{\theta\theta} &= c_{12}^D S_{rr} + c_{11}^D S_{\theta\theta} + c_{33}^D S_{zz} - h_{31} D_z \\ T_{zz} &= c_{13}^D S_{rr} + c_{13}^D S_{\theta\theta} + c_{33}^D S_{zz} - h_{33} D_z \\ E_z &= -h_{31} S_{rr} - h_{31} S_{\theta\theta} - h_{33} S_{zz} + D_z / \epsilon_{33}^s \end{aligned}\right\} \tag{3.7}$$

Where, c_{ij}^D are the coefficients of the elastic constant tensor; ϵ_{33}^s is the dielectric constant of the ring in a compressed state; h_{ij} are elements of the piezoelectric constant tensor $(i, j = 1, 2, 3)$.

Relations between components of the relative deformations tensor (S) and mechanical displacement vector (u) are expresed in Equation 3.8 [69]:

$$(S_{pq} = 0, \text{if } p \neq q) : S_{rr} = \partial u_r/\partial r, S_{\theta\theta} = u_r/r, S_{zz} = \partial u_z/\partial z \tag{3.8}$$

In addition, the partial differential equations that describe the oscillations of a piezoceramic ring in radial and thickness directions given in Equation 3.9:

$$\left.\begin{aligned} \frac{\partial T_{rr}}{\partial r} + \frac{T_{rr} - T_{\theta\theta}}{r} &= \rho \frac{\partial^2 u_r}{\partial t^2} \\ \frac{\partial T_{ss}}{\partial z} &= \rho \frac{\partial^2 u_z}{\partial t^2} \end{aligned}\right\} \tag{3.9}$$

By substituting Equation 3.7 in Equation 3.9, the equations of oscillation in radial and thickness direction take the following form.

$$\left.\begin{aligned} c_{11}^D \left(\frac{\partial^2 u_r}{\partial r} + \frac{1}{r}\frac{\partial u_r}{\partial r} - \frac{u_r}{r^2} \right) &= \rho \frac{\partial^2 u_r}{\partial t^2} \\ c_{33}^D \frac{\partial^2 u_z}{\partial z^2} &= \rho \frac{\partial^2 u_z}{\partial t^2} \end{aligned}\right\} \tag{3.10}$$

On assumption that the waves were harmonic, components of the mechanical displacement in the radial and thickness direction are solutions of Equation 3.10 and they are presented through two orthogonal wave functions:

$$\left.\begin{aligned} u_r &= [AJ_1(k_r, r) + BY_1(k_r, r)]\mathbf{e}^{j\omega t} \\ u_z &= [C\sin(k_z, z) + D\cos(k_z, z)]\mathbf{e}^{j\omega t} \end{aligned}\right\} \tag{3.11}$$

Where, $k_r = \omega/V_r$, $k_z = \omega/V_z$, $V_r = \sqrt{c_{11}^D/\rho}$ and $V_z = \sqrt{c_{33}^D/\rho}$ are wave (characteristic, eigenvalue) numbers and phase velocities of two uncoupled waves in the radial and

thickness direction, respectively; ω is angular frequency; ρ is density of the piezoceramic; J_1 and Y_1 are Bessel functions of the first and the second kind respectively. A, B, C, and D are constants [71]. Assuming that the outer surfaces are in contact with external media and and there is continuity of the velocities on these surfaces ($\dot{u}_i = \partial u/\partial t$):

$$\left.\begin{aligned} \dot{u}_r(a_1) &= v_1 \mathbf{e}^{j\omega t}; & \dot{u}_r(a_2) &= -v_2 \mathbf{e}^{j\omega t}; \\ \dot{u}_z(b) &= -v_3 \mathbf{e}^{j\omega t}; & \dot{u}_z(-b) &= v_4 \mathbf{e}^{j\omega t}. \end{aligned}\right\} \tag{3.12}$$

Obtaining:

$$\left.\begin{aligned} A &= A_1 v_1 + A_2 v_2; & B &= B_1 v_1 + B_2 v_2; \\ C &= -\frac{v_3 + v_4}{2j\omega \sin(k_z b)}; & D &= \frac{v_4 - v_3}{2j\omega \cos(k_z b)}. \end{aligned}\right\} \tag{3.13}$$

where:

$$\left.\begin{aligned} A_1 &= \frac{Y_1(k_r a_2)}{j\omega[J_1(k_r a_1)Y_1(k_r a_2) - J_1(k_r a_2)Y_1(k_r a_1)]}; \\ A_2 &= \frac{Y_1(k_r a_1)}{j\omega[J_1(k_r a_1)Y_1 k_r a_2 - J_1(k_r a_2)Y_1(k_r a_1)]}; \\ B_1 &= \frac{J_1(k_r a_2)}{j\omega[J_1(k_r a_2)Y_1 k_r a_1 - J_1(k_r a_1)Y_1(k_r a_2)]}; \\ B_2 &= \frac{J_1(k_r a_1)}{j\omega[J_1(k_r a_2)Y_1 k_r a_1 - J_1(k_r a_1)Y_1(k_r a_2)]}. \end{aligned}\right\} \tag{3.14}$$

The external behavior of the element was computed imposing the continuity between the stresses and the forces on its surfaces in an integral form [72]:

$$\left.\begin{aligned} \int_{\sigma_1} T_{rr}(a_1) d\sigma &= -F_1; & \int_{\sigma_2} T_{rr}(a_2) d\sigma &= -F_2; \\ \int_{\sigma_3} T_{zz}(b) d\sigma &= -F_3; & \int_{\sigma_4} T_{zz}(-b) d\sigma &= -F_4; \end{aligned}\right\} \tag{3.15}$$

3.2.5 Radial vibration of a piezoceramic ring

Axisymmetric radial vibration can be set up in a thin ceramic ring with radial poling and electrodes connected on its inner and outer surfaces [73,74] as shown in Figure 3.11.

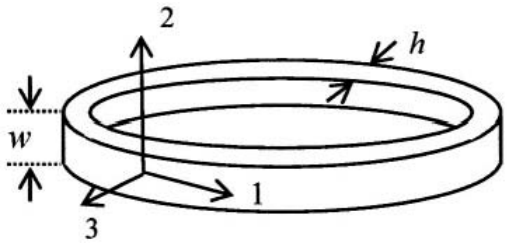

Figure 3.11: A piezoceramic ring with radial poling.

Taking R, w and h as the mean radius, width and thickness of the ring respectively and making the assumption that $R >> w >> h$, then in cylindrical coordinates and using the boundary conditions, Equations 3.16 are approximated as true throughout the ring:

$$\left.\begin{aligned} &T_{ii} \neq 0, \\ &T_{ij} = 0 \text{ for } i \neq j \\ &E_\theta = E_z = 0 \end{aligned}\right\} \tag{3.16}$$

Let (θ, z, r) correspond to $(1, 2, 3)$. The radial electric field and the tangential strain are given by

$$\left.\begin{aligned} S_{11} = S_{\theta\theta} &= \frac{u_r}{R}, \\ E_3 = E_r &= -\frac{V}{h}. \end{aligned}\right\} \tag{3.17}$$

The relevant constitutive relations are

$$\left.\begin{aligned} S_{11} = S_{\theta\theta} = s_{11}T_{\theta\theta} + d_{31}E_r, \\ D_3 = D_r = d_{31}T_{\theta\theta} + \epsilon_{33}E_r, \end{aligned}\right\} \tag{3.18}$$

which on solving give

$$\left.\begin{aligned} T_{\theta\theta} = \frac{1}{s_{11}}\frac{u_r}{R} - \frac{d_{31}}{s_{11}}E_r, \\ D_r = \frac{d_{31}}{s_{11}}\frac{u_r}{R} + \bar{\epsilon}_{33}E_r, \end{aligned}\right\} \tag{3.19}$$

where

$$\bar{\epsilon}_{33} = \epsilon_{33} - d_{31}^2/s_{11} \tag{3.20}$$

The equation of motion takes the following form [75]

$$-\frac{T_{\theta\theta}}{R} = \rho\ddot{u}_r \tag{3.21}$$

Substitution of Equation 3.19 into Equation 3.21 yields

$$-\frac{1}{s_{11}}\frac{u_r}{R^2} + \frac{d_{31}}{s_{11}R}E_r = \rho\ddot{u}_r \tag{3.22}$$

substituting Equation 3.17 in Equation 3.22 gives

$$-\frac{1}{s_{11}}\frac{u_r}{R^2} - \frac{d_{31}}{s_{11}R}\frac{V}{h} = \rho\ddot{u}_r \tag{3.23}$$

which can be written in the form

$$\rho\ddot{u}_r + \frac{1}{s_{11}R^2}u_r = -\frac{d_{31}}{s_{11}R}\frac{V}{h} \tag{3.24}$$

Equation 3.24 can be compared with the differential equation of a spring-mass system (Equation 3.25) with a forcing function, F [76].

$$\left.\begin{aligned} m\ddot{x} + kx &= F \\ \text{whose natural frequency, } \omega^2 &= \frac{k}{m} \end{aligned}\right\} \tag{3.25}$$

Similarly, the natural frequency of vibration of the piezoceramic ring is given by [74],

$$\omega^2 = \frac{1}{\rho s_{11}R^2}. \tag{3.26}$$

which gives

$$\omega = \sqrt{\frac{1}{\rho s_{11}R^2}} \tag{3.27}$$

3.3 Analysis of Axisymmetric Waves in an Infinitely Long Hollow Cylinder

A traveling wave propagating along an infinitely long hollow cylinder can be analyzed in the Pochhammer and Chree manner [77]. Neglecting the propagating attenuation, the equation of motion for an isotropic elastic medium is

$$\left.\begin{aligned} \rho\frac{\partial^2\mathbf{U}}{\partial t^2} &= (\lambda+\mu)\text{grad div } \mathbf{U} + \mu(\text{grad div } \mathbf{U} \text{ - rot rot } \mathbf{U}) \\ &= (\lambda+\mu)\nabla\nabla.\mathbf{U} + \mu\nabla^2\mathbf{U}, \end{aligned}\right\} \tag{3.28}$$

with

$$U = \mathbf{U}_1 + \mathbf{U}_2 + \mathbf{U}_3, \tag{3.29}$$

$$\mathbf{U}_1 = \text{grad } \phi, \mathbf{U}_2 = \text{rot } \mathbf{L}, \mathbf{U}_3 = \text{rot rot } \mathbf{L} \tag{3.30}$$

where ϕ is a scalar potential and L is a vector potential given in the form,

$$A = (0, 0, \psi), \tag{3.31}$$

and λ and μ, ρ and ψ are Lame's elastic constants, density and the z-coordinate respectively.

The displacement vector $\mathbf{U}_2$ is not relevant in this analysis since it represents non-axisymmetric shear horizontal (**SH**) waves, which are independent from $\mathbf{U}_1$ and $\mathbf{U}_3$.

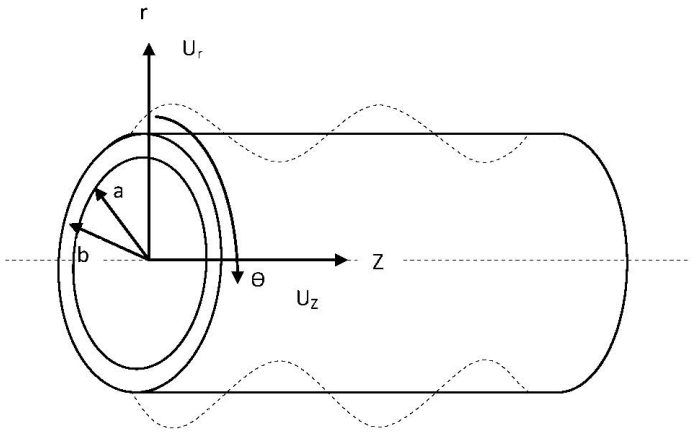

Figure 3.12: Reference coordinates and dimensions.

In the cylindrical coordinates shown in Figure 3.12, individual components of displacement vectors $\mathbf{U}_1$ and $\mathbf{U}_3$ can be described as

$$\mathbf{U}_1 : \mathrm{u}_r = \frac{\partial \phi}{\partial r}, \quad \mathrm{u}_\theta = \frac{\partial \phi}{r \partial \theta}, \quad \mathrm{u}_z = \frac{\partial \phi}{\partial z} \tag{3.32}$$

$$\mathbf{U}_3 : \mathrm{u}_r = \frac{\partial^2 \psi}{\partial r \partial z}, \quad \mathrm{u}_\theta = \frac{\partial^2 \psi}{r \partial r \partial \theta}, \quad \mathrm{u}_z = -(\frac{\partial^2 \psi}{\partial r^2} + \frac{1}{r}\frac{\partial \psi}{\partial r} + \frac{1}{r^2}\frac{\partial^2 \psi}{\partial \theta^2}) \tag{3.33}$$

Substituting Equations 3.32 and 3.33 into Equation 3.28 yields

$$\frac{\partial^2 \phi}{\partial r^2} + \frac{1}{r}\frac{\partial \phi}{\partial r} + \frac{\partial^2 \phi}{\partial z^2} = \frac{1}{\mathrm{C}^2{}_d}\frac{\partial^2 \phi}{\partial t^2} \tag{3.34}$$

$$\frac{\partial^2 \psi}{\partial r^2} + \frac{1}{r}\frac{\partial \psi}{\partial r} + \frac{\partial^2 \psi}{\partial z^2} = \frac{1}{\mathrm{C}^2{}_t}\frac{\partial^2 \psi}{\partial t^2} \tag{3.35}$$

The solutions for the above equations for axisymmetric harmonic waves, for a wave propagating in the z-axis direction at an angular frequency ω can be expressed in the forms

$$\phi = \phi_0(r) \exp(-j\mathrm{k}_0 z) \exp(j\omega t), \tag{3.36}$$

$$\psi = \psi_0(r) \exp(-j\mathrm{k}_0 z) \exp(j\omega t), \tag{3.37}$$

Where, k_0 is the wave number. Taking C_d and C_t as the sound speeds for dilatational and transverse waves respectively, then [20],

$$\mathrm{C}_d = \sqrt{\frac{\lambda + 2\mu}{\rho}} \qquad \text{and} \qquad \mathrm{C}_t = \sqrt{\frac{\mu}{\rho}} \tag{3.38}$$

Functions $\phi_0(r)$ and $\psi_0(r)$ are solutions for the equations

$$\frac{\partial^2\phi_0}{\partial r^2} + \frac{1}{r}\frac{\partial\phi_0}{\partial r} + k_d^2\phi_0 = 0 \tag{3.39}$$

and

$$\frac{\partial^2\psi_0}{\partial r^2} + \frac{1}{r}\frac{\partial\psi_0}{\partial r} + k_t^2\psi_0 = 0, \tag{3.40}$$

where

$$k_d^2 = (\omega/C_d)^2 - k_0^2 \qquad \text{and} \qquad k_t^2 = (\omega/C_t)^2 - k_0^2 \tag{3.41}$$

The general solutions for equations 3.39 and 3.40 are expressed in terms of Bessel functions as

$$\phi_0 = AJ_0(k_d r) + BY_0(K_d r) \tag{3.42}$$

and

$$\psi_0 = CJ_0(k_t r) + DY_0(K_t r) \tag{3.43}$$

where A, B, $C$and D are arbitrary real constants. Displacements u_r and u_z are respectively given by

$$u_r = \frac{\partial\phi}{\partial r} + \frac{\partial^2\psi}{\partial r\partial z} \tag{3.44}$$

and

$$u_z = \frac{\partial \phi}{\partial z} - \frac{\partial^2 \psi}{\partial r^2} - \frac{1}{r}\frac{\partial \psi}{\partial r} \tag{3.45}$$

For traction-free boundary conditions (free motion), the stresses must vanish on the inner and outer surfaces of the hollow-cylinder [78], i.e.,

$$T_{rr} = 0 \quad \text{and} \quad T_{zr} = 0 \quad \text{at} \quad r = b \quad \text{and} \quad r = a, \tag{3.46}$$

where T_{rr} and T_{zr} are stress components obtained from

$$\left.\begin{aligned} T_{rr} &= \lambda(\frac{\partial u_r}{\partial r} + \frac{u_r}{r} + 2\mu\frac{\partial u_z}{\partial z}) \\ &= 2(\lambda+\mu)((1-\sigma)\frac{\partial u_r}{\partial r} + \sigma\frac{u_r}{r} + \sigma\frac{\partial u_z}{\partial z}) \end{aligned}\right\} \tag{3.47}$$

and

$$T_{rz} = \mu(\frac{\partial u_r}{\partial z} + \frac{\partial u_z}{\partial z}) \tag{3.48}$$

where γ is the Poisson's ratio for the medium, expressed in terms of Lame's constants as

$$\sigma = \lambda/[2(\lambda+\mu)]. \tag{3.49}$$

Actual conditions on the inside surface of $r = a$ are evidently not traction free, due to the presence of powder, which should be fed forward. However, it is fairly light in normal usage, thus the assumption above is allowed in order to find the vibrational behaviour regarding elliptic particle motion. With these boundary conditions, Equations 3.42 and

3.43 yield the characteristic equations expressed in the matrix representation [20].

$$\begin{pmatrix} C_{11} & C_{12} & C_{13} & C_{14} \\ C_{21} & C_{22} & C_{23} & C_{24} \\ C_{31} & C_{32} & C_{33} & C_{34} \\ C_{41} & C_{42} & C_{43} & C_{44} \end{pmatrix} \begin{pmatrix} A \\ B \\ C \\ D \end{pmatrix} = C \begin{pmatrix} A \\ B \\ C \\ D \end{pmatrix} = \begin{pmatrix} 0 \\ 0 \\ 0 \\ 0 \end{pmatrix} \tag{3.50}$$

The components for the matrix are given as follows:

$$\left.\begin{aligned} C_{11} &= (-1/2)(\beta^2 - K^2)J_0(\alpha) + \alpha J_1(\alpha), \\ C_{12} &= (-1/2)(\beta^2 - K^2)Y_0(\alpha) + \alpha Y_1(\alpha), \\ C_{13} &= jk_0[\beta^2 J_0(\beta) - \beta J_1(\beta)], \\ C_{14} &= jk_0[\beta^2 Y_0(\beta) - \beta Y_1(\beta)], \\ C_{21} &= j2k_0k_a J_1(\alpha), \qquad C_{22} = j2k_0k_a Y_1(\alpha), \\ C_{23} &= (k_0^2k_t - k_t^3)J_1(\beta)), \qquad C_{24} = (k_0^2k_t - k_t^3)Y_1(\beta) \\ C_{31} &= (-1/2)[(\beta p)^2 - (Kp)^2]J_0(\alpha p) + (\alpha p)J_1(\alpha p), \\ C_{32} &= (-1/2)[(\beta p)^2 - (Kp)^2]Y_0(\alpha p) + (\alpha p)Y_1(\alpha p), \\ C_{33} &= jk_0[(\beta p)^2 J_0(\beta p) - (\beta p)J_1(\beta p)], \\ C_{34} &= jk_0[(\beta p)^2 Y_0(\beta p) - (\beta p)Y_1(\beta p)], \\ C_{41} &= j2k_0k_a J_1(\alpha p), \qquad C_{42} = j2k_0k_a Y_1(\alpha p), \\ C_{43} &= (k_0^2k_t - k_t^3)J_1(\beta p), \qquad C_{24} = (k_0^2k_t - k_t^3)Y_1(\beta p) \end{aligned}\right\} \tag{3.51}$$

where

$$\alpha = k_d b, \quad \beta = k_t b, \quad K = k_0 b, \quad \text{and the ratio} \quad p = a/b$$

Defining the normalized angular frequency,

$$\Omega = (\omega b/C_d), \tag{3.52}$$

then from Equation 3.41,

$$\alpha^2 = \Omega^2 - K^2 \qquad \text{and} \qquad \beta^2 = (C_d/C_t)^2\Omega^2 - K^2 \tag{3.53}$$

Since λ and μ can be written in terms of Young's Modulus, E and Poisson's ratio, γ as

$$\lambda + 2\mu = \frac{(1-\sigma)E}{(1-2\sigma)(1+\sigma)}, \qquad \mu = \frac{E}{2(1+\sigma)} \tag{3.54}$$

the ratio C_d/C_t is derived from Equation 3.38 as

$$\frac{C_d}{C_t} = \left(\sqrt{\frac{\lambda+2\mu}{\rho}} \Big/ \sqrt{\frac{\mu}{\rho}}\right) = \sqrt{\frac{2(1-\sigma)}{1-2\sigma}} \tag{3.55}$$

In order for Equation 3.50 to have a set of nontrivial solutions, the determinant of matrix C must be zero. Therefore, the elliptic particle motion can accordingly be obtained from Equations 3.44 and 3.45, as

$$\left.\begin{aligned} u_r &= A\{-k_a J_1(\alpha X) - k_d(B/A)Y_1(\alpha X) + jk_0k_t[(C/A)J_1(\beta X) \\ &\quad + (D/A)Y_1(\beta X)]\}\exp[j(\omega t - k_0 z)] \\ &\equiv (u_{rR} + ju_{rI})\exp[j(\omega t - k_0 z)] \end{aligned}\right\} \tag{3.56}$$

and

$$\left.\begin{aligned} u_z &= A\{-jk_0[J_0(\alpha X) + (B/A)Y_1(\alpha X)] + k_t^2[(C/A)J_0(\beta X) \\ &\quad + (D/A)Y_0(\beta X)]\}\exp[j(\omega t - k_0 z)] \\ &\equiv (u_{zR} + ju_{zI})\exp[j(\omega t - k_0 z)], \end{aligned}\right\} \tag{3.57}$$

where A, B, C and D are the solutions given by Equation 3.50, and X is the normalized radius, that is, the coordinate r divided by the outer radius of the cylinder b. The real parts of u_r and u_z are given by

$$\Re[u_r] = u_{rR}\cos(\omega t - k_0 z) - u_{rI}\sin(\omega t - k_0 z) \tag{3.58}$$

and

$$\Re[u_z] = u_{zR}\cos(\omega t - k_0 z) - u_{zI}\sin(\omega t - k_0 z) \tag{3.59}$$

The locus of a particle is obtained by eliminating the terms $(\omega t - k_0 z)$ from the above equations. When both α and β are real, the terms u_{rI} and u_{zR} vanish and the locus equation is

$$\left(\frac{\Re[u_r]}{u_{rR}}\right)^2 + \left(\frac{\Re[u_z]}{u_{zI}}\right)^2 = 1 \tag{3.60}$$

Hence Equation 3.60 shows that the elliptic motion can be realized by a traveling wave [20].

3.4 Particle manipulation by the traveling wave

A body subjected to an acoustic wave field, experiences a steady force called acoustic radiation pressure and a time varying force caused by the periodic variation of the pressure in the surrounding fluid. The radiation pressure is always repulsive meaning that it is directed as the wave vector while the time varying force oscillates at the frequency of the acoustic wave and its time average is equal to zero. The radiation pressure F_R exerted on a rigid spherical particle by a plane progressive wave is derived as [79]:

$$F_R = \frac{64\pi^5 d^6}{\lambda^4} \bar{E} F(\rho_\circ/\rho_1) \tag{3.61}$$

where

d = Particle diameter,

λ = wavelength of the acoustic wave,

$\bar{E}$ = acoustic energy density.

The parameter $F(\rho_\circ/\rho_1)$ is called relative density factor being given by:

$$F(\rho_\circ/\rho_1) = \frac{1 + \frac{2}{9}(1 - \rho_\circ/\rho_1)^2}{(2 + \rho_\circ/\rho_1)^2} \tag{3.62}$$

where $\rho_\circ$ and ρ_1 are air and particle density, respectively. For most solids, $\rho_\circ/\rho_1 << 1$ implying that $F(\rho_\circ/\rho_1) = 0.305$. For a plane progressive acoustic wave, energy density is [80].

$$\bar{E} = \frac{p_s^2}{\rho_\circ c^2} \tag{3.63}$$

where

p_s = sound pressure $[N/m^2]$,

c = the speed of propagation of the acoustic wave $[m/s]$

Sound pressure can be estimated according to the formula which defines the sound pressure level, SPL [81]:

$$SPL = 20 \log_{10} \frac{p_s}{p_{ref}} \tag{3.64}$$

where $p_{ref} = 2 \times 10^{-5} N/m^2$ is the standard reference pressure. Sound pressure level (SPL) is expressed in dB and can be experimentally measured by using sound level meters.

King [79], as an intermediate result, obtained the velocity of a spherical particle placed in an acoustic wave field as:

$$\frac{dr}{dt} = -\frac{A_1}{\alpha^3} k_\circ \frac{\rho_\circ}{\rho_1} \frac{1}{F_1 - iG_1} \tag{3.65}$$

where $k_\circ = w/c$, $\alpha = k_\circ d/2$ where w is the angular frequency of the acoustic wave. If $\rho_\circ/\rho_1 << 1$ and $\alpha << 1$ then $F_1(\alpha) \simeq 2/\alpha^3$ and $G_1 \simeq 1/3$. The quantity A_1 is a measure of wave intensity given by $|A_1| = 3cv/w$. Therefore, for a plane progressive acoustic wave, the amplitude of the acoustic oscillating force exerted on the particle may be written as [82]:

$$F_A = |M \frac{d^2 r}{dt^2}| = \frac{wM|A_1|}{\alpha^3} k_\circ \frac{\rho_\circ}{\rho_1} \frac{1}{F_1 - iG_1} \tag{3.66}$$

where M is the mass of the particles in Kg and $|A_1|$ is $3cv/\omega$. Taking into account

expressions for F_1, G_1, $|A_1|$, α and $k_\circ$, written above, Equation 3.66 becomes:

$$F_A = 2wMv\frac{\rho_\circ}{\rho_1} \tag{3.67}$$

The quantity v represents the amplitude of the velocity of the surrounding fluid particles (air in this case), which are oscillating due to the acoustic wave, and is related to the sound pressure by the relation:

$$v = \frac{\sqrt{2}p_s}{\rho_\circ c} \tag{3.68}$$

Considering $\rho_\circ/\rho_1 << 1$ and $\alpha << 1$, the amplitude of the oscillating force becomes

$$F_A = \frac{2\sqrt{2}wMp_s}{\rho_1 c} \tag{3.69}$$

Consequently, the Total force, F is given by;

$$F = F_R + F_A \tag{3.70}$$

The acoustic radiation pressure F_R is several order of magnitude less than that of oscillating force amplitude F_A and can therefore be neglected [82]. Hence

$$F \approx F_A \tag{3.71}$$

CHAPTER FOUR

4.0 METHODOLOGY

In this chapter, the procedure of carrying out research is detailed.

4.1 Introduction

The model of the powder transport system is shown in Figure 4.1.

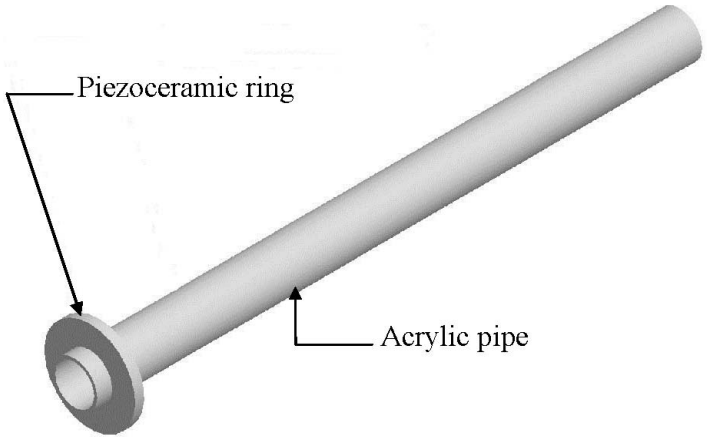

Figure 4.1: The powder transport prototype.

The ANSYS 12.0 Finite Element Analysis software was used for modeling purposes. First, the modal analysis was done in order to determine the vibration characteristics (natural frequencies and mode shapes) of the structure during free vibrations. The normal modes of the system are the shapes where all parts of the system move sinusoidally with the same frequency (natural frequency) and in phase. Thereafter, the harmonic analysis was carried out in order to determine the steady-state response of the structure to loads that vary sinusoidally (harmonically) with time. Harmonic analysis calculates the response of the system to cyclic loads over a frequency range (a sine sweep) and

obtains a graph of displacements versus frequency. During this analysis, the following parameters were varied as illustrated in Figure 4.2:

1. The offset position of placing the transducer on the acrylic pipe.
2. The length of the acrylic pipe.
3. The inner and outer diameter of the pipe.

These parameters were varied as compared to the trial device that had been developed [18].

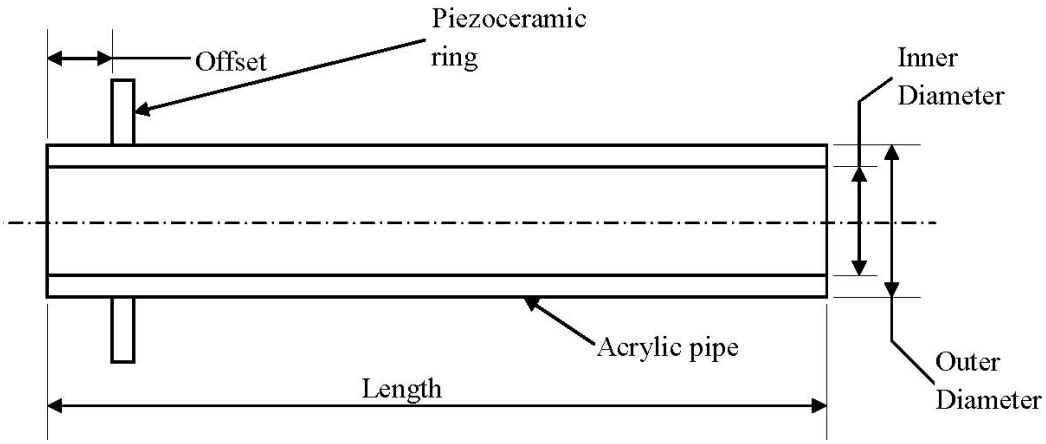

Figure 4.2: Various parameters considered during optimization.

The prototype was then built in order to verify the modeling results with the schematic diagram shown in Figure 4.3.

4.2 Modeling

Harmonic analysis of the whole model was done by varying the parameters. The engineering materials used were selected from the ANSYS library, but for acrylic, the material properties were input and saved into the ANSYS library as follows:

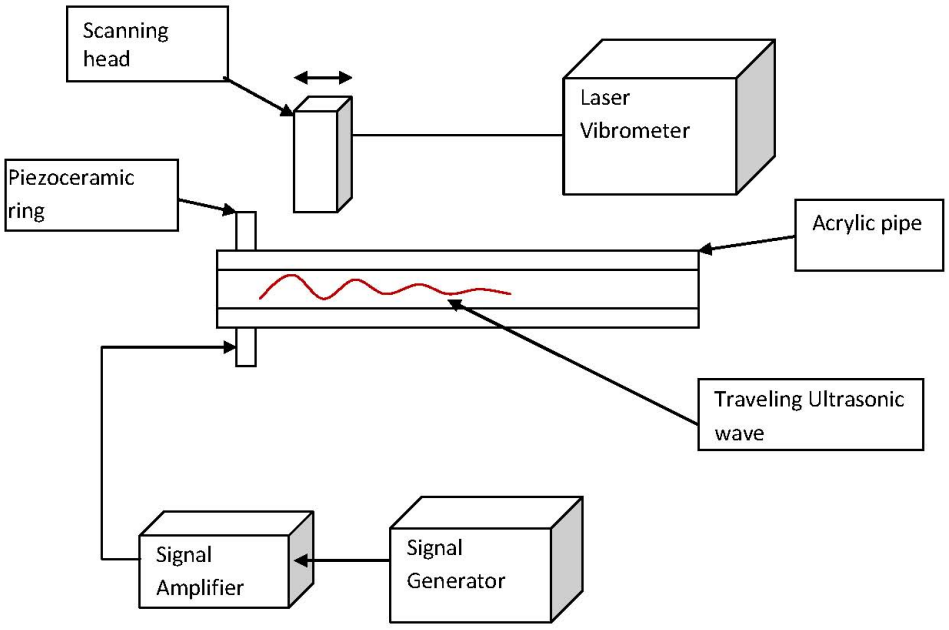

Figure 4.3: Schematic diagram for the experimental set-up.

(a) Density = 1.18×10^3 kg/m^3.

(b) Young's modulus = 3.3×10^9 Pa.

(c) Poisson's ratio = 0.43

The geometry was then drawn, saved as two different solids, and all the parameters were named. Consequently the model was then set up for analysis. In the geometry cell, the two solids were assigned to their respective materials. However, the material properties for the piezoceramic ring were given as commands after converting the properties provided by the manufacturer to ANSYS format as explained in Appendix **B**. Thenceforth, the piezoceramic ring and the acrylic pipe were bonded and then meshed. The model was first freely meshed, and then refined as shown in Figures 4.4a and 4.4b respectively. The next stage of the analysis involved naming of the faces of the model in order to use them as the electrodes as illustrated in Figure 4.5. The faces were named as `PIE1` and `PIE2` whereas the whole piezoceramic ring was named as `PIEZO`. The naming of the

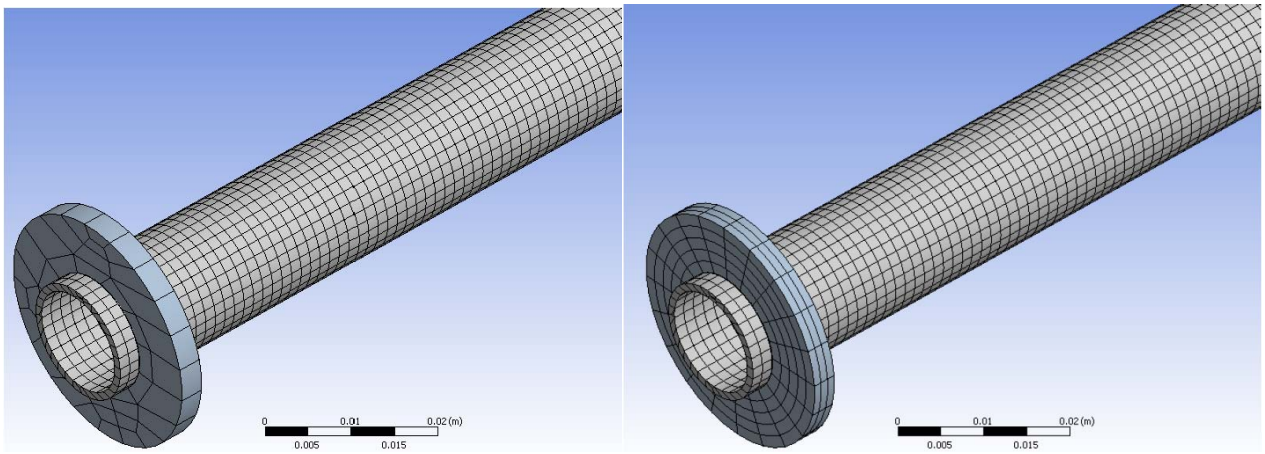

(a) Automatic meshes (b) Refined meshes

Figure 4.4: Generated mesh for the prototype during modeling.

piezoceramic ring helped in selecting the type of solid it was assigned to in ANSYS, and in this case, it was assigned as solid 226 which is a 3-D 20-Node Coupled-Field Solid with piezoelectric capabilities. Thereafter, the load to be used in the model was

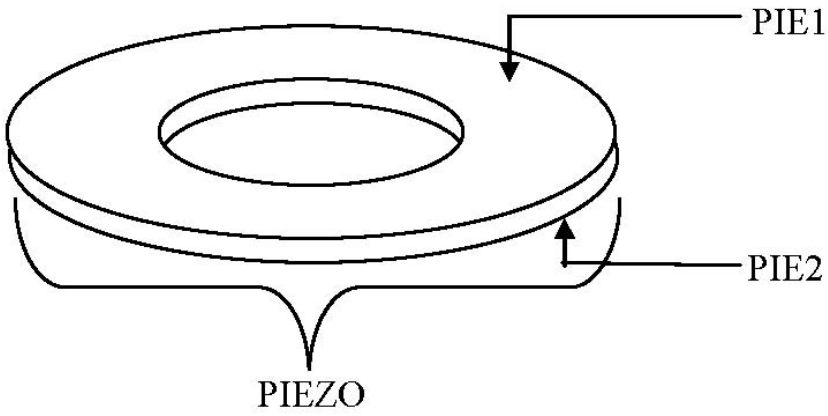

Figure 4.5: Naming of the piezoceramic ring.

applied, where in this case, voltage was applied to the electrodes of the piezoceramic ring. Finally, the solution for the deformation frequency response model was obtained.

The first parameter that was varied was the offset position of placing the transducer on the pipe. It was varied from the edge of the pipe to halfway through, taking advantage of the symmetry. Subsequently, the same was done for various lengths of acrylic pipe

varying from 300 mm to 1000 mm. This length was used in order to have enough acrylic material to dissipate the reflected wave. The optimum length was obtained as the one that gave the highest amplitude of the wave while the optimum offset position was the position of the piezoceramic ring at the optimum length.

Thereafter, with the optimum offset position and length determined, the inner and outer diameters of the model were varied. The outer diameter was kept constant while varying the inner diameter to a value close to the outer diameter. This analysis was done for values of the outer diameter varying between 10 mm to 20 mm with this range being related to the trial device that had been developed. This analysis resulted in the optimum diameter being determined as the diameter giving the highest amplitude of the ultrasonic wave.

4.2.1 Model

Due to the limited availability of all sizes of the acrylic pipe and corresponding size of piezoceramic rings in the market, a model that was available was chosen, analyzed and compared experimentally. The available size of the pipe and the ring had an external and internal diameter of 13 mm by 15 mm and 15 mm by 30 mm respectively.

4.2.1.1 Modal Analysis

The properties of the piezoceramic material provided by the manufacturer were converted into the format used by ANSYS as explained in Appendix **B**. It was then meshed using automatic meshes as shown in Figure 4.6a, and later refined using mapped face meshing and body sizing so as to arrange the elements in a regular manner as shown in Figure 4.6b.

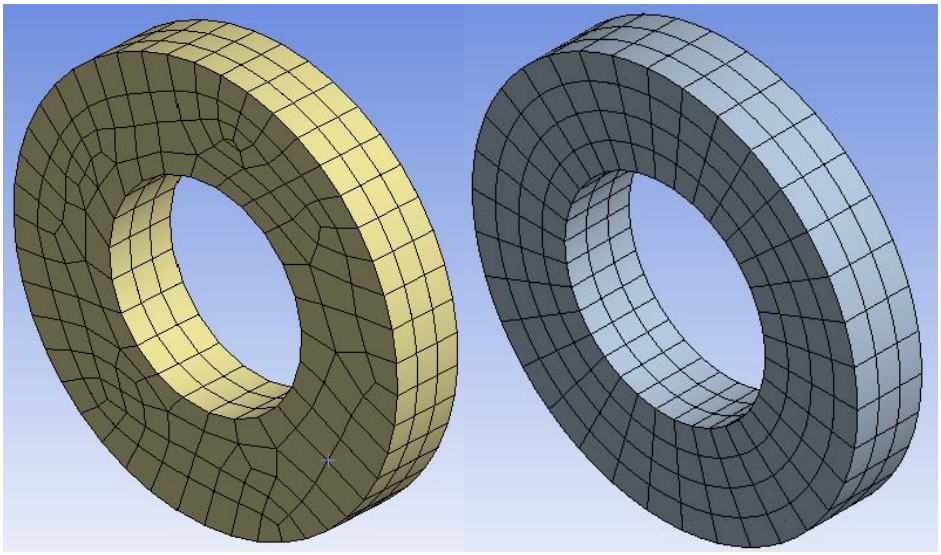

(a) Automatic meshes (b) Refined meshes

Figure 4.6: Mesh for the piezoceramic ring model

The modal shape was obtained as shown in Figure 4.7.

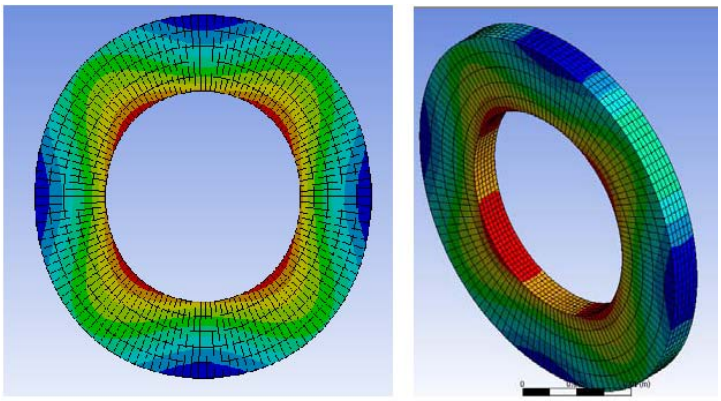

Figure 4.7: Modal shape for the piezoceramic ring.

Afterwards, the acrylic pipe was analyzed. The meshes generated were similar in shape to those of the piezoceramic ring and appeared as shown in Figure 4.8. The pipe was supported on both sides and then the deformation shapes for the whole pipe model was obtained.

The acrylic pipe had its modal shapes and natural frequencies investigated appearing

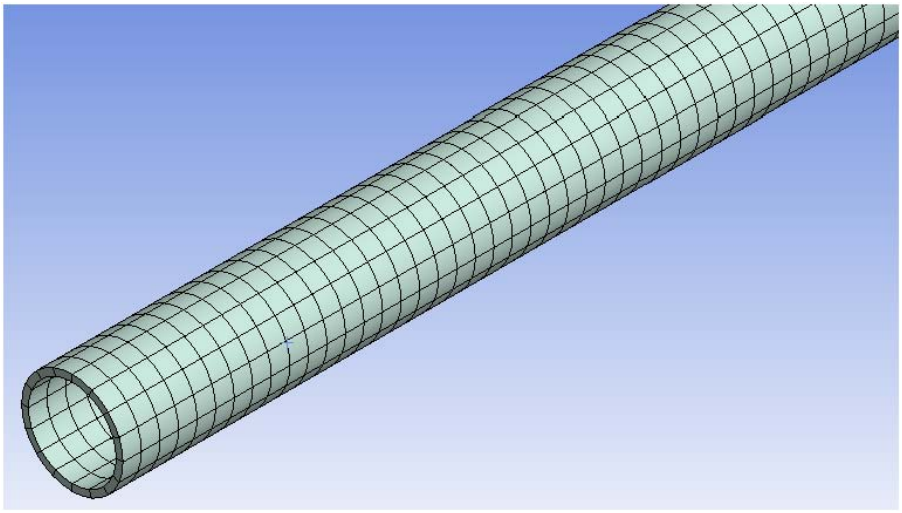

Figure 4.8: Elements for the acrylic pipe.

as shown in Figure 4.9.

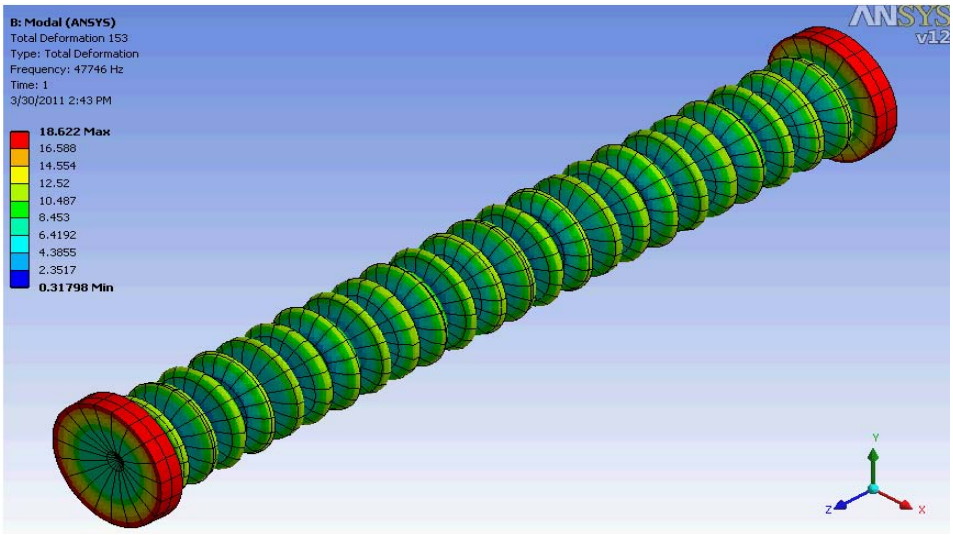

Figure 4.9: Modal shape for the acrylic pipe.

Finally, the whole set-up was analyzed. In this analysis, the piezoceramic ring and the acrylic pipe were bonded together. The model was meshed automatically and later refined as shown in Figures 4.4a and 4.4b respectively. Thereafter, the piezooceramic ring was loaded and the modal shapes of deformation obtained as shown in Figure 4.10.

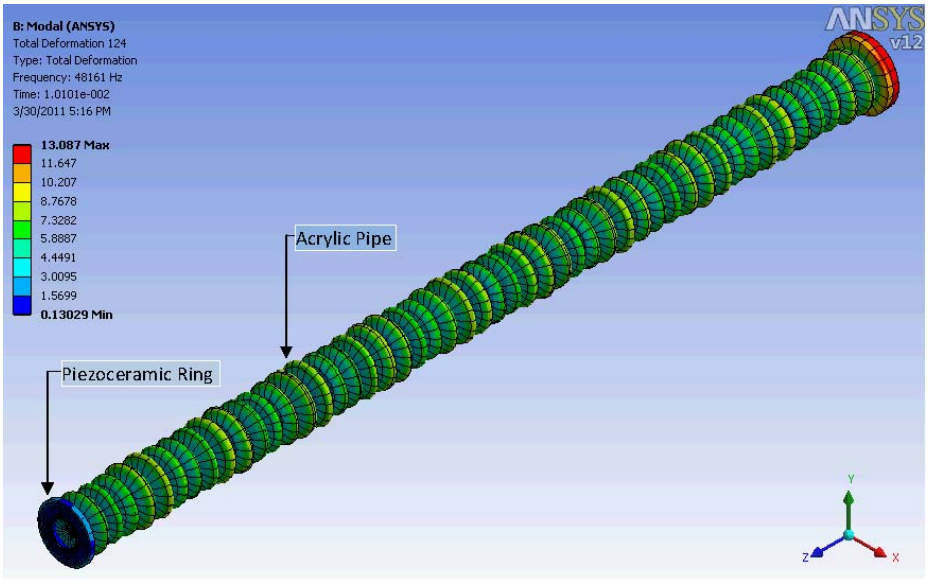

Figure 4.10: Modal shape for the whole set-up.

4.2.1.2 Harmonic analysis

First, the deformation of the piezoceramic rings was investigated on feeding with a 10 V ac voltage, which was the ideal voltage for operating the piezoceramic ring as provided by the manufacturer. Using the frequency response, the deformation of the two edges shown in Figure 4.11 was investigated in order to find out whether there was any difference in their deformation. Further, the inner and outer diameter faces were analyzed in order to obtain their velocities at resonant frequency.

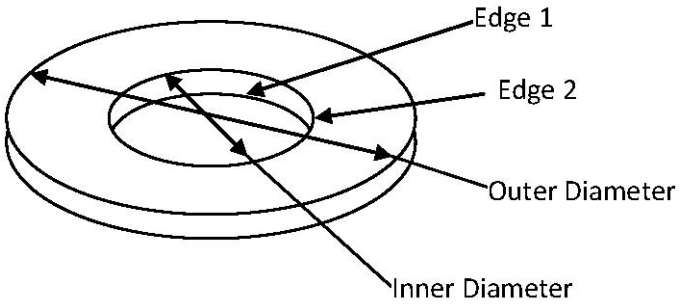

Figure 4.11: Piezoelectric inner edges.

The whole set-up was modeled at frequency ranging from 20kHz to 70kHz, taking ad-

vantage of the low ultrasonic frequency spectrum. The deformation was investigated and the kind of waves produced at the frequencies analyzed.

4.3 Laboratory Experiments

Various experiments were conducted to verify the model results. First the piezoceramic ring had the electrodes connected to its faces as shown in Figure 4.12.

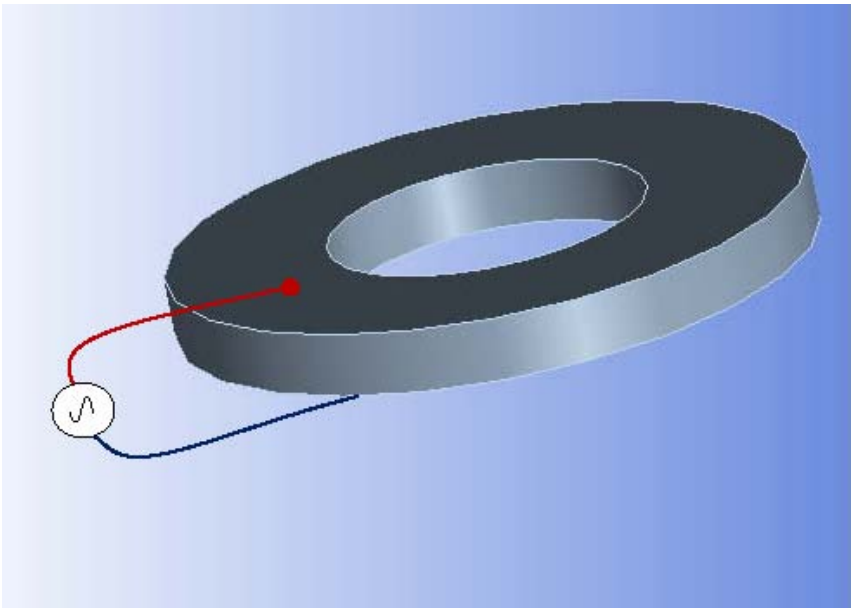

Figure 4.12: Electrodes connection on the piezoceramic ring.

Thereafter, the ring was subjected to 10 V ac and then the deformation graph was viewed using a digital oscilloscope. The frequency of the voltage was then varied until the deformation and the voltage curves were in phase. This state indicated that the peizoceramic ring was vibrating at its resonant frequency. Two rings were used, and the velocity of vibration of the inner and the outer faces were compared.

Subsequently, the ring and the pipe were thoroughly cleaned, and then bonded at the optimum position using Loctite Hysol 3425 adhesive. The pipe was used at the optimum length and offset position and the set-up, shown in Figure 4.13 was left overnight in

order to thoroughly dry up. Thereafter, a thin reflecting foil was placed outside along the length of the pipe so that the vibrometer could measure the wave velocity along the pipe.

Figure 4.13: The constructed prototype.

Figure 4.14 shows the experimental set-up that was used during the experiments to verify the model results. When the power was generated by the power supply, it was taken through an amplifier in order to amplify to 10V AC. This signal was taken to a wave generator, where the required frequency was set and then connected to the workpiece through the electrodes on the piezoceramic ring. The oscilloscope was used to monitor the sinusoidal signals generated by the power supply and the signal fed to the electrodes of the piezoceramic ring. The laser scanning vibrometer consisted of three modules; the input/output module, the vibrometer controller and the data management system as shown in Figure 4.15. The input/output module was used to get the velocity of the traveling wave inside the acrylic pipe, which was computed and presented graphically through the graphical user interface by the data management system. The vibrometer controller was responsible for powering and controlling the functions of the laser vibrometer.

The scanning head of the vibrometer was used to take measurements of the wave at the scanning points along the reflecting foil on the acrylic pipe which appeared as shown in Figure 4.16. In order to improve on the accuracy, the scanning points were placed 5

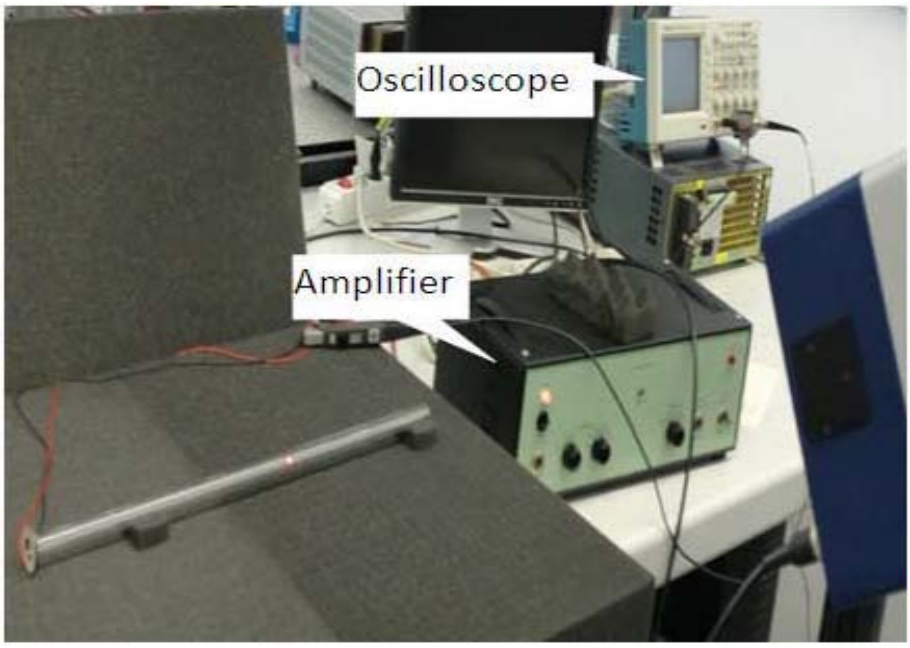

(a)

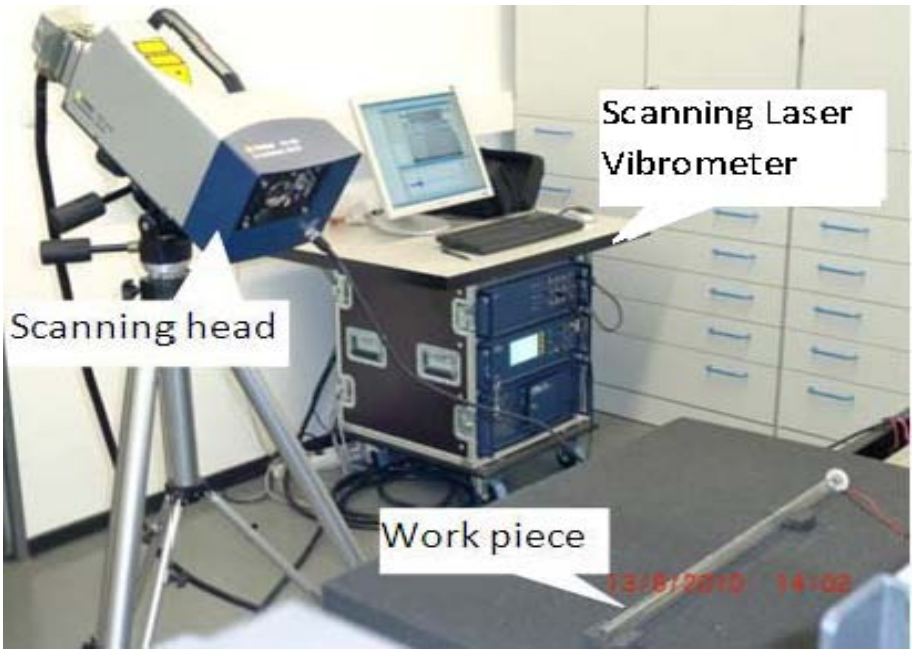

(b)

Figure 4.14: The experimental setup

mm apart and the measurement at each point was taken three times as shown in the Figure 4.17. The laser scanning head had a video camera that enabled the capturing of the prototype. The scanning points were therefore set on the monitor of the vibrometer. The laser head was first moved from the first point to the last point in order to check

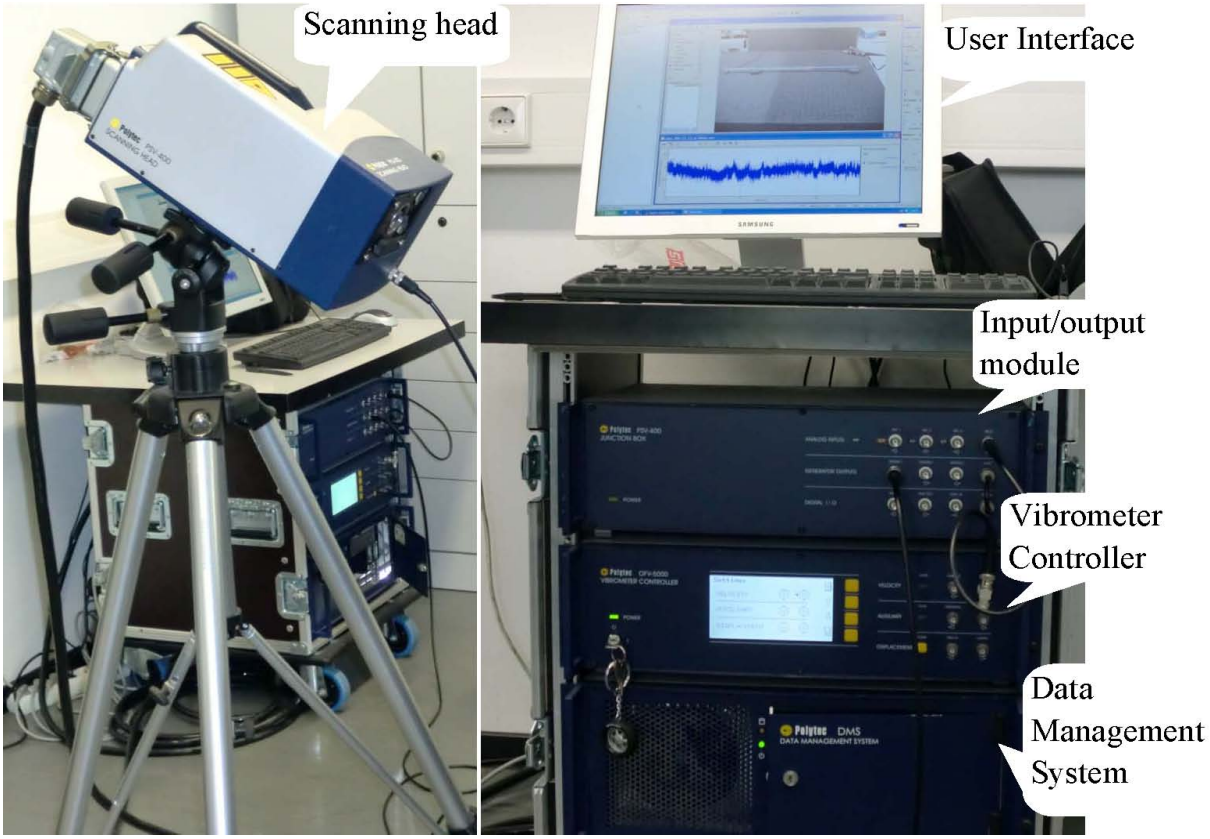

Figure 4.15: The Laser scanning vibrometer

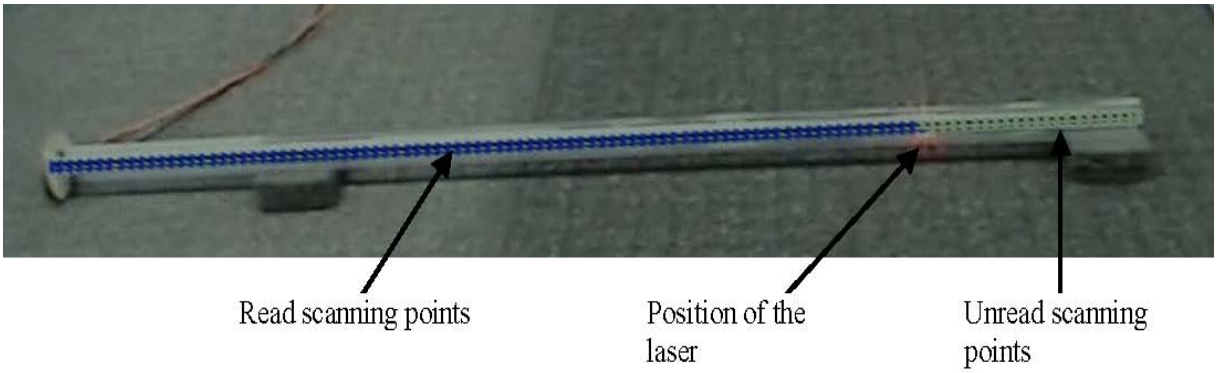

Figure 4.16: The scanning points during the experiment

whether all the points were on the reflecting foil. Once all the points were determined to be correctly positioned, the set-up was subjected to a series of tests. First, the resonant frequency was tested through a procedure similar to that of the piezoceramic ring. Then, the prototype was fed with a frequency ranging from 20 kHz to 70 kHz. The vibrometer then analyzed the data and displayed the type of the wave produced in an animated

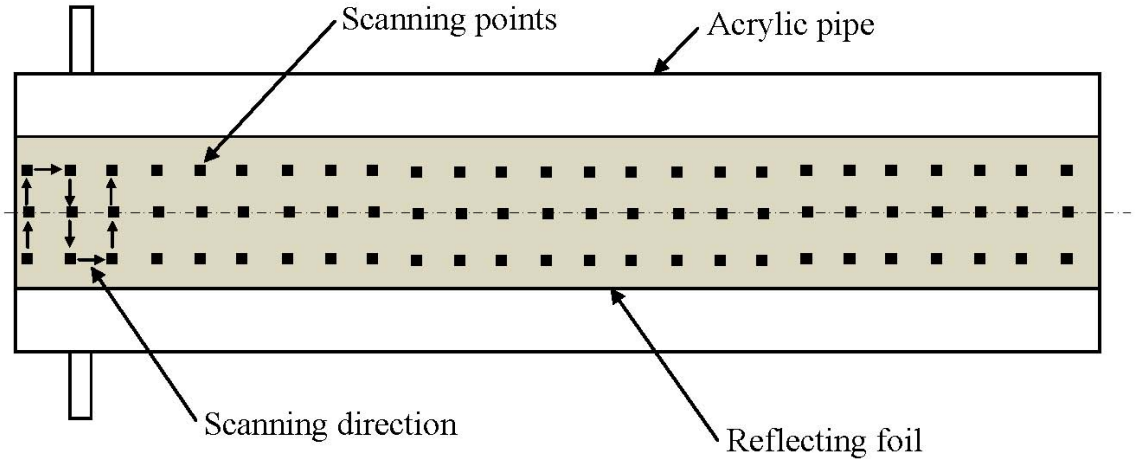

Figure 4.17: The arrangement of scanning points along the pipe.

form on the monitor.

CHAPTER FIVE

5.0 RESULTS AND DISCUSSION

In this chapter, detailed results from modeling and laboratory experiments are discussed.

5.1 Modeling

The results obtained after the variation of the offset position of the transducer along the pipe for different lengths are as shown in Figure 5.1.

From each graph, the optimum position of placing the transducer was obtained as the highest value of the amplitude in a particular length of the acrylic pipe. It was observed that there was erratic deformation in the first 20% of the pipe which then decayed to an almost constant minimal value. In addition the amplitude was affected by the length of the pipe and the offset position of the transducer. When the transducer was at the edge of the pipe, the deformation was at the minimum position in all the instances considered since the wave was only transmitted in one direction along the pipe. However, as the transducer was moved along the pipe, the wave was transmitted both in the right and the left side of the transducer. The erratic deformation was consequently caused by the interference of strong reflected waves coming from the left side of the acrylic pipe which was small length hence the properties of the acrylic pipe could not reduce its effect.

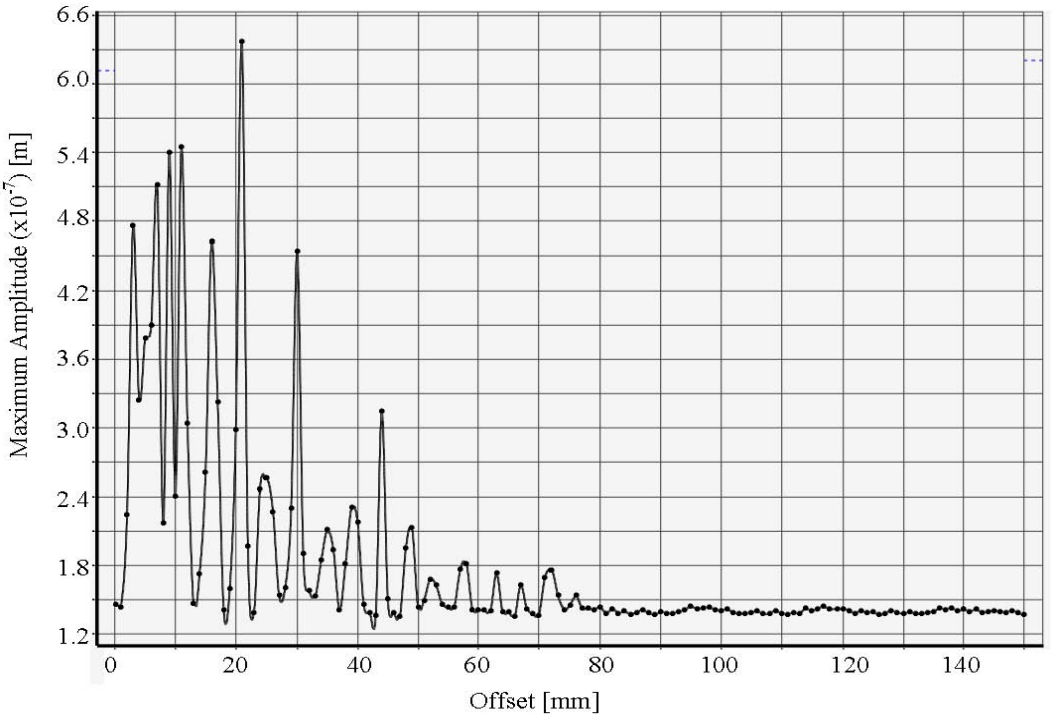

(a) 300mm pipe

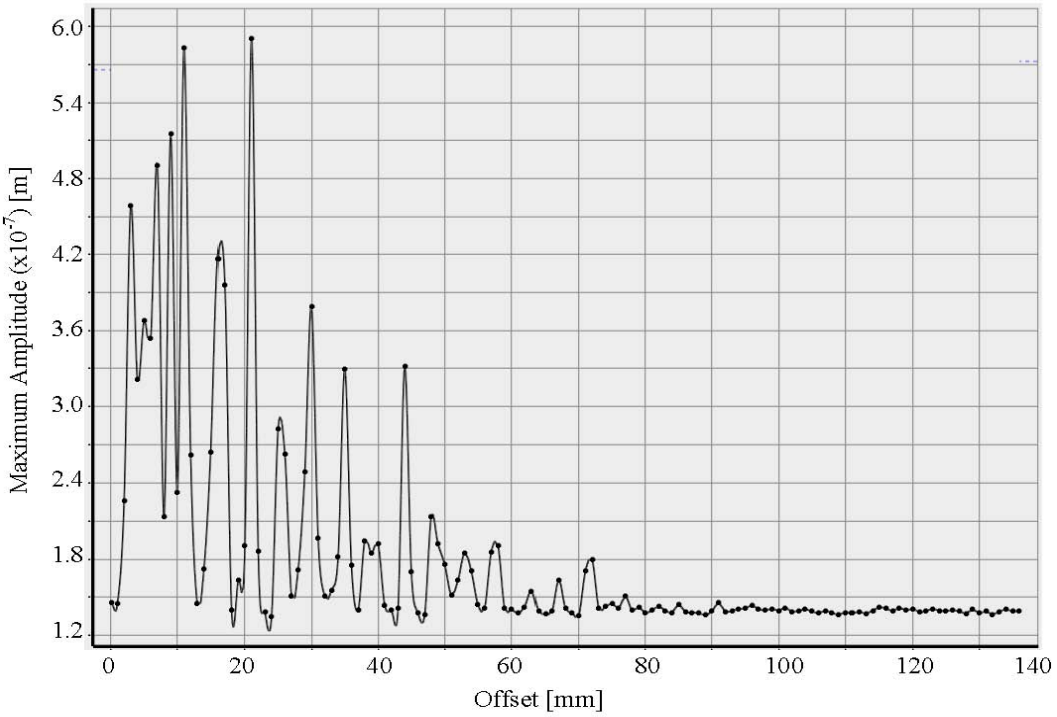

(b) 400mm pipe

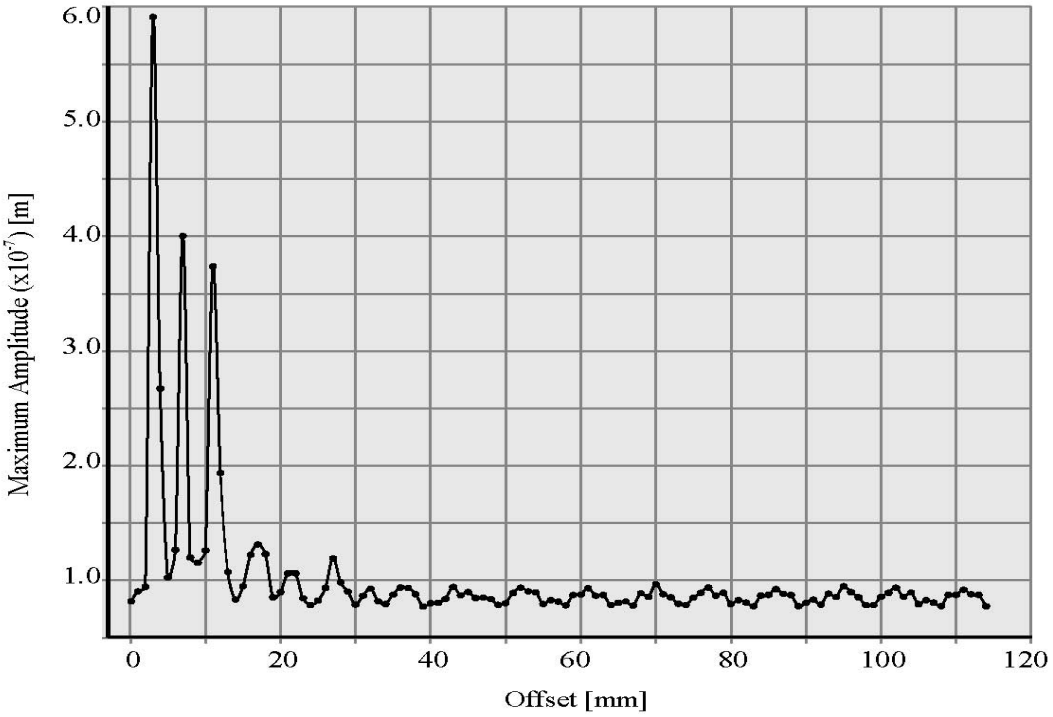

(c) 500mm pipe

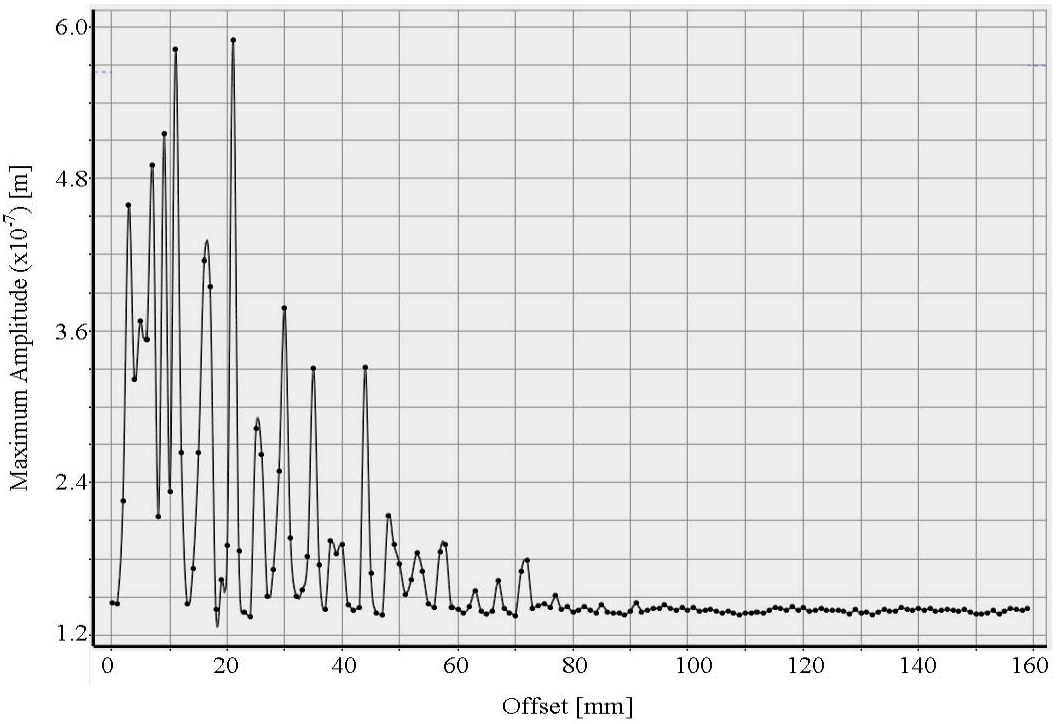

(d) 600mm pipe

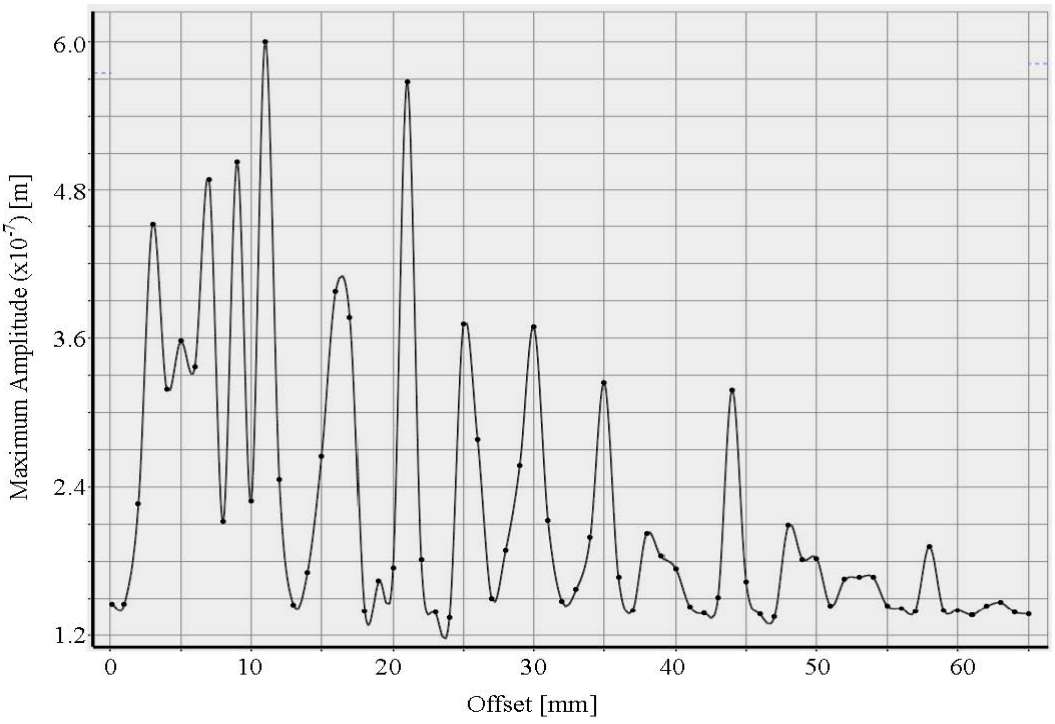

(e) 700mm pipe

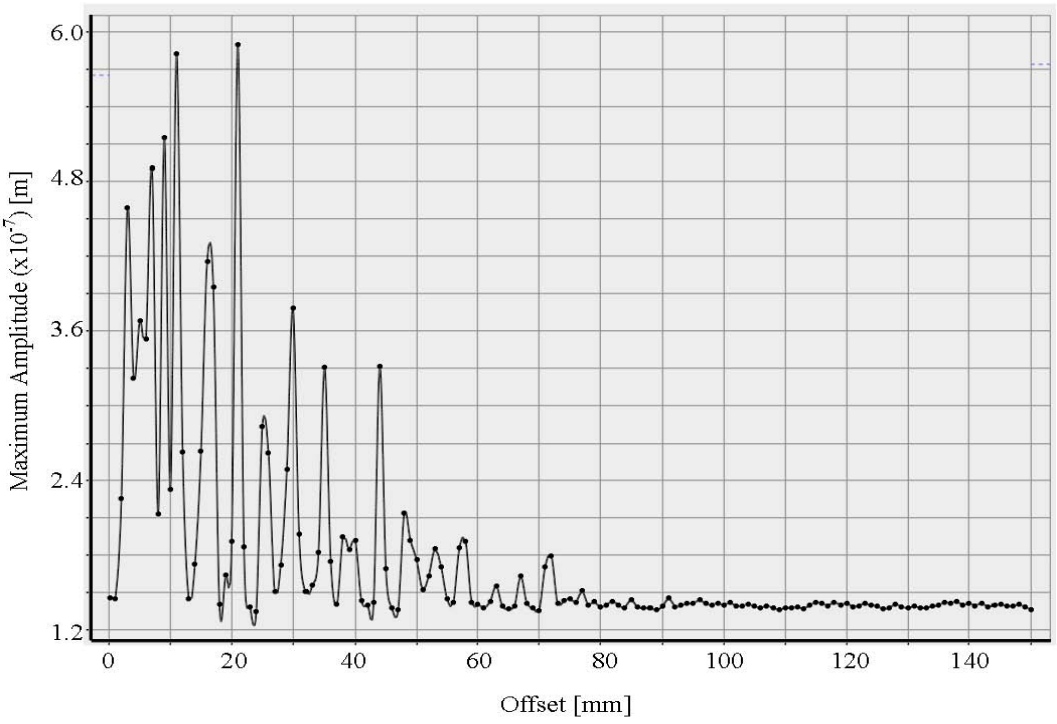

(f) 800mm pipe

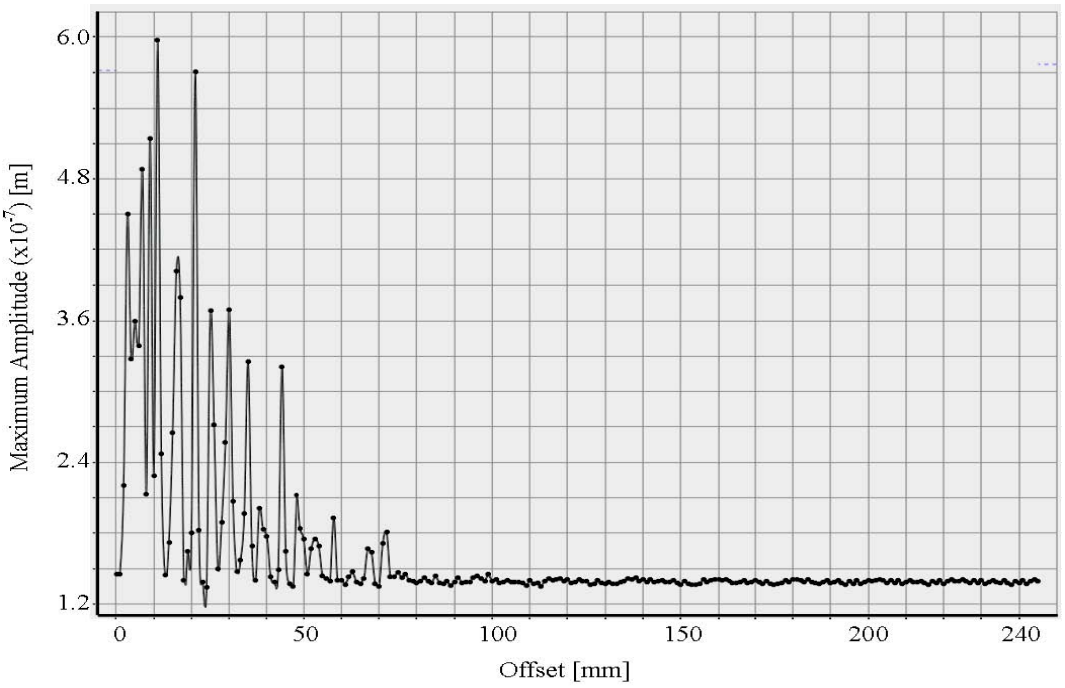

(g) 900mm pipe

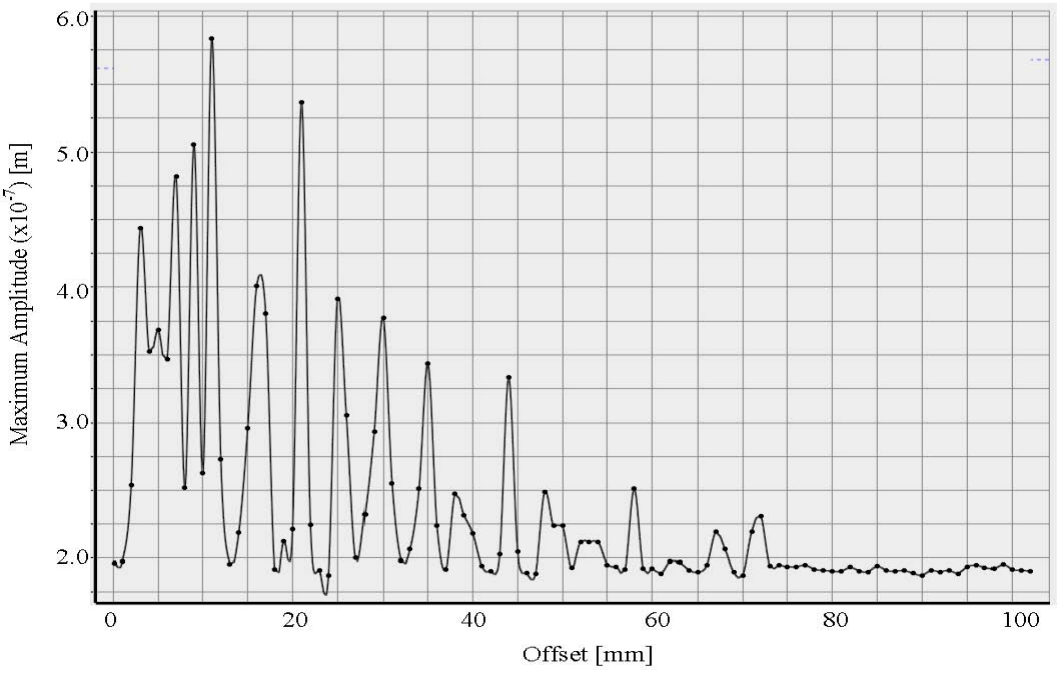

(h) 1000mm pipe

Figure 5.1: Waves in pipes of various lengths

Consequently, the optimum length was obtained by plotting the various maximum amplitudes at the optimum offset positions against the lengths of the pipe as shown in

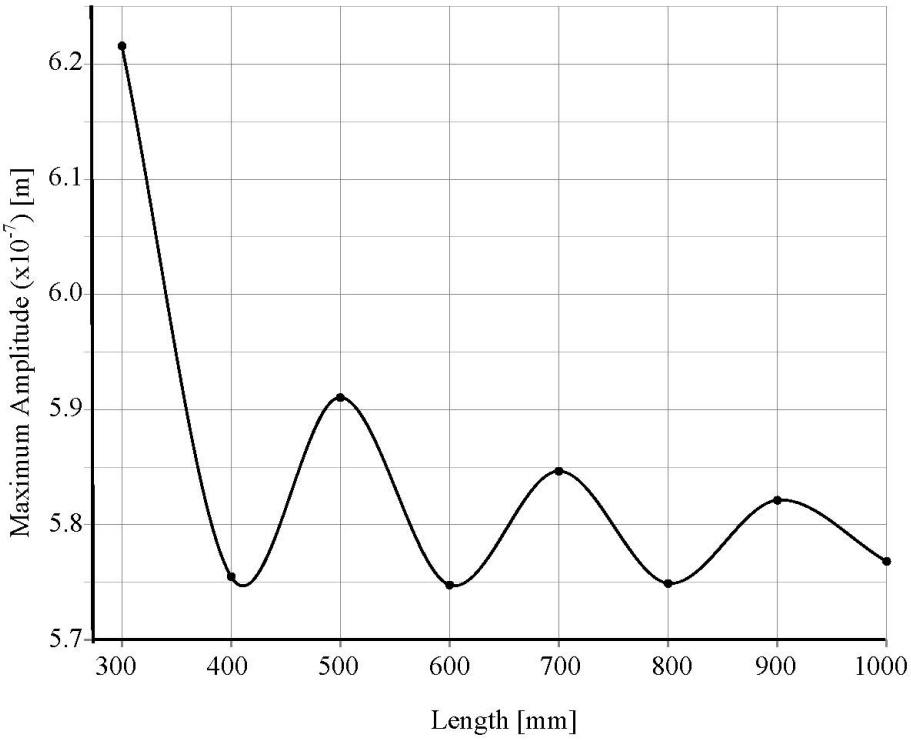

Figure 5.2: Maximum amplitude versus Length

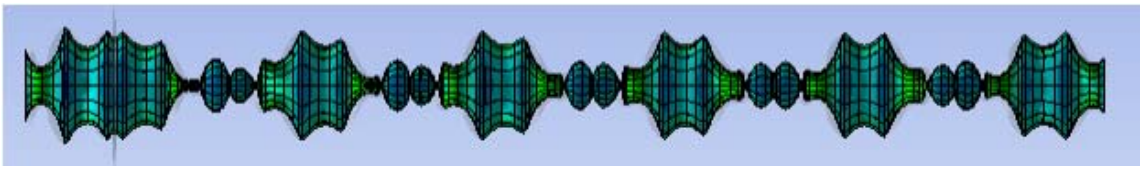

Figure 5.3: The ultrasonic wave produced in the 300mm pipe length

Figure 5.2. It is clear from the graph that th amplitude of the ultrasonic wave continuously reduced due to the wave being damped by the properties of the longer acrylic pipe From this graph, the length of the pipe with the maximum amplitude of displacement was found to be 300 mm length at an optimum offset positions of 21 mm. Unfortunately, for this length of the pipe, the effect of reflected waves was significant from both ends of the pipe, implying that a traveling wave could not be produced. The type of a resulting wave produced in the pipe was as shown in Figure 5.3. The effect of the reflected waves were caused by inadequate material of acrylic due to the short length of the pipe implying that the damping was not as much as desired.

Therefore, the optimum length was taken as 500 mm at an offset position of 3 mm, since this gave the next highest amplitude of the ultrasonic wave produced.

Using the optimum length, the results from the variation of the inner and outer diameter were obtained as shown in Figures 5.4. The external diameter was varied from 10mm to 20mm and in each case, the inner diameter was varied so as to investigate the effect of the material thickness. From the curves, when the thickness of the material was too thick, the wave will be damped leading to a low amplitude. Likewise, when the material was too thin, the wave damping was minimal. As a result, the interference of the incident and the reflected wave, where their amplitudes are quite significant led to a low amplitude due to the destructive interference.

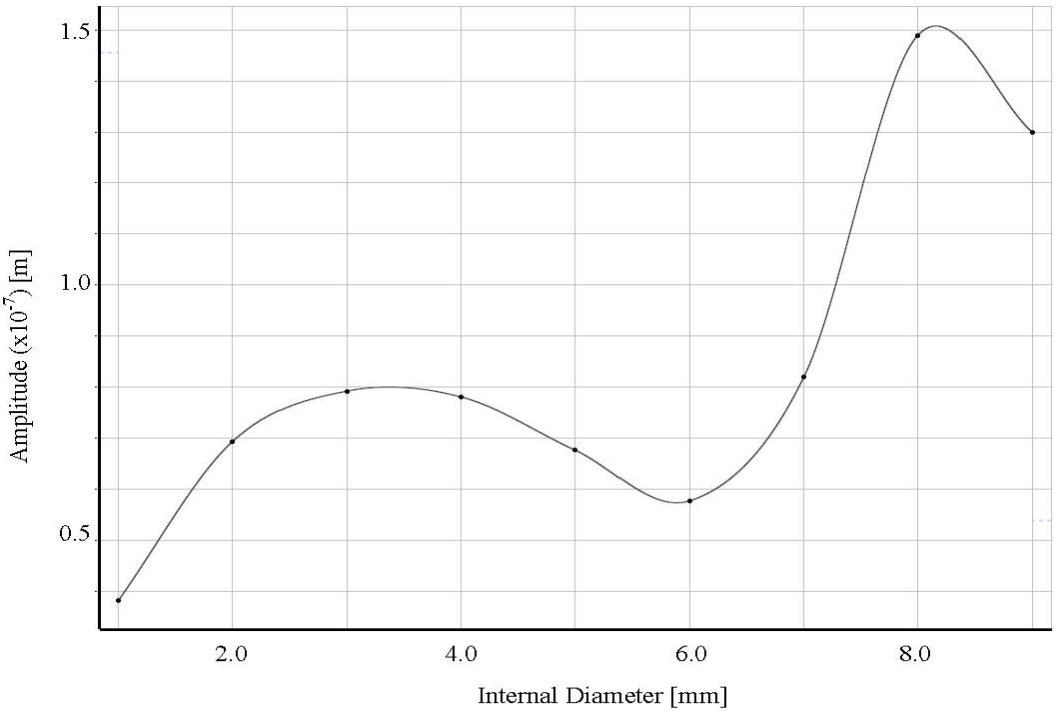

(a) 10 mm External Diameter

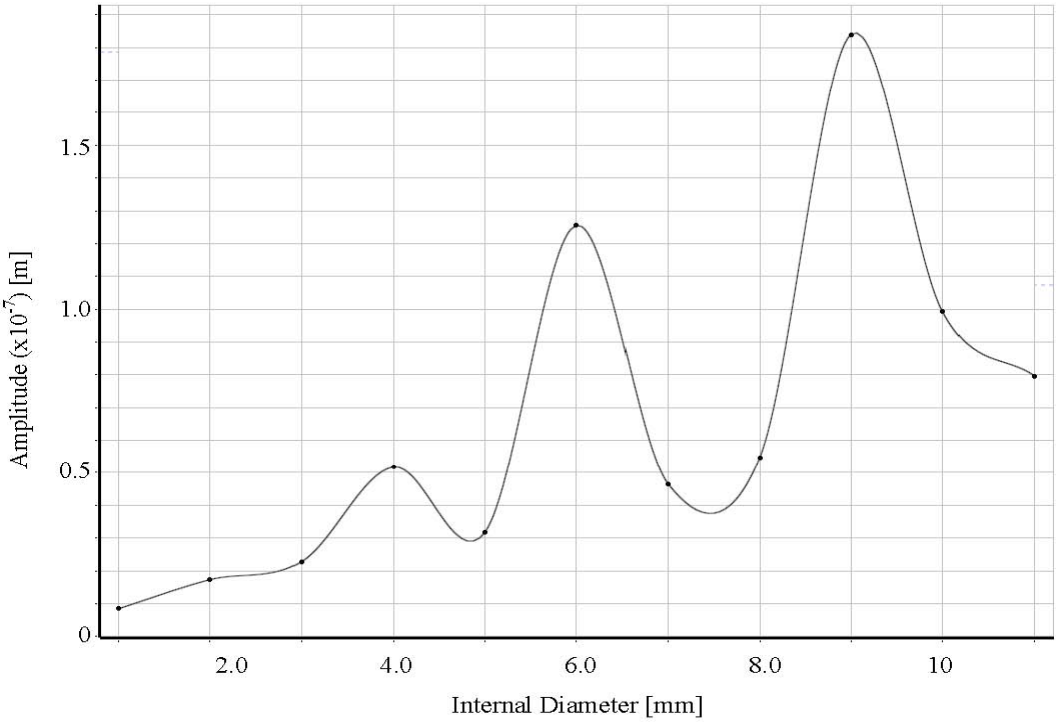

(b) 12 mm External Diameter

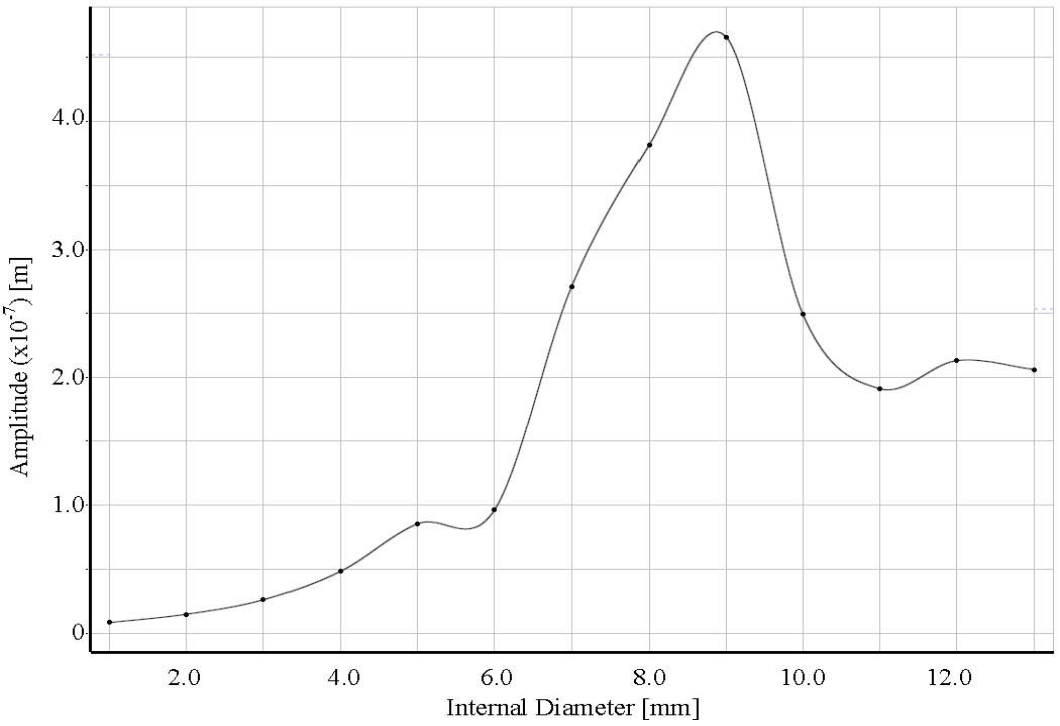

(c) 14 mm External Diameter

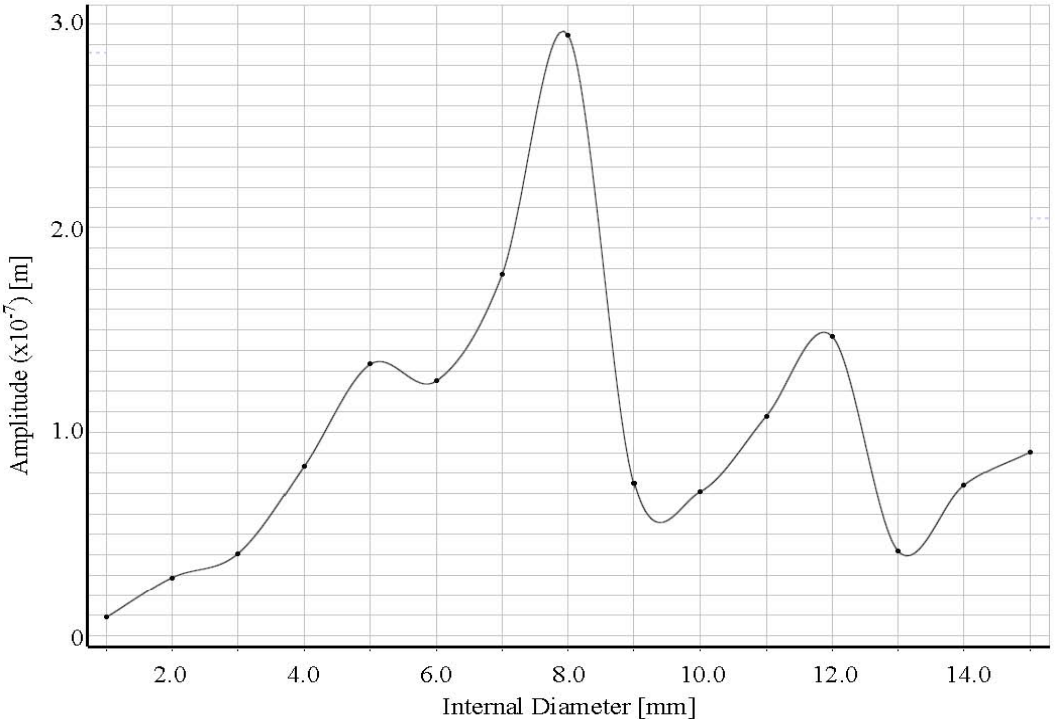

(d) 16 mm External Diameter

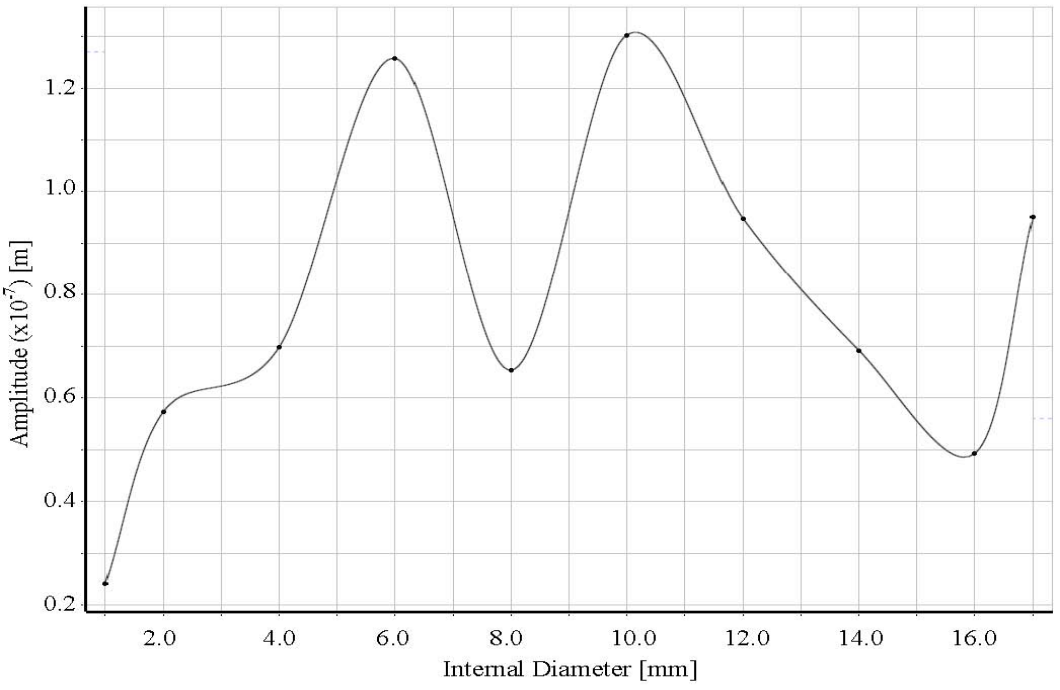

(e) 18 mm External Diameter

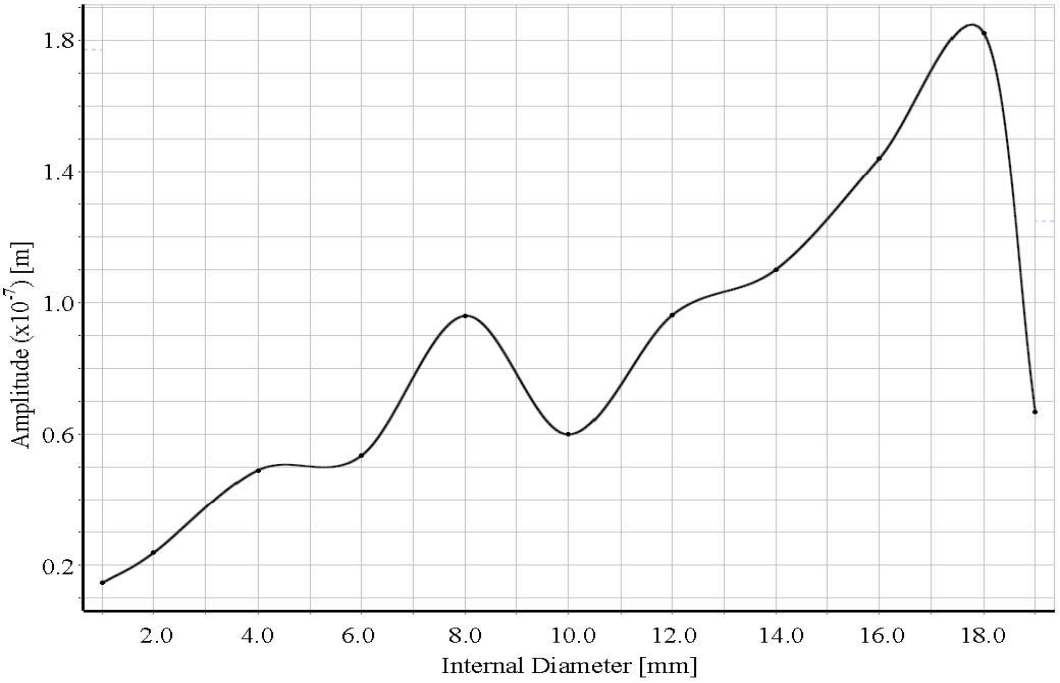

(f) 20 mm External Diameter

Figure 5.4: Maximum amplitude vs inner diameter for various external diameter pipe.

From the graphs, various maximum amplitudes were obtained in each pipe diameter variation. The maximum amplitudes were plotted against the external diameter in order to obtain the optimal diameter. The results are as shown in Figure 5.5.

Therefore, the maximum amplitude was obtained with the pipe having an external diameter of 14mm. From Figure 5.4c, the maximum internal diameter is 9mm. Hence, the optimal thickness was obtained when the pipe's internal and external diameters were 9mm and 14mm respectively.

5.2 Model for analysis

A model, whose dimensions were closest to the optimum model, that was available in the market was analyzed. The dimensions of the acrylic pipe were external and internal

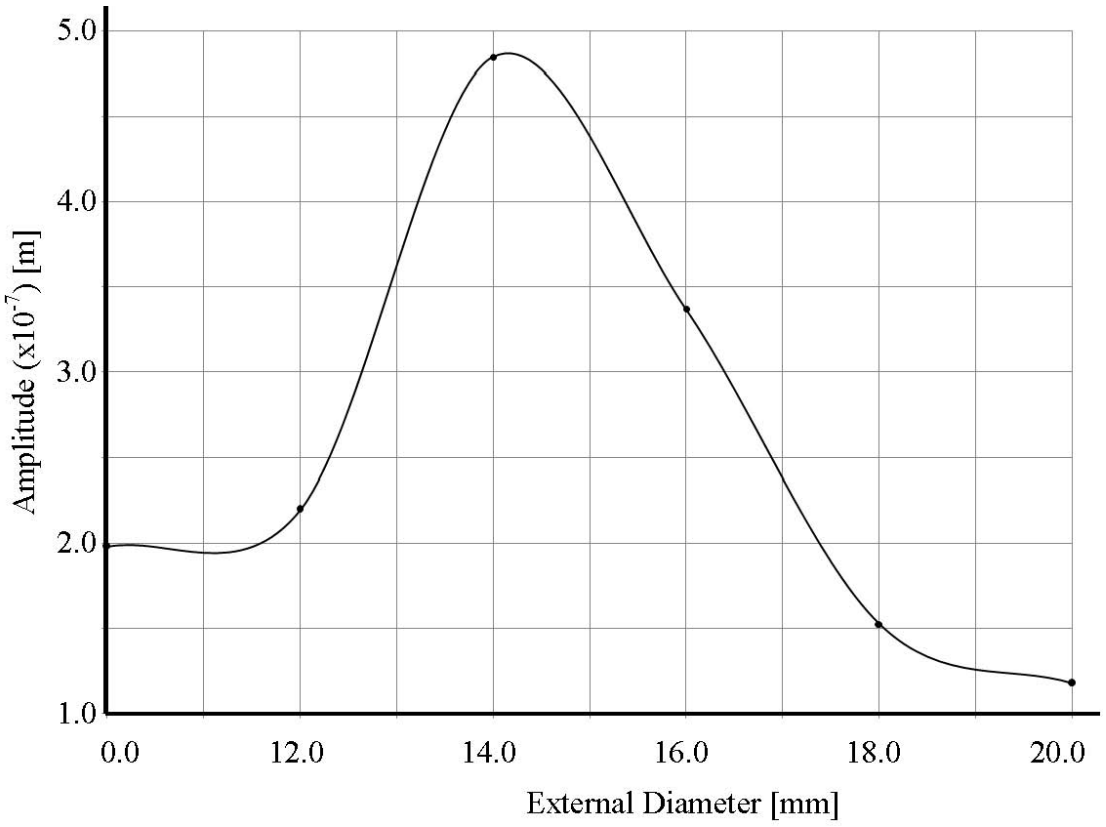

Figure 5.5: Variation of the maximum amplitudes with external diameters of the pipe

diameters of 15mm by 13mm respectively while those of the piezoceramic ring were 30mm by 15mm respectively.

5.2.1 Piezoceramic Ring

From the modal analysis, the piezoceramic ring was found to have a natural frequency of 47.9 kHz. Additionally, from the harmonic analysis, the ratio of deformation of the inner ring edges was obtained as shown in Table 5.1. This showed that the ratio of the

Table 5.1: Deformation of the piezoceramic inner face and edges.

Offset (mm)	Amplitude at Edge 1 (m)	Amplitude at Edge 2 (m)	Amplitude Ratio
0.1	1.05E-008	1.06E-008	0.9858
1	1.05E-008	1.07E-008	0.9868
2	1.06E-008	1.07E-008	0.9894
3	1.03E-008	1.05E-008	0.9896
4	9.93E-009	9.87E-009	1.0060
5	9.97E-009	9.97E-009	1.0000
6	1.02E-008	1.01E-008	1.0124
7	1.03E-008	1.02E-008	1.0102
8	9.51E-009	9.11E-009	1.0438
9	9.39E-009	8.99E-009	1.0446
10	8.45E-009	8.22E-009	1.0282
11	9.59E-009	9.66E-009	0.9925
12	9.82E-009	9.62E-009	1.0204
13	9.91E-009	9.73E-009	1.0184
14	9.76E-009	9.50E-009	1.0274
15	9.31E-009	9.15E-009	1.0185
16	9.35E-009	9.17E-009	1.0186
17	9.66E-009	9.70E-009	0.9957
18	9.55E-009	9.58E-009	0.9971
19	9.80E-009	9.86E-009	0.9942
20	9.95E-009	9.87E-009	1.0082

deformation was approximately 1 at the various offsets considered implying that there was no significant variation to the deformation of the inner edges of the ring. As a result, the whole of the inner face was used during the modeling of the deformation of the whole set-up.

An analysis around the resonant frequency of the piezoceramic ring was done in order to obtain the maximum velocity of vibration of the inner and outer diameter faces.

Tables 5.2 and 5.3 show the results of the face displacements. From the frequency, f, of excitation and the Amplitude, A, the velocity, V, was calculated using Equation 5.1.

$$V = 2\pi f A. \tag{5.1}$$

Table 5.2: Velocity for the deformation of the inner face of the ring

Frequency (Hz)	Amplitude (m)	Velocity (mm/s)
47000	9.02E-08	2.66E+01
47200	1.02E-07	3.03E+01
47400	1.18E-07	3.51E+01
47600	1.33E-07	3.99E+01
47800	1.44E-07	4.32E+01
48000	1.45E-07	4.37E+01
48200	1.36E-07	4.11E+01
48400	1.21E-07	3.68E+01
48600	1.06E-07	3.23E+01
48800	9.22E-08	2.83E+01
49000	8.08E-08	2.49E+01

Table 5.3: Velocity for the deformation of the outer face of the ring

Frequency (Hz)	Amplitude (m)	Velocity (mm/s)
47000	6.99E-08	2.06E+01
47200	7.82E-08	2.32E+01
47400	8.93E-08	2.66E+01
47600	1.00E-07	3.00E+01
47800	1.74E-07	5.23E+01
48000	1.07E-07	3.23E+01
48200	9.95E-08	3.01E+01
48400	8.80E-08	2.68E+01
48600	7.62E-08	2.33E+01
48800	6.58E-08	2.02E+01
49000	5.72E-08	1.76E+01

The resonant frequency of the ring was also obtained numerically using Equation 3.5, whereas the mean radius of the ring in Figure 3.7 was calculated as 11.25 mm using Equation 5.2.

$$R = \frac{d_{outer} + d_{inner}}{4} \tag{5.2}$$

From Equation 3.26, the natural frequency in radial mode for the ring was obtained as 4.4350×10^4 Hz.

The resonant frequency in radial mode, f_{r-rad} was obtained as 4.4350×10^4 Hz using Equation 5.3.

$$f_{r-rad} = \frac{\omega}{2\pi} \tag{5.3}$$

5.2.2 Acrylic pipe

The natural frequency of the acrylic pipe was obtained as 47.7 kHz and the modal shape is shown in Figure 4.9.

5.2.3 Model Whole Set-up

The modal shape of the whole set-up whose natural frequency was 47.8 kHz was obtained as shown in Figure 4.10.

At this frequency the greatest amplitude, and consequently, the greatest velocity of the wave was obtained, and the traveling wave produced is shown in Figure 5.6. The

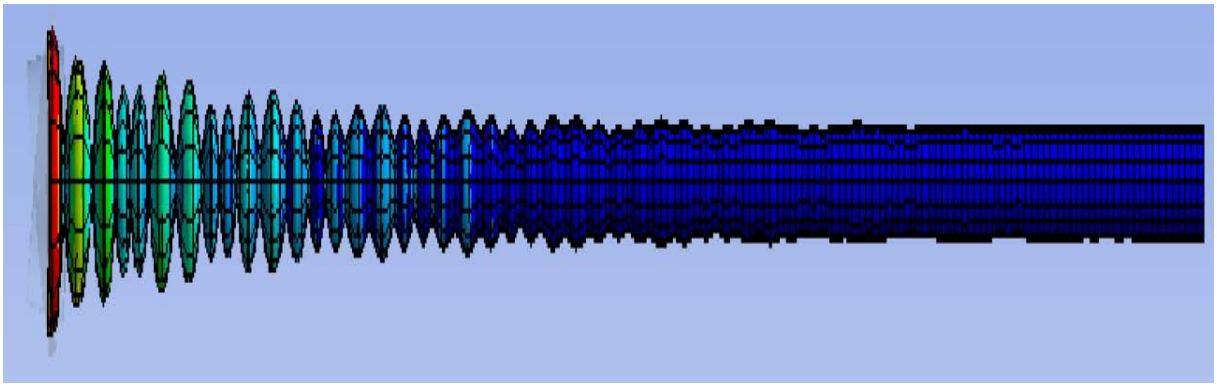

Figure 5.6: The waveform in the pipe at the resonant frequency.

maximum amplitude of the wave was evident at the piezoceramic ring which decayed along the length of the pipe.

Further analysis was done on the waves produced along the pipe when the frequency of the voltage was varied from 20kHz to 70kHz, and the waveforms are shown in Figure 5.7.

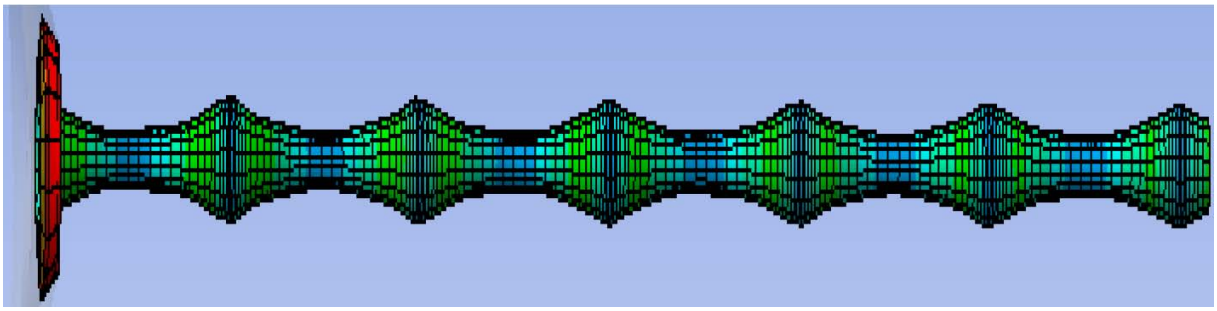

(a) 20kHz

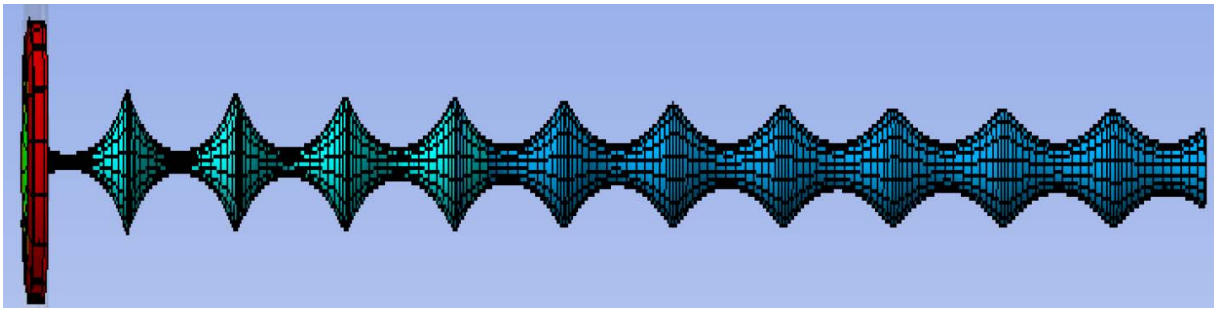

(b) 30kHz

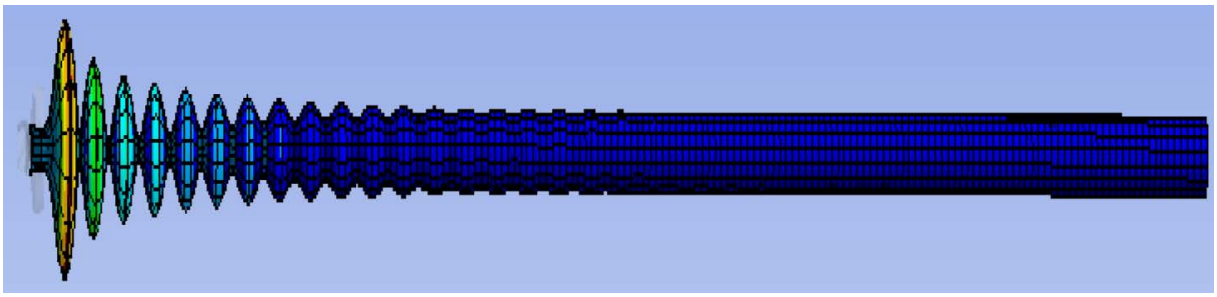

(c) 40kHz

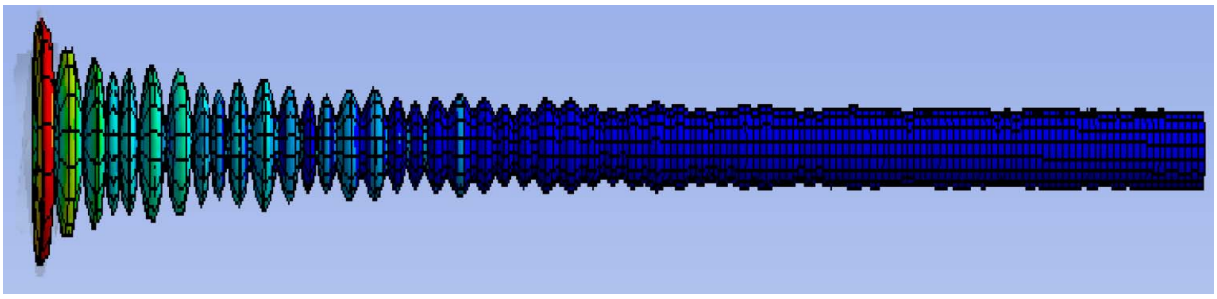

(d) 50kHz

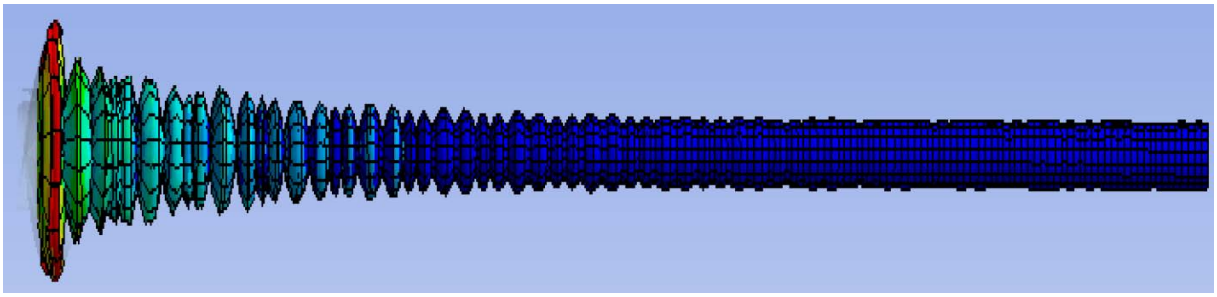

(e) 60kHz

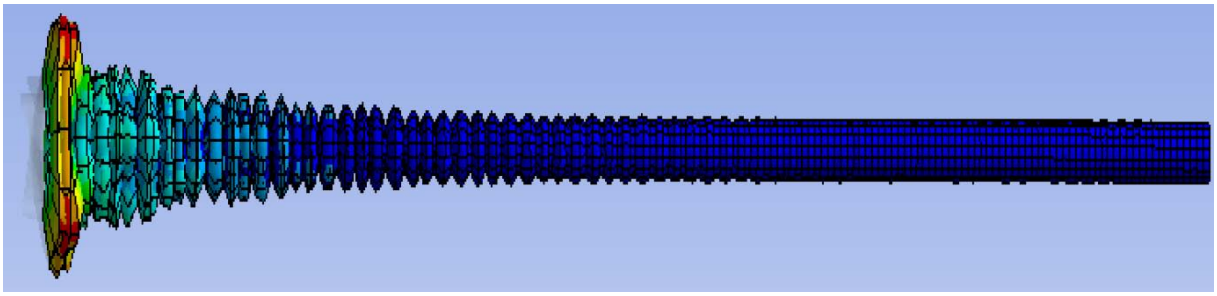

(f) 70kHz

Figure 5.7: Waves produced at various frequencies in the model.

It was evident from the waveforms that the wavelength reduced as the frequency was increased. In addition, the rate of attenuation of the wave along the length of the pipe increased with frequency. This was due to the viscoelastic properties of the acrylic pipe whereby damping increases with increase in frequency. This showed that at low frequencies, the damping was not so much meaning some reflected wave was able to travel back along the pipe.

5.3 Experimental Results

5.3.1 Piezoceramic ring

The results after testing the vibration of the piezoceramic rings were compared to the modeling ones as shown in Table 5.4. Although the resonant frequencies were compara-

ble, there was a small deviation in the velocities of the faces. This error was attributed to the deterioration of the piezoelectric properties with time.

Table 5.4: Results for model and experimental values for the piezoceramic ring.

		Model	Experimental	
			Ring 1	Ring 2
Resonant Frequency(kHz)		47.91	47.96	47.99
Velocity (mm/s)	Inner Diameter	43.70	37.00	37.00
	Outer Diameter	52.30	50.00	50.00

5.3.2 Experiment Whole set-up

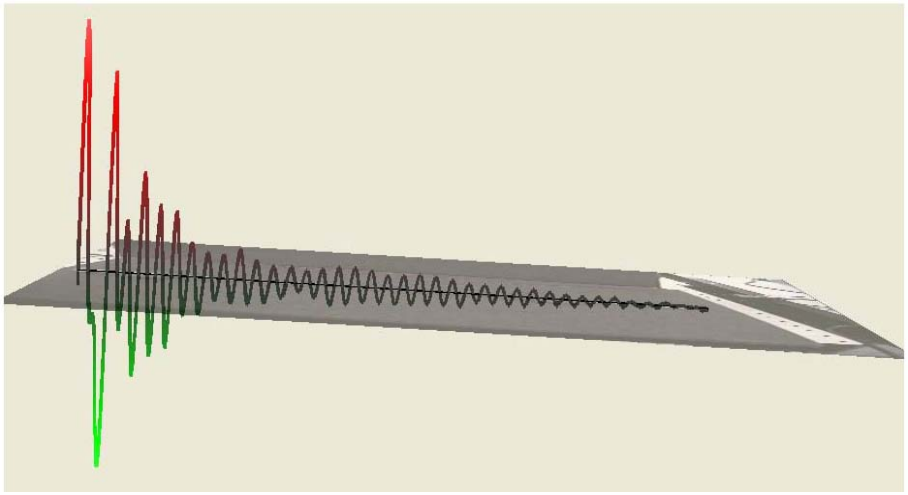

Figure 5.8: Traveling wave at Resonant frequency, 48.4kHz along various scanning points.

Figure 5.8 shows the traveling wave at resonant frequency of 48.4 kHz for the whole set-up along the various scan points on the acrylic pipe. The traveling waves produced at various frequencies between 20kHz to 70kHz are shown in Figure 5.9.

On comparing the wave shapes from the model and experimental results, the amplitude of the wave reduced along the pipe. It was clear that a traveling wave was produced,

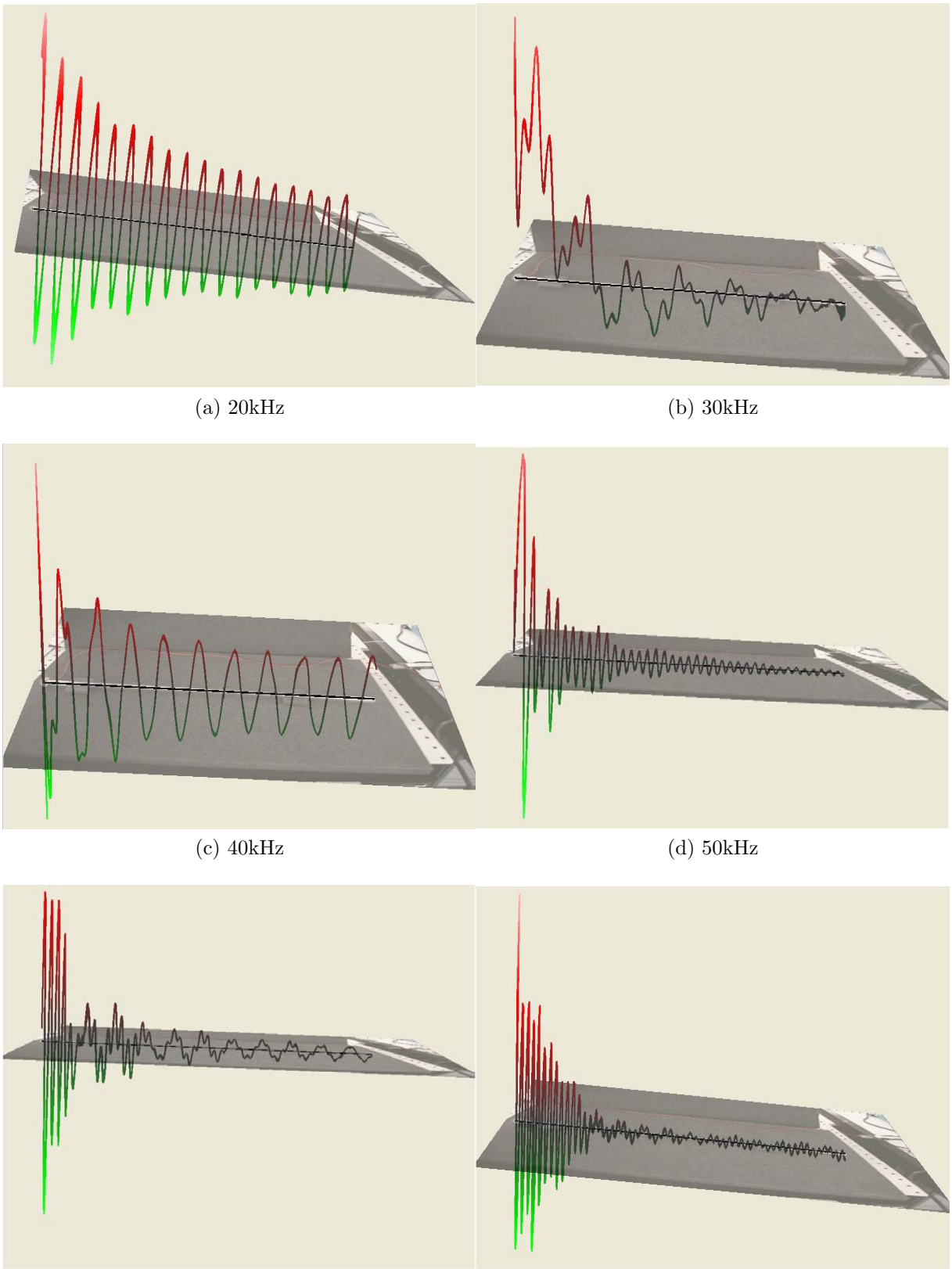

(a) 20kHz (b) 30kHz

(c) 40kHz (d) 50kHz

(e) 60kHz (f) 70kHz

Figure 5.9: Traveling wave produced at various frequencies along the scanning points during the experiment.

and the acrylic pipe played a major role in damping the waves. When the frequency of the alternating voltage was increased, the wavelength decreased as the frequency is inversely proportional to the wavelength. The attenuation of the wave was also observed to increase with increasing frequency. This was because the damping properties of the acrylic pipe significantly increased with the frequency.

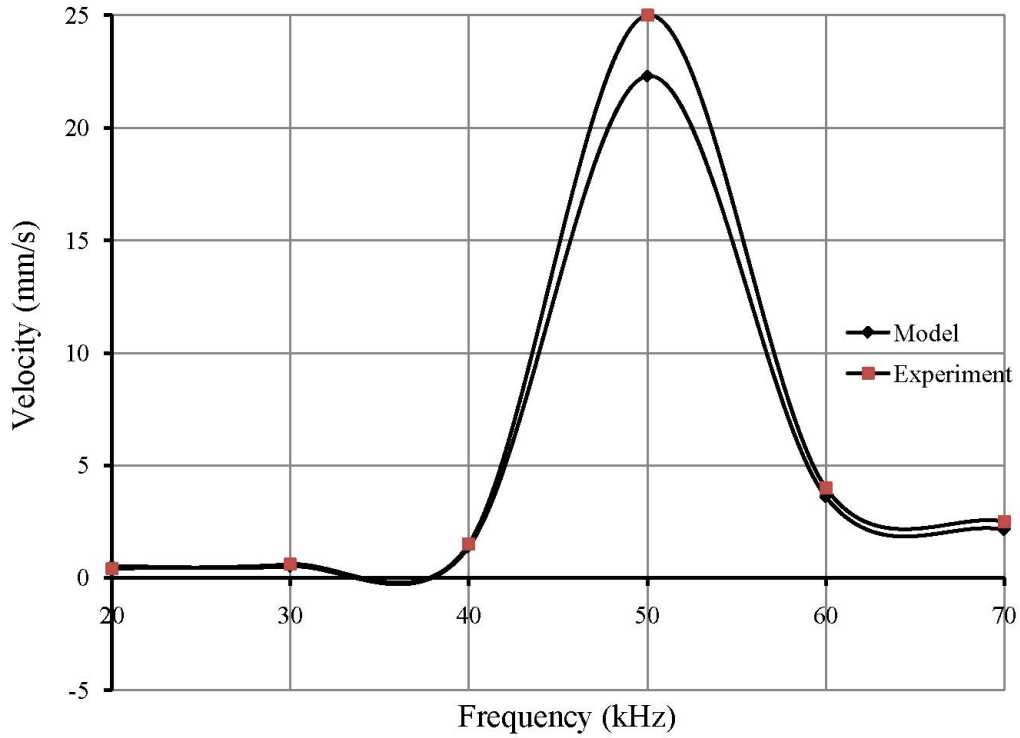

Figure 5.10: Plot comparing the velocity of model and experimental results.

From the plot in Figure 5.10, the velocities obtained from modeling and experimentally were comparable at lower frequencies. However, as frequency increased, especially around the resonant frequency, about 20% error was noticed, with the experimental velocity being higher than the modeled. These errors were as a result of the continuously increasing damping with frequency due to the viscoelastic properties of the acrylic material.

5.4 Force produced by the traveling wave

In this research, the sound pressure, p_s in Equation 3.64 was obtained as 0.356 N/m^2.

By taking the speed of sound in air, c as 343 m/s and density of air as 1.2 kg/m^3 then the energy density of the traveling wave produced in Equation 3.63 was obtained as $8.96 \times 10^{-7} J/m^3$

The spherical micro-particles consisting of Al_2O_3 powder, 60-200 μm in diameter, density 3700 kg/m^3, stored at normal pressure and temperature were considered.

The Oscillating force amplitude, F_A, from Equation 3.69, for 60 μm and 200 μm particles was obtained as $9.92 \times 10^{-11} N$ and $3.68 \times 10^{-9} N$ respectively. The operating conditions in Ovidiu's research [82] with the same powder are shown in Table 5.5.

Table 5.5: Comparison of critical values from Ovidiu's research and those obtained in this research.

Parameter	**Values for smallest particle**	**Values for largest particle**
particle diameter, d	6×10^{-5} m	2×10^{-4} m
particle density, (Al_2O_3) ρ_1	3700 kg/m^3	3700 kg/m^3
sound frequency, f	100 Hz	100 Hz
particle mass, M	4.18×10^{-10} kg	1.55×10^{-8} kg
particle weight, Mg	4.10×10^{-9} N	1.51×10^{-7} N
Critical Oscillation force Amplitude, F_A	2.08×10^{-13}	7.71×10^{-12}
Obtained Oscillation force Amplitude, F_A	9.92×10^{-11}	3.68×10^{-9}

The amplitudes of the oscillating force are greater than the critical values implying that it is possible to transport the particles using the traveling ultrasonic wave produced.

CHAPTER SIX

6.0 CONCLUSIONS AND RECOMMENDATIONS

6.1 Conclusions

This research involved modeling and validation of the results experimentally using the market available materials. The results from the model showed that it was possible to produce traveling ultrasonic waves in an acrylic pipe while using only one transducer. The modeling results showed that the optimal position of placing the transducer was 3mm from the edge of the acrylic pipe of 500mm optimal length. With this length, the optimal thickness was obtained when the pipe's internal and external diameters were 9mm and 14mm respectively.

Experiments conducted verified the modeling results and indeed the ultrasonic wave was produced inside the pipe, with the strongest wave produced at the resonant frequency of the system. However, a small effect of the reflected wave was found at the end of the pipe, and the damping of the acrylic pipe was found to be affected by the frequency of the signal.

6.2 Recommendations

This research showed that the developed optimum prototype can be used in powder transportation for powders in micro range. More optimization could be carried out in the material properties of the acrylic pipe and the piezoceramic ring in order to allow for more damping of the wave and higher deformations with less power requirements.

Further research on this powder transporting system could be carried out. Possible

areas of furthering this research could be:

(i) Carrying out experiments using different powders.

(ii) Effect on the powder transportation rate when the device is inclined.

(iii) Miniaturization of the system.

(iv) Use of the powder transport system to transport suspended particles in liquids.

(v) Feasibility of the transportation system to feed liquids in small doses.

(vi) Relate the forces and the mass rate of the powder that can be transported.

REFERENCES

[1] Anthony Barber, *Pneumatic Handbook*. Elsevier Advanced Technology, 1997.

[2] X. Lu, S. Yang and J. Evans, "Studies on ultrasonic microfeeding of fine powders," *Journal of Physics D: Applied Physics*, vol. 39, pp. 2444–2453, 2006.

[3] S. Bryant, I. Gill, D. Edwards, I. Smith, "Advances in powder dosing technology."

[4] Byoung-Gook Loh, Paul I. Ro, "An Object Transport System Using Flexural Ultrasonic Progressive Waves Generated by Two-Mode Excitation," *IEEE transactions on ultrasonics, ferroelectrics and frequency control.*, vol. 47, pp. 994–999, 2000.

[5] D. Koyama, K. Nakamura, "Noncontact Ultrasonic Transportation of Small Objects Over Long Distances in Air Using a Bending Vibrator and a Reflector," *IEEE*, vol. 57, pp. 1152–1159, 2010.

[6] S. Jeong, G. Kim, S. Choi, J. Park, K. Cha, "A Study on an Object Transport System Using Ultrasonic Wave Excitation," *Journal of Mechanical Science and Technology*, vol. 21, pp. 941–945, 2007.

[7] S. N. Sen, *Acoustics, Waves and Oscillations*. Wiley Eastern Ltd, 1990.

[8] G. S. J. Blitz, *Ultrasonic methods of Non destructive testing*. Chapman & Hall, 1996.

[9] R. Huber, D. Chinn, O. Balogun, T. Murray, "High frequency laser-based ultrasound," tech. rep., Lawrence Livermore National Laboratory, 2005.

[10] S. Gurevich, Y. Petrov, A. Shusharin, E. Golubev, "Analysis of Ultrasonic waves excited in a metal plate by nanosecond laser pulses," *Russian journal of nondestructive testing*, vol. 45, pp. 247–251, 2009.

[11] Jan Kocbach, "Finite Element Modeling of Ultrasonic Piezoelectric Transducers," tech. rep., University of Bergen, Department of Physics, 2000.

[12] Allan G. Piersol, Thomas L. Paez, *Harris' Schock and Vibration handbook*. McGraw-hill, 2010.

[13] T. Pritz, "Frequency power law of material damping," *Applied Acoustics*, vol. 65, pp. 1027–1036, 2004.

[14] A. Kirekawa, Y. Ito and K. Asano, "A study of structural control using viscoelastic material," in *Eathquake engineering, Tenth World Conference*, 1992.

[15] F. Kreith and R. Mahajan, eds., *Vibration Damping, Control, and Design*. Taylor & Francis Group, LLC, 2007.

[16] T. Takano, Y. Tomikawa, "Excitation of a progressive wave in a lossy ultrasonic transmission line and an application to a powder feeding device," tech. rep., Tohoku Institute of Technology, Yamagata university., 1997.

[17] Zhou Zhizhi, "Powder Transport with the Piezoelectric Motor," tech. rep., College of Energy and Electrical Engineering, Hohai University, NanJing 210098, 2010.

[18] M. Mracek, J. Wallaschek, "A system for powder transport based on piezoelectrically excited ultrasonic progressive waves," *Materials chemistry and physics*, vol. 90, pp. 378–380, 2005.

[19] T. Takano, T. Suzuki, K. Adachi, Y. Tomikawa, "Basic studies on powder-sending devices using ultrasonic vibration," in *Proceedings of 11th symposium on ultrasonic electronics*, 1990.

[20] N. Kanbe, Y Tomikawa, K. Adachi, "Analysis of axisymmetric waves propagating along a hollow cylindrical ultrasonic transmission line," *Acoustical Society of America*, vol. 93, pp. 3235–3241, 1993.

[21] J. Melcher, E. Warren, R. Kotwal, "Traveling-Wave Delivery of Single-Component Developer," *IEEE*, vol. 25, pp. 956–961, 1989.

[22] R. Moroney, R. White, R. Howe, "Ultrasonically Induced Microtransport," tech. rep., Department of EECS and the Electronics Research Laboratory, University of California., 1991.

[23] S. Yang, J. Evans, "Metering and dispensing of powder; the quest for new solid freeforming techniques," *Powder Technology*, vol. 178, p. 5672, 2007.

[24] F. Norton, *Elements of Ceramics*. Addison Wesley, MA, second ed., 1974.

[25] B. Tay, J. Evans, M. Edirisinghe, "Solid freeform fabrication of ceramics," *International Material Reviews*, vol. 48, pp. 341–370, 2003.

[26] Z. Tadmor, C. Gogos, *Principles of Polymer Processing*. Wiley, NY, 1979.

[27] G. Vetter, *The dosing handbook*. Elsevier advanced technology, Oxford, 1998.

[28] J. N. Keraita, "Optimum vibration angle for transporting granular materials on linear conveyors," *Precision engineering and manufacturing*, vol. 9, pp. 3–7, 2008.

[29] E.M. Sloot, N.P. Kruyt, "Theoretical and experimental study of the transport of granular materials by inclined vibratory conveyors," *Powder technology*, vol. 87, pp. 203–210, 1996.

[30] H. Colijn, *Weighing of bulk solids*. Bulk solids handling, 1991.

[31] T. Crowder, V. Sethuraman, T. Fields, A. Hickey, "Signal Processing and Analysis Applied to Powder Behavior in a Rotating Drum," *WILEY-VCH*, vol. 16, pp. 191–196, 1999.

[32] Timothy M. Crowder, "Vibration Technology for Active Dry-Powder Inhalers," tech. rep., Oriel Therapeutics, Inc., 2004.

[33] Michael J. R. Young, "Transport system for material in powder or like form." Patent Number 4648557, March 1987.

[34] Aleksandar I. Ribic, eljko V. Despotovic,, "High-Performance Feedback Control of Electromagnetic Vibratory Feeder," *IEEE*, vol. 57, pp. 3087–3094, 2010.

[35] R. G. Holdich, *Fundamentals of particle technology.* Midland information technology and publishing, 2002.

[36] W. Chen, M. Hou, K. Lu, Z. Jiang, L. Lam, "Granular flows through vertical pipes controlled by an electric field," *Phys. Rev., E Stat. Phys. Plasmas Fluids Relat. Interdiscip. Topics*, vol. 64, pp. 061305–1–061305–6., 2001.

[37] W. Chen, M. Hou, Z. Jiang, L. Lam, "Retardation and transition of dilute and dense granular flows in a vertical pipe induced by electric fields," *Applied Physics Letters*, vol. 80, pp. 2213–2215, 2002.

[38] S. Thompson, S. Law, W. Balachandran, "Metering of bulk material with an electrostatic valve," *Trans. ASAE*, vol. 38, pp. 1189–1194, 1995.

[39] W. Balachandran, D. Hu, M. Ghadiri, S.E. Law, S.A. Thompson, "The study of the performance of an electrostatic valve used for bulk transport of particulate materials," *IEEE*, vol. 33, pp. 871–878, 1997.

[40] M. Ghadiri, C. Martin, J. Morgan, R. Clift, "An electromechanical valve for solids," *Powder Technology*, vol. 73, p. 2135, 1992.

[41] J. Olansen, P. Dunn, "Dispensing particles under atmospheric and vacuum conditions using an electrostatic valve," *Journal of Applied Physics*, vol. 66, pp. 6098–6109, 1989.

[42] Y. Yang, X. Li, "Experimental and analytical study of ultrasonic micro powder feeding," *Journal of Physics*, vol. 36, pp. 1349–1354, 2003.

[43] B. Loh, S. Hyun, P. Ro, C. Kleinstreuer, "Acoustic streaming induced by ultrasonic flexural vibrations and associated enhancement of convective heat transfer," *Acoustical Society of America*, vol. 111, pp. 875–883, 2002.

[44] Y. Bar-Cohen, X. Bao, W. Grandiab, "Rotary Ultrasonic Motors Actuated By TravelingF lexural Waves," *Smart Structures and Materials Symposium*, pp. 1–5, 1998.

[45] T. Kozuka, T. Tuziuti, H. Mitome and T. Fukuda, "Noncontact micromanipulation using an ultrasonic standing wave field," *IEEE*, vol. 91, pp. 435–440, 1996.

[46] W. Nyborg, "Radiation pressure on a small rigid sphere," *Acoustical Society of America*, vol. 42, pp. 947–952, 1967.

[47] J. Wu, "Acoustical tweezers," *Acoustical Society of America*, vol. 89, pp. 2140–2143, 1991.

[48] T. Kozuka, T. Tuziuti, H. Mitome, "Control of Position of a Particle Using a Standing Wave Field Generated by Crossing Sound Beams," *IEEE ultrasonics symposium*, vol. 1, pp. 357–660, 1998.

[49] K. Yamada, T. Nakagawa, K. Nakamura, "Powder transportation by unidirectional ultrasound radiated from a pair of phase-shifted bending vibrators," tech. rep., Department of Electrical Communications, Faculty of engineering, Tohoku University, dai 980, Japan, 1993.

[50] H. Yamane, Y. Ito, M. Kawamura, "Sound radiation from rectangular plates vibrating in stripes mode," *Acoustical Society of Japan*, vol. 39, pp. 380–387, 1983.

[51] M. Kuribayashi, S. Ueha, E. Mori, "Excitation conditions of flexural traveling waves for a reversible ultrasonic linear motor," *Acoustical Society of America*, vol. 77, pp. 1431–1435, 1985.

[52] Y. Hashimoto, Y. Koike and S. Ueha, "Transporting objects without contact using flexural traveling waves," *Acoustical Society of America*, vol. 103, pp. 3230–3233, 1998.

[53] D. Sun, S. Wang, J.i Sakurai, S. Hata, K. Choi, and A.Shimokohbe, "A Traveling Wave Type of Piezoelectric Ultrasonic Bidirectional Linear Microactuator," *The Japan Society of Applied Physics*, vol. 2, pp. 046503–1–046503–3, 2009.

[54] S. Moaveni, *Finite Element Analysis: Theory and application with ANSYS*. Prentice Hall, Inc., 1999.

[55] R. Ndeda, "Modeling of bulge formation in polymers during laser micromachining," Master's thesis, Jomo Kenyatta University of Agriculture and Technology, 2011.

[56] E. Madenci and I. Guven, *The Finite Element Method and Applications in Engineering using ANSYS*. Springer Science + Business Media, LLC, 2006.

[57] S. Bhavikatti, *Finite Element Analysis*. New Age International (P) Ltd, 2005.

[58] E. Barkanov, *Introduction to the Finite Element Method*. Riga, 2001.

[59] M. Petyt, *Introduction to Finite Element Vibration Analysis*. Cambridge University press, 2010.

[60] V. Vishal, A. Fernandes, "Piezo electricity: Powering the Future." M.I.T. Manipal, 2009.

[61] T. Jordan, Z. Ounaies, "Piezoelectric Ceramics Characterization," tech. rep., NASA Langley Research Center, 2001.

[62] W. Cady, *Piezoelectricity*. Dover Publications, New York, 1964.

[63] APC International Ltd., *Piezoelectric Ceramics: Principles and Applications*. APC International Ltd., 2002.

[64] W. Mason, *Piezoelectric crystals amd their applications to ultrasonics*. D. Van Nostrand, New York, 2000.

[65] T. Hueter, R. Bolt, *Sonics*. John Wiley and Sons, Inc., 1955.

[66] K. Cheng, H. Chan, "Characterization of Piezoelectric Ring Used for Wire Bonding Transducer Application," tech. rep., The Hong Kong Polytechnic University, Hunghom, Kowloon, Hong Kong, 1998.

[67] IEC standard, "Guide to dynamic measurements of piezoelectric ceramics with high electromechanical coupling." 1976.

[68] M. Radmanovic, D. Mancic, Z. Petrusic, G. Stancic, "Components of the Mechanical displacements of the piezoceramic ring points," *Working and Living Environmental Protection*, vol. 5, pp. 49 – 57, 2008.

[69] M. Radmanovic, D.Mancic, "Design and modeling of the power ultrasonic transducers." Nis, Faculty of Electronic Engineering, 2004.

[70] A. Iula, N. Lamberti, M. Pappalardo, "An approximated 3-D model of cylinder-shaped piezoceramic elements for transducer design," *IEEE Trans. Ultrason., Ferroelect., Freq. Control*, vol. 45, pp. 1056–1064, 1998.

[71] D. Mancic, M. Radmanovic, "Piezoceramic ring loaded on each face: a three-dimensional approach," *Electronic Journal Technical Acoustics*, vol. 2, pp. 1.1–1.7, 2002.

[72] G. Hayward, D. Gillies, "Block diagram modeling of tall, thin parallelepiped piezoelectric structures," *Acoustical Society of America*, vol. 86, pp. 1643–1653, 1989.

[73] J. Yang, *An introduction to the theory of piezoelectricity*. Springer Science, 2005.

[74] Jiashi Yang, *The Mechanics of Piezoelectric Structures*. World Scientific Publishing Co. Pte. Ltd, 2006.

[75] J. Portelles, J. Fuentes, E. L. Rodriguez, L. Soto, O. Raymond, V. Garcia, J. Heiras and J. Siqueiros, "Piezoelectricity: Measurement of the resonant response of the radial mode at different temperatures," *Latin-American Journal of Physics Education*, vol. Vol. 5, pp. 129–133, 2011.

[76] S. G. Kelly, *Fundamentals of Mechanical Vibrations*. McGraw-Hill, 2000.

[77] M. Redwood, *Mechanical Waveguides*. Pergamon, 1960.

[78] V. Protopappas, I. Kourtis, L. Kourtis, K. Malizos, C. Massalas and D. Fotiadisa, "Three-dimensional finite element modeling of guided ultrasound wave propagation in intact and healing long bones," *Acoustical Society of America*, vol. 121, pp. 3907–3921, 2007.

[79] L. V. King, "On the Acoustic Radiation Pressure on Spheres," *The Royal Society*, vol. 147, pp. 212–240, 1934.

[80] L. Kinsler, A. Frey, A. Coppens, J. Sanders, *Fundamentals of Acoustics*. John Wiley & Sons, Inc, 2000.

[81] R. P. Vila, ed., *Waves in Fluids and Solids*. InTech, 2011.

[82] S. Ovidiu, "Studies on the interaction between an acoustic wave and levitated microparticles," in *Waves in Fluids and Solids*, InTech, 2011.

[83] S. Imaoka, "Conversion of piezoelectric material data." Collaborative Solutions Inc., 1999.

APPENDIX A

20 Node Brick Element

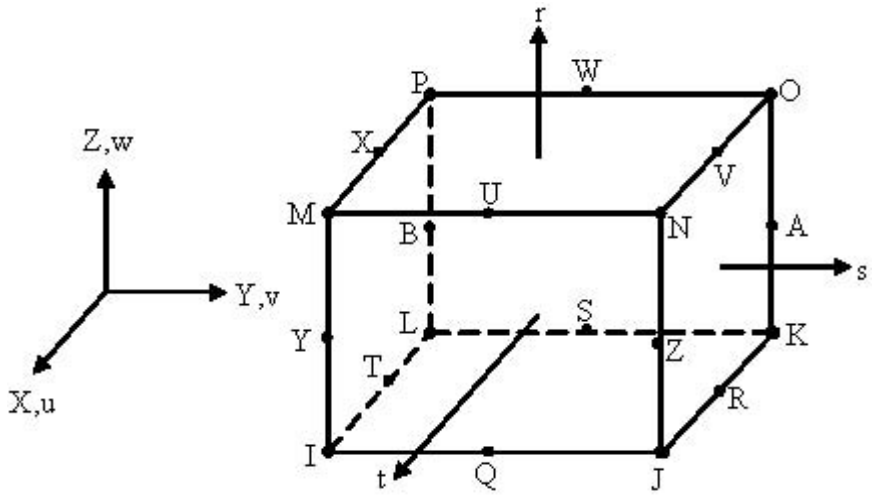

Figure A.1: SOLID 226 geometry element used by ANSYS.

The element has twenty nodes with up to five degrees of freedom per node. Structural capabilities are elastic only and include large deflection, stress stiffening effects, and prestress effects. For solid mechanic problems using the element (Figure A.1), the elements displacement field in terms of the nodal displacements and the shape functions is given by

$$
\left.
\begin{aligned}
u = \frac{1}{8}\big\{ & u_I(1-s)(1-t)(1-r)(-s-t-r-2) + u_J(1+s)(1-t)(1-r)(s-t-r-2) \\
& + u_K(1+s)(1+t)(1-r)(s+t-r-2) + u_L(1-s)(1+t)(1-r)(-s+t-r-2) \\
& + u_M(1-s)(1-t)(1+r)(-s-t+r-2) + u_N(1+s)(1-t)(1+r)(s-t+r-2) \\
& + u_O(1+s)(1+t)(1+r)(s+t+r-2) + u_P(1-s)(1+t)(1+r)(-s+t+r-2)\big\} \\
& + \frac{1}{4}\big\{u_Q(1-s^2)(1-t)(1-r) + u_R(1+s)(1-t^2)(1-r) \\
& + u_S(1-s^2)(1+t)(1-r) + u_T(1-s)(1-t^2)(1-r) \\
& + u_U(1-s^2)(1-t)(1+r) + u_V(1+s)(1-t^2)(1+r) \\
& + u_W(1-s^2)(1+t)(1+r) + u_X(1-s)(1-t^2)(1+r) \\
& + u_Y(1-s)(1-t)(1-r^2) + u_Z(1+s)(1-t)(1-r^2) \\
& + u_A(1+s)(1+t)(1-r^2) + u_B(1-s)(1+t)(1-r^2)\big\}
\end{aligned}
\right\}
\tag{A.1}
$$

The v and w components of displacement are similar to u component in Equation (A.1) and are given in Equations (A.2) and (A.3) respectively.

$$
v = \frac{1}{8}\big\{v_I(1-s)\ldots(\text{analogous to u}) \tag{A.2}
$$

$$
w = \frac{1}{8}\big\{w_I(1-s)\ldots(\text{analogous to u}) \tag{A.3}
$$

APPENDIX B

Conversion of Piezoelectric Material Data

Conversion of material properties of piezoelectric ceramics (such as PZT) can cause confusion because of the difference between manufacturer-supplied data and the format required by ANSYS [83].

B.1 Background Information

The constitutive relationship usually given by manufacturers or published data/reports is in the form of Equations B.1 and B.2:

$$\{S\} = \left[s^E\right]\{T\} + [d]\{E\} \tag{B.1}$$

$$\{D\} = [d]^t\{T\} + \left[\varepsilon^T\right]\{E\} \tag{B.2}$$

Where,

$\{T\}$ = stress vector (six components x, y, z, yz, xz, xy)

$\{S\}$ = strain vector (six components x, y, z, yz, xz, xy)

$\{D\}$ = electric displacement vector (three components x, y, z)

$\{E\}$ = electric field vector (three components x, y, z)

$\left[s^E\right]$ = compliance matrix evaluated at constant electric field, i.e. short circuit

$[d]$ = piezoelectric matrix relating strain/electric field

$[d]^t$ = piezoelectric matrix relating strain/electric field (transposed)

$\left[\varepsilon^T\right]$ = dielectric matrix evaluated at constant stress, i.e. mechanically free

On the other hand, ANSYS requires data in the form in Equations B.3 and B.4.

$$\{T\} = \left[c^E\right]\{S\} - [e]\{E\} \tag{B.3}$$

$$\{D\} = [e]^t\{S\} + \left[\varepsilon^S\right]\{E\} \tag{B.4}$$

Where,

$\{T\}$ = stress vector (six components x, y, z, yz, xz, xy)

$\{S\}$ = stress vector (six components x, y, z, yz, xz, xy)

$\{D\}$ = electric displacement vector (three components x, y, z)

$\{E\}$ = electric field vector (three components x, y, z)

$\left[c^E\right]$ = stiffness matrix evaluated at constant electric field, i.e. short circuit

$[e]$ = piezoelectric matrix relating stress/electric field

$[e]^t$ = piezoelectric matrix relating stress/electric field (transposed)

$\left[\varepsilon^S\right]$ = dielectric matrix evaluated at constant strain, i.e. mechanically clamped

In order to convert the manufacturers data presented in the form of Equations B.1 and B.2 to ANSYS notation (Equations B.3 and B.4), Equation B.1 needs to be based on stress rather than strain. The following manipulations can be performed:

$$\{S\} = \left[s^E\right]\{T\} + [d]\{E\} \tag{B.5}$$

$$\left[s^E\right]\{T\} = \{S\} - [d]\{E\} \tag{B.6}$$

$$\{T\} = \left[s^E\right]^{-1}\{S\} - \left[s^E\right]^{-1}[d]\{E\} \tag{B.7}$$

Since Equation B.2 relates electric displacement to strain rather than stress, Equation B.7 can then be substituted back into Equation B.2 giving:

$$\{D\} = [d]^t\{T\} + \left[\varepsilon^T\right]\{E\} \tag{B.8}$$

$$\{D\} = [d]^t\Big(\left[s^E\right]^{-1}\{S\} - \left[s^E\right]^{-1}[d]\{E\}\Big) + \left[\varepsilon^T\right]\{E\} \tag{B.9}$$

$$\{D\} = [d]^t\left[s^E\right]^{-1}\{S\} + \Big(\left[\varepsilon^T\right] - [d]^t\left[s^E\right]^{-1}[d]\Big)\{E\} \tag{B.10}$$

Upon comparison of Equation B.7 and B.10 with Equations B.3 and B.4, the relationship between manufacturer-supplied data and ANSYS-required value can be obtained using Equations B.11, B.12 and B.13.

$$\left[c^E\right] = \left[s^E\right]^{-1} \tag{B.11}$$

$$\left[\varepsilon^S\right] = \left[\varepsilon^T\right] - [d]^t\left[s^E\right]^{-1}[d] \tag{B.12}$$

$$[e] = \left[s^E\right]^{-1}[d] = [d]^t\left[s^E\right]^{-1} \tag{B.13}$$

B.2 Stiffness/Compliance Matrix

There are three ways in which stress-strain data can be input. `MP` commands can be used to specify orthotropic material properties (`EX`, `NUXY`, `GXY`). Otherwise, an anisotropic elastic matrix can be input using `TB,ANEL` commands.

Assuming polarization in the 3-axis (z-axis), the manufacturer data can be mapped to

ANSYS data to generate a compliance matrix B.14:

$$\left[s^E\right] = \left[c^E\right]^{-1} = \begin{bmatrix} s_{11}^E & s_{12}^E & s_{13}^E & 0 & 0 & 0 \\ & s_{11}^E & s_{13}^E & 0 & 0 & 0 \\ & & s_{33}^E & 0 & 0 & 0 \\ & & & s_{66}^E & 0 & 0 \\ & & & & s_{44}^E & 0 \\ & & & & & s_{44}^E \end{bmatrix} \tag{B.14}$$

If s_{66}^E is not available, it can be determined from Equation B.15.

$$s_{66}^E = \frac{1}{G_{xy}} = \frac{2(1+\upsilon_{xy})}{E_x} = 2\left(s_{11}^E - s_{12}^E\right) \tag{B.15}$$

For the `TB,ANEL` command, either matrix (stiffness matrix or compliance matrix) can be input. To input this data as compliance, the following commands can be issued:

```
TB,ANEL,1,1,,1              ! Material #1, 1 TEMP, TBOPT=1
                              for compliance input
TBDATA, 1,se11,se12,se13    ! Input first row
TBDATA, 7,se11,se13         ! Input second row
TBDATA,12,se33              ! Input third row
TBDATA,16,se66              ! Input fourth row
TBDATA,19,se44              ! Input fifth row
TBDATA,21,se44              ! Input sixth row
```

On the other hand, to input this data as stiffness, the following commands can be issued:

```
TB,ANEL,1,1,,0              ! Material #1, 1 TEMP, TBOPT=0
                              for stiffness input
TBDATA, 1,ce11,ce12,ce13    ! Input first row
TBDATA, 7,ce11,ce13         ! Input second row
TBDATA,12,ce33              ! Input third row
TBDATA,16,ce66              ! Input fourth row
TBDATA,19,ce44              ! Input fifth row
TBDATA,21,ce44              ! Input sixth row
```

$$[D]^{-1} = \begin{bmatrix} 1/E_x & -\upsilon_{xy}/E_y & -\upsilon_{xz}/E_z & 0 & 0 & 0 \\ & 1/E_y & -\upsilon_{yz}/E_z & 0 & 0 & 0 \\ & & 1/E_z & 0 & 0 & 0 \\ & & & 1/G_{xy} & 0 & 0 \\ & & & & 1/G_{yz} & 0 \\ & & & & & 1/G_{xz} \end{bmatrix} \tag{B.16}$$

$$= \left[s^E\right] = \left[c^E\right]^{-1}$$

An alternative method instead of using `TB,ANEL` is to use `MP` commands. Assuming polarization in the 3-axis (z-axis), manufacturer data can be converted to ANSYS data.

From Equation B.16, the stiffness via orthotropic MP commands can be input as follows;

$$\left.\begin{aligned} E_x &= \frac{1}{s_{11}^E} = E_x \\ E_z &= \frac{1}{s_{33}^E} \\ G_{xy} &= \frac{1}{s_{66}^E} = \frac{1}{2(s_{11}^E - s_{12}^E)} \\ G_{yz} &= \frac{1}{s_{44}^E} = G_{yz} \\ \gamma_{xy} &= -\frac{s_{12}^E}{s_{11}^E} \\ \gamma_{yz} &= -\frac{s_{13}^E}{s_{33}^E} = \gamma_{xz} \end{aligned}\right\} \tag{B.17}$$

where

$E_x =$ Young's modulus in the x direction (input as EX on MP command

$\gamma_{xy} =$ major Poisson's ratio (input as PRXY on MP command)

$\gamma_{yx} =$ minor Poisson's ratio (input as NUXY on MP command)

$G_{xy} =$ shear modulus in the xy plane (input as GXY on MP command)

To input this data, the following commands can be issued;

```
MP,EX ,1,1/se11        ! Material #1, Elastic modulus
MP,EY ,1,1/se11
MP,EZ ,1,1/se33
MP,NUXY,1,-se12/se11   ! minor Poissons ratio
MP,NUYZ,1,-se13/se33
MP,NUXZ,1,-se13/se33
MP,GXY ,1,1/se66       ! Shear modulus
```

```
MP,GYZ ,1,1/se44
MP,GXZ ,1,1/se44
```

B.3 Permittivity Matrix

The permittivity matrix evaluated at constant strain is input into ANSYS. Often times, manufacturers data has permittivity evaluated at constant stress, so conversion is necessary. From Equation B.12, the dielectric constants based on constant strain can be calculated. The permittivity matrix (Equation B.18) has diagonal terms only:

$$\left[\varepsilon^s\right] = \begin{bmatrix} \varepsilon_{11}^s & 0 & 0 \\ & \varepsilon_{11}^s & 0 \\ & & \varepsilon_{33}^s \end{bmatrix} = \varepsilon \begin{bmatrix} K_{11}^s & 0 & 0 \\ & K_{11}^s & 0 \\ & & K_{33}^s \end{bmatrix} \tag{B.18}$$

where $K_{11}^s = \varepsilon_{11}^s/\varepsilon_0$ is relative permittivity. In ANSYS, although there is a choice of inputting permittivity as an absolute value ε_{33}^T or relative value K_{33}^T, the relative value is the recommended choice. Assuming polarization in the 3-axis (z-direction), this can be input with the MP commands as follows:

```
EMUNIT,EPZRO,8.85e-12   ! Define free-space permittivity
MP,PERX,1,r-eps11       ! Material #1
MP,PERY,1,r-eps11
MP,PERZ,1,r-eps33
```

B.4 Material Density

Density does not require conversion. It is input with the MP command as follows;

```
MP,DENS,1,dens  ! Material #1
```

B.5 Piezoelectric Constant Matrix

Usually, manufacturers data has $[d]$, which relates mechanical strain to electric field. However, ANSYS requires $[e]$, relating mechanical stress to electric field, so conversion is necessary. From Equation B.13, a relationship between $[e]$ and $[d]$ is established. assuming polarization in the 3-axis (z-direction) and symmetry in the unpolarized directions ($d_{32} = d_{31}$ and $d_{24} = d_{15}$);

$$[d]^t = \begin{bmatrix} 0 & 0 & 0 & 0 & 0 & d_{15} \\ 0 & 0 & 0 & 0 & d_{15} & 0 \\ d_{31} & d_{31} & d_{33} & 0 & 0 & 0 \end{bmatrix} \tag{B.19}$$

Manufacturers data assumes the mechanical vector as $\{x, y, z, yz, xz, xy\}$ corresponding to $\{1, 2, 3, 4, 5, 6\}$ indexes. Row 4 needs to be shifted to Row 5, and, likewise, Row 5 $\rightarrow$ Row 6, Row 6 $\rightarrow$ Row 4. Hence, d_{15} and d_{24} are shifted one across. Using matrix with

$\left[s^E\right] = \left[c^E\right]^{-1}$ to evaluate $[e]$ (with rows 4, 5, 6 properly modified), gives;

$$\begin{bmatrix} 0 & 0 & e_{31} \\ 0 & 0 & e_{31} \\ 0 & 0 & e_{33} \\ 0 & 0 & 0 \\ 0 & e_{15} & 0 \\ e_{15} & 0 & 0 \end{bmatrix} \tag{B.20}$$

To input this data, the following commands can be issued:

```
TB,PIEZ, 1       ! Material #1, piezo matrix
TBDATA,  3, e31  ! Input first row
TBDATA,  6, e31  ! Input second row
TBDATA,  9, e33  ! Input third row
TBDATA, 14, e15  ! Input fifth row
TBDATA, 16, e15  ! Input sixth row
```